

Final Report
(CSM Project 4-42339)

Phase II
Joint Research Program between MMS and IMP
Underwater Wet Welding for Offshore Structures and Pipelines in the Gulf
of Mexico: Process Maturation and Technology Transfer

Submitted to:
Mr. Michael Else
Minerals Management Service
Engineering and Research Branch
381 Elden St. Herndon, VA 20170
and
Instituto Mexicano del Petroleo
Eje Central Lazaro Cardenas No. 152
Mexico City, 07734

Prepared by:
Stephen Liu and Faustino Perez Guerrero
Center for Welding, Joining and Coatings Research
Colorado School of Mines
Golden, Colorado 80401
CSM Report #: MT-CWJCR-006-002

Research Performed Under Contract:
0101PO18117

May 2006

TABLE OF CONTENTS

	Page
Executive summary	1
1 Introduction	3
1.1 Background	3
1.2 Objectives of this Research	3
1.3 Organization of the report	4
1.4 Participants	4
2 Tasks in Phase II	5
2.1 Underwater wet welding at 150 m	5
2.2 Performance of cellulosic electrodes	14
2.3 Out-of-position welding	33
2.4 Performance of rutile electrodes with nickel additions	56
2.5 Mitigation of porosity	64
2.6 Welding with covered electrodes using a constant voltage power source	72
3 General Conclusions and Recommendations	77
3.1 Conclusions	77
3.2 Recommendations	79
4 Acknowledgments	80

List of Tables

Table 2.1.1. Task 1 Experimental matrix.....	5
Table 2.1. 2. Welding current used for the different water depths and electrode grades.	5
Table 2.1.3. Tensile test results of the wet welds deposited at 150 m.	11
Table 2.2.1. Welding parameters selected to deposit the bead-on-plate welds with E6010 electrodes.....	16
Table 2.2.2. Tensile testing results from all weld metal specimens.	31
Table 2.3.1. Experimental matrix for out-of-position wet welding at three water depths (0.5, 50 and 100 m).....	34
Table 2.3.2. Welding parameters for the 3.2 mm electrode diameter.....	37
Table 2.3.3. Weld bead morphologies.	39
Table 2.3. 4. Bead morphologies of the bead-on-plate wet welds.....	43
Table 2.3. 5. Bead morphologies of the bead-on-plate wet welds.....	45
Table 2.3. 6. Bead morphologies of the bead-on-plate wet welds.....	47
Table 2.3. 7. Bead morphologies of the bead-on-plate wet welds.....	49
Table 2.3. 8. Weld metal porosity measured on the cross-sections.	49
Table 2.3. 9. Bead morphologies of the bead-on-plate wet welds.....	51
Table 2.3. 10. Weld metal porosity measured on the cross-sections	51
Table 2.3. 11. Reinforcement volume of the wet welds deposited at 0.5, 50, and 100 m water depth with E6013 electrodes.	52
Table 2.4.1. Main ingredients used for experimental rutile-grade electrode with nickel addition.	58
Table 2.5.1. Porosity of droplets collected during welding in dry conditions	65
Table 2.5.2. Gaseous species detected in pores, Sanchez-Osio (1995).	66
Table 2.6.1. Experimental matrix for the wet welds deposited in the hyperbaric chamber.....	72

List of Figures

Figure 2.1.1. Steel plate arrangement for V-groove wet welds to be deposited at 150 m water depth using the gravity welding system.	6
Figure 2.1.2. (a) Hyperbaric chamber used to perform the wet welds and (b) gravity welder inside the chamber.	6
Figure 2.1.3. (a) Multipass V-groove wet weld deposited with E6013 electrodes on A36 steel plates at 150 m and (b) its radiographic image. The weld passes started at the left-hand side.	7
Figure 2.1.4. (a) Multipass V-groove wet weld deposited with E7024 electrodes on A36 steel plates at 150 m and (b) its radiographic image. The weld passes started at the left-hand side.	8
Figure 2.1.5. (a) Multipass V-groove wet weld deposited with E6013 electrodes on API 5L Gr. B steel plates at 150 m and (b) its radiographic image. The weld passes started at the left-hand side.	8
Figure 2.1.6. Arc voltage signal acquired during wet welding with E6013 electrode on A36 steel. The average and standard deviation are 35.5 and 5.5 V, respectively.	9
Figure 2.1.7. Arc voltage signal acquired during wet welding with E7024 electrode on A36 steel. The average and standard deviation are 60.0 and 8.7 V, respectively.	9
Figure 2.1.8. Cross-section macrographs showing porosity of the V-groove deposited with E6013 electrode on A36 steel at 150 m (the scale is in millimeters).	10
Figure 2.1.9. Cross-section macrographs showing porosity of the V-groove wet welds deposited with E7024 electrode on A36 steel at 150 m (the scale is in millimeters).	10
Figure 2.1.10. Cross-section macrographs showing porosity of the V-groove wet welds deposited with E6013 electrode on API 5L Gr. B steel at 150 m (the scale is in millimeters).	11
Figure 2.1.11. Shape and dimensions of the tensile specimens extracted from the wet welds deposited at 150 m.	11
Figure 2.1.12. Fracture surfaces of wet weld made with (a) E6013 electrodes on A36 steel, (b) E7024 electrodes on A36 steel, and (c) E6013 electrodes on API 5L Gr. B steel. Arrows are pointing to communicating pores (the width is 19 mm and the high is 8 mm).	12
Figure 2.2.1. Hyperbaric chamber at the Colorado School of Mines for underwater wet welding where different water depths can be simulated (maximum pressure 300 psig).	15
Figure 2.2.2. Bead-on-plate wet welds deposited with E6010 electrode type.	16
Figure 2.2.3. V-groove multipass wet weld after a weld pass. Note the amount of spatter on the weld and plate.	17
Figure 2.2.4. V-groove multipass wet weld inside the hyperbaric chamber.	17
Figure 2.2.5. Voltage signals acquired during welding at depths of (a) 0.3 and (b) 50 m, and (c) power spectrum density of a voltage signal acquired during wet welding at 50m.	18
Figure 2.2.6. Cross-section macrographs of the BOP weld deposited with the E6010 electrode at water depths of (a) 0.30m, (b) 14m, (c) 28m, (d) 42m, and (e) 50 m. The dimension of the white scale is 6 mm.	19
Figure 2.2.7. Variation of width and penetration with water depth of the weld beads deposited with E6010 electrodes. The width and penetration of a wet weld made with E6013 electrode at 50 m are given for comparison.	19
Figure 2.2.8. Cracking at the fusion line of a bead-on-plate wet welds deposited at (a) 14 m and (b) 50 m water depth (Note the differences in scale).	20
Figure 2.2.9. Cross-section macrographs of the bead-on-plate wet welds deposited at four water depths, (a) 14 m, (b) 28 m, (c) 42 m, and (d) 50m. The dimension of scale is 6 mm.	20
Figure 2.2.10. Porosity percent versus water depth from the cross-section macrographs of the BOP welds.	21
Figure 2.2.11. Cross-section macrographs parallel to the top surface of the plate showing the porosity in the weld metal. The welds were deposited at (b) 14m, (c) 28m, (d) 42 and (e) 50m of water depth. The white scale represents 6 mm.	21
Figure 2.2.12. Porosity variation as a function of water depth. From the cross-section macrographs shown in Figure 2.2.11.	22
Figure 2.2.13. Cross-section macrograph of the V-groove wet weld deposited at 50 m of water depth with E6010 electrodes.	22
Figure 2.2.14. Manganese content as a function of water depth In the weld metal of the welds deposited with E6010 electrodes.	23

Figure 2.2.15. Silicon content as a function of water depth in the weld metal deposited with E6010 electrodes.....	23
Figure 2.2.16. Carbon content as a function of water depth in the weld metal of the welds deposited with E6010 electrodes.....	24
Figure 2.2.17. Oxygen content as a function of water depth in the weld metal of the welds deposited with E6010 electrodes.....	24
Figure 2.2.18. Micrographs showing oxide inclusions in a wet weld deposited at 50 m water depth with E6010 electrode. (a) Large oxide inclusion with 39 μm in diameter and (b) two smaller oxide inclusions with 14 and 16 μm in diameter. Note also the inclusions with diameters around 1 μm in diameter.	25
Figure 2.2.19. (a) SEM micrograph and electron dot maps of a large inclusion, (b) iron, (c) manganese, (d) oxygen, (e) silicon, and (f) titanium distribution in the weld metal.	26
Figure 2.2.20. (a) SEM micrograph of the EDS mapped region showing two inclusions, (b) iron, (c) manganese, (d) oxygen, (e) silicon, and (f) titanium distribution in the weld metal.	26
Figure 2.2.21. Micrographs from the bead-on-plated wet weld deposited with E6010 electrodes (a) and (b) at surface in dry conditions, (c) and (d) at 0.3 m, and (e) and (f) at 50m (the scale box represents 25 μm).	28
Figure 2.2.22. Additional micrographs from bead-on-plate wet welds deposited at (a) surface and (b) 50 m water depth; (c) and (d) are high magnification views from (a) and (b) respectively.	29
Figure 2.2.23. Diamond pyramid hardness or Vickers Hardness (500 g load) from the.....	30
Figure 2.2.24. Diamond pyramid hardness or Vickers hardness (500 g load) from V-groove wet welds made with E6010 and E6013 electrodes at 50 m.	30
Figure 2.2.25. Toughness of wet welds deposited with E6010 grade and rutile-type electrodes tested at two temperatures.	31
Figure 2.3. 1. Schematic illustration of the replacement of part of a damaged structural member (2), which is welded to a main column (3). A slightly large diameter sleeve (1) is wet welded to the remaining end of the damaged member.	33
Figure 2.3. 2. Gravity feed system for out-of-position welding (a) vertical-down and (b) vertical-up.	34
Figure 2.3. 3. Vertical-down gravity welding system inside a water tank for initial tests.....	35
Figure 2.3. 4. Steel plates to deposit bead-on-plate wet weld in vertical position.....	35
Figure 2.3. 5. Flux-covered electrodes E6010, E7018 and E6013 (from top to bottom).	35
Figure 2.3. 6. Location and identification of cross-sections extracted from the dead on plate-wet-welds.	36
Figure 2.3. 7. Welding current values tested in the vertical-down position with two electrode diameters.	36
Figure 2.3. 8. Bead-on-plate wet welds deposited in vertical-down position with E6010, E7018, and E6013 electrode on API 5L Gr. B steel plates.....	38
Figure 2.3. 9. Weld liquid metal with vertical support.	38
Figure 2.3. 10. Cross-section macrographs of the bead-on-plate wet weld deposited using electrodes with 3.3 mm in diameter.	39
Figure 2.3. 11. Cross-section macrographs of the bead-on-plate wet weld deposited using electrodes with 4 mm in diameter.	39
Figure 2.3. 12. Arc voltage signals recorded for the three electrode types.....	40
Figure 2.3. 13. Arc current signals recorded for the three electrode types.	41
Figure 2.3. 14. Three BOP wet welds deposited in the vertical-down position with E6013 electrodes at 0.5 m water depth.....	42
Figure 2.3. 15. Cross-sections from the bead-on-plate wet welds deposited with E6013 electrodes at 0.5 in the vertical-down position. The scales are in millimeters.....	43
Figure 2.3. 16. Three BOP wet welds deposited in the vertical-down position with E6010 electrodes at 0.5 m water depth.....	44
Figure 2.3. 17. Cross-sections from the bead-on-plate wet welds deposited with E6010 electrodes at 0.5 in the vertical-down position.	45
Figure 2.3. 18. Three BOP wet welds deposited in the vertical-down position with E7018 electrodes at 0.5 m water depth.....	46
Figure 2.3. 19. Cross-sections from the bead-on-plate wet welds deposited with E7018 electrodes at 0.5 in the vertical-down position.....	47

Figure 2.3. 20. Three BOP wet welds deposited in the vertical-down position with E6013 electrodes at 50 m water depth.....	48
Figure 2.3. 21. Cross-sections from the bead-on-plate wet welds deposited with E6013 electrodes at 50 in the vertical-down position.	48
Figure 2.3. 22. Three BOP wet welds deposited in the vertical-down position with E6013 electrodes at 100 m water depth.	50
Figure 2.3. 23. Cross-sections from the bead-on-plate wet welds deposited with E6013 electrodes at 100 in the vertical-down position.	50
Figure 2.3. 24. Wet weld made with E7018 electrode type at 50 m.	52
Figure 2.3. 25. Weld liquid metal without vertical support.	53
Figure 2.3. 26. Bead-on-plate wet welds deposited in the vertical-up position at 0.5 m using E6013, E6010 and E7018 electrodes, respectively.	54
Figure 2.4.1. Effect of nickel on impact toughnes of wet welds deposited with rutile and oxidizing electrodes at 32 F, Perez (2003).	56
Figure 2.4.2. Impact toughnes versus nickel content tested at different tempratures – Surface welds Perez (2003).	57
Figure 2.4.3. Fracture surfaces of Charpy V-notch specimens tested at –58 F.	57
Figure 2.4.4. (a) Electrode extruder at CSM and (b) extruder illustration, Perez (2003).	58
Figure 2.4.5. Set of standard Charpy V-notch specimens made from a multipass wet weld deposited at 50 m with rutile electrodes with nickel additions. These specimens show the bottom side of the multipass weld.	58
Figure 2.4.6. Average impact toughness of the three multipass wet welds made with rutile electrodes and nickel additions.	60
Figure 2.4.7. SEM photographs taken from the fracture surfaces showing dimples, the scale bar indicates 23 μm	61
Figure 2.4.8. SEM photographs taken from the fracture surfaces showing (a) cleavage fracture and (b) a mixture of dimples and cleavage facets, the scale bar indicates 50 μm	61
Figure 2.4.9. Fracture surface of Charpy V-notch specimens made from the multipass wet weld with 2.4 wt. pct. nickel showing defects such as porosity and slag entrapment.	62
Figure 2.4.10. Micrographs taken from the Charpy V-notch specimens extracted from the multipass wet welds showing the fine grains in the reheated zone	63
Figure 2.5.1. (a) Droplet attached to the tip of the electrode and (b) collected droplets (Brandi, S., Taniguchi C. and Liu S. (1991)).	64
Figure 2.5.2. Weld metal porosity as a function of water pressure, by Suga and Hasui (1986).	66
Figure 2.5.3. Arc voltage signals acquired during wet welding at 50 m (top) and 100 m (bottom) water depths.	67
Figure 2.5.4. Illustrations of droplet formation and growth at the electrode tip, gas diffusion, and gas entrapment in the weld metal.	68
Figure 2.5.5. Top view of a bead-on-plate wet weld deposited with E6010 electrode at 50 m.	70
Figure 2.5.6. Longitudinal section from a bead-on-plate wet weld deposited with E6010 electrode at 75 m water depth using constant current. The porosity percentage measured is 10.3 %.	70
Figure 2.5.7. Longitudinal section from a bead-on-plate wet weld deposited with E6010 electrode at 75 m water depth using constant current. The porosity percentage measured is 3.2 %.	71
Figure 2.6.1. Welding system used for wet welding with flux-covered electrodes and constant voltage.	73
Figure 2.6.2. Bead-on-plate wet welds made with E6013 electrodes, electrode positive polarity, and constant voltage at 50 m water depth. The numbers on the plate from left to right indicate water depth, voltage and weld number.	74
Figure 2.6.3. Close-up of the bead-on-plate wet welds shown previously.	74
Figure 2.6.4. Width versus selected voltage of the BOP welds.	75
Figure 2.6.5. Penetration versus selected voltage of the BOP welds.	75
Figure 2.6.6. Porosity percent versus selected voltage of the BOP welds.	76

EXECUTIVE SUMMARY

This report presents the results obtained in six different research tasks carried out in Phase II of the MMS-IMP sponsored underwater wet welding program.

Multipass underwater wet welds were deposited at 150 m water depth using a gravity welding system placed inside a hyperbaric chamber. Cross-section macrographs of the welds exhibited porosity that ranged from 7.3 to 23.5 pct., which affected the tensile strength of the weld metal by approximately 30 ksi (nearly 50 % the strength of the base metal). The AWS E6013 grade electrode reported the smallest porosity percentages. Similar to the results presented in Phase I, the welds exhibited more porosity at the beginning side of the weld and less porosity at the end side.

Cellulosic electrodes, particularly the AWS E6010 grade, exhibited good performance in wet welding conditions with deeper penetration than rutile-grade electrodes. This electrode produced light slag that was easily removed and with the deep weld penetration, slag entrapment was not a problem. Although large hydrogen-assisted cracks were observed in the heat-affected zone of single bead-on-plate wet welds, only a few micro-cracks were observed in the weld metal in multipass welds. Loss of alloying elements such as manganese, silicon, and carbon was observed with increasing water depth. Also, large oxide inclusions were observed in the weld metal. These inclusions contain manganese, silicon, oxygen, and a few traces of titanium. These findings indicate that the alloying elements detected by bulk chemical analyses in wet welds deposited at 50 m could be in the form of oxide inclusions, which are detrimental to the mechanical properties of the wet welds. Good agreements were observed between chemical analyses, observed microstructures, and mechanical properties.

Out-of-position wet welds were deposited at 0.5, 50 and 100 m water depth, the results obtained showed that acceptable welds could be produced in the vertical-down position while unacceptable weld were deposited in the vertical-up position. In the vertical-down position, the pressure of the arc ahead gives support to the liquid weld metal, while in the vertical-up position the liquid metal runs down and away from the arc due to the lack of support. Even with the arc support in the vertical down position, liquid metal can still run away from the weld, as observed in the welds deposited at 50 and 100 m. Wet welds deposited in the vertical-down position exhibited less porosity than wet welds deposited in flat position.

Toughness of wet welds deposited at very shallow water depths has been improved when small amounts of nickel were added to oxidizing and rutile-grade electrodes. Therefore, experimental rutile electrodes with nickel additions were extruded to deposit wet welds at 50 m water depth. Although the toughness values obtained are smaller than those obtained from wet welds deposited at surface. It was evident that nickel does improve the impact toughness of wet welds at low temperatures. Up to 20 ft-lb. was obtained at -54 F when the weld metal nickel content was 0.9 wt. pct., which is greater than the 8 ft-lb. reported for a surface wet weld with very low nickel content. In this comparison, it is important to consider that wet welds deposited at 50 m contain larger defects such as porosity and slag entrapment than surface wet welds. Facets of plastic fracture were observed on all the specimens tested at three temperatures. Due to the nickel additions, large regions with small grains (less than 4 μm) were observed in the wet welds. Small grains are desirable to improve the mechanical properties of steel welds.

Porosity in wet welds becomes more important as the water depth increases, becoming one of the main problems in wet welds. Reducing porosity in wet welds deposited at water depth beyond 50 m can increase the mechanical properties and quality of the wet welds. Results in the literature and in this work indicate that as water depth increased, porosity increased. This increase is caused by an enrichment of the gas content in the liquid drops that hang from the tip of the electrode. Therefore, when these droplets

are transferred into the weld pool, the entrapped gas also transfers. Unable to escape, porosity results. A possible reason for porosity formation could be that the pressure of the arc is greater than the entrapped gas pressure. Based on this reasoning, porosity could be reduced if the size of the droplets transferred to the weld pool is diminished. Initial results show that pulsed welding current can reduce weld metal droplet size and porosity. However, more research work is required to identify the proper welding parameters for the flux-covered electrodes being used.

One of the disadvantages of the shielded metal arc welding process in wet welding with a gravity welder is the initiation of the arc. A paste with low electrical conductivity was developed that can be placed between the electrode tip and the base metal to initiate the arc. Even though electrode-welding process relationships are very well established, i.e. the matching of a welding process with particular type of consumables, this disadvantage in wet welding can be avoided if the constant voltage process (typically used with wire electrode) is used with the flux-covered electrodes. Experiments showed that wet welds were successfully deposited at simulated water depth of 25, 50, and 75 m using a constant voltage power source with 5/32" rutile-grade electrodes. When proper welding parameters were selected, the arc readily started when the electrode contacted the base metal. A better control of the arc length was also achieved with constant voltage. One disadvantage is that at short-circuiting, the welding current could surge to the maximum output value, posing risk for the operator.

1 INTRODUCTION

1.1 Background

Based on the results obtained in Phase I, six tasks were included in Phase II of this underwater wet welding program conducted at the Colorado School of Mines. The tasks are listed in the following:

- a) Underwater wet welding at 150 m.
- b) Performance of cellulosic electrodes.
- c) Out-of-position welding.
- d) Performance of rutile electrodes with nickel additions.
- e) Mitigation of porosity.
- f) Welding with covered electrodes using a constant voltage power source.

The first task was not included in Phase I due to technical problems to deposit the planned wet welds. Wet welds performed at 150 m water depth showed severe weld metal porosity and resulted in poor mechanical properties. As such, the original experimental matrix was reduced.

Cellulosic electrodes are typically used in pipe welding because of its ability to produce deep penetrating welds, which is a requirement for all-position welding and good weld metal toughness. Requested by one of the sponsors, IMP, this task was performed to study the performance of cellulosic electrodes in wet conditions.

Even though most of the experimental wet welds were made in the flat position, actual repairs with wet welding are typically made out-of-position. Thus, experimental vertical-up and vertical-down wet welding positions were considered in this task.

It has been demonstrated that nickel improves toughness of underwater wet welds deposited at surface. Although the same effect is expected in wet welds deposited at deeper waters (i.e. 50 m) no experimental results are available. Experimental electrodes with different amounts of nickel were used to produce welds at greater depths.

Since weld metal porosity is one of the main problems in wet welding that result in poor mechanical properties, it is a top priority to reduce weld metal porosity. Several approaches were explored to minimize the formation of pores.

In terms of industrial practice, arc welding processes are very well established. For example, constant current power sources are typically used with flux-covered electrodes and constant voltage power sources, with solid wire, flux-cored wire or metal-core wire. As such, constant current type power sources are used for wet welding using covered electrodes. When a gravity welding system is used, one of the main disadvantages observed is the difficulty in initiating an arc without short-circuiting the electrode on the base plate. A low conductivity flux paste was developed and placed between the tip of the electrode and the base metal to initiate the arc. This inconvenient step can be avoided with the use of a constant voltage welding machine.

1.2 Objectives of this research

The general objective of Phase II of this program is to carry out different tasks in order to understand problems associated with underwater wet welding and recommend possible solutions to the problems.

Specific task objectives are as follows:

Task	Objectives
1	To investigate feasibility of depositing multipass wet welds using a gravity welding system at 150 m simulated water depth.
2	To evaluate the performance of E6010 (cellulosic) electrodes in wet welding conditions.
3	To investigate the difficulties in depositing wet welds in vertical-down and vertical-up positions.
4	To assess the effect of nickel additions in rutile-grade electrodes on impact toughness of wet welds made at greater water depths (i.e. 50 m).
5	To identify mechanisms of porosity formation in order to recommend mitigating measures.
6	To evaluate the performance of constant voltage power source in wet welding with flux-covered electrodes.

1.3 Organization of the report

This report contains four sections. Section 1 contains the executive summary, followed by the introduction. The specific tasks in Phase II are reported in Section 2, each task has an introduction, experimental procedures, results, and conclusions. Section 3 presents general conclusions and recommendations of the program and the acknowledgments are presented in Section 4.

1.4 Participants

In Phase II of this program, the participants are the Center for Welding, Joining and Coatings Research (CWJCR) of the Colorado School of Mines (CSM) and the Department of Mechanical Engineering at the Federal University of Minas Gerais (UFMG), which is located in Belo Horizonte, Brazil. Tasks 1 and 3 were conducted at UFMG and tasks 2, 4, 5, and 6 were performed at CSM. The final analysis and integration of the results were carried out at CSM.

Having the capabilities, interest, and the experience obtained in Phase I work of this project, UFMG was subcontracted by CSM to perform the two tasks previously mentioned.

2 TASKS IN PHASE II

2.1 Underwater wet welding at 150 m.

2.1.1 Introduction

Underwater wet welds at 150 m water depth were not reported in Phase I due to technical and operational difficulties. After solving these problems in Phase II, three multipass V-groove wet welds were made with a gravity welder to assess porosity and tensile strength of the weld metals. AWS E6013 and E7024 grade commercial electrodes were used along with ASTM A-36 and API 5L Gr. B steel plates. Based on the results obtained in Phase I, the use of the E7018 electrode grade was not advised for this water depth. Also based on the porosity observed in the initial welds, the experimental matrix was reduced (see below).

2.1.2 Experimental procedures

Initially three steels were considered for welding with three commercial electrodes at 150 m water depth. However, based on the results obtained in phase I and the difficulties encountered during welding at 150 m water depth, only three multipass V-groove wet welds were made as indicated in Table 2.1.1.

AWS E6013 and E7024 grade commercial electrodes were used. These electrodes measured 5 mm X 356 mm (diameter and length), and had 1 and 3 mm flux thickness, respectively. The electrodes were waterproofed with commercial varnish to protect the flux coating from water absorption.

Table 2.1.1. Task 1 Experimental matrix.

Steel plates	Electrodes		
	E6013	E7018 ¹	E7024
ASTM A-36	√	X	√
ASTM A572 Gr. 50 ²	X	X	X
API 5L Gr. B	√	X	X ²

Note:

1. Base on phase I results, the E7018 electrode grade was considered unsuitable for wet welding due to the large porosity percentages observed.
2. Due to large porosity percentage observed in the first V-groove wet welds, no multipass wet welds were deposited with E6013 and E7024 grade electrodes on ASTM A572 Gr. 50 steel nor E7024 electrodes on API 5L Gr. B steel.

In order to overcome the water pressure equivalent to 150 m water depth and the corresponding arc instability, welding current had to be increased by about 10% with respect to previous welding experiments at lower pressures (shallower water depths), see Table 2.1.2. Larger current values were also used with the E7024 than the E6013 grade electrodes because of the thicker flux coating of those electrodes.

Table 2.1. 2. Welding current used for the different water depths and electrode grades.

Electrode/water depth, m	Welding Current (A)		
	50	100	150
E6013	260	280	300
E7024	310	310	330

Multipass V-groove wet welds were deposited on steel plates according to the matrix shown in Table 2.1.1 and with the plate arrangement shown in Figure 2.1.1. Wet welding with the gravity welding system inside the chamber at 150 m water depth pressure is a more time-consuming process because of cycle time (weld setup, close chamber, pressurize, weld, depressurize, drain water, open chamber). Therefore, thicker electrode diameters (steel rod diameter of 5 mm) were selected to increase the weld metal deposition rate.

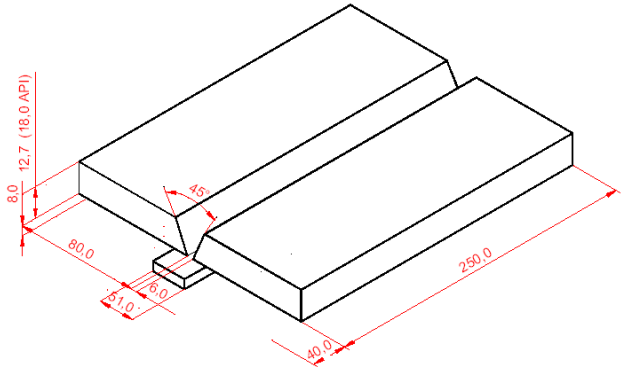


Figure 2.1.1. Steel plate arrangement for V-groove wet welds to be deposited at 150 m water depth using the gravity welding system.

This task was carried out at UFMG, which has the facilities and experience to perform experimental wet welding. Figure 2.1.2 shows the hyperbaric chamber and the gravity welder inside the chamber. Water depths from 0 to 200 m can be simulated in this chamber.

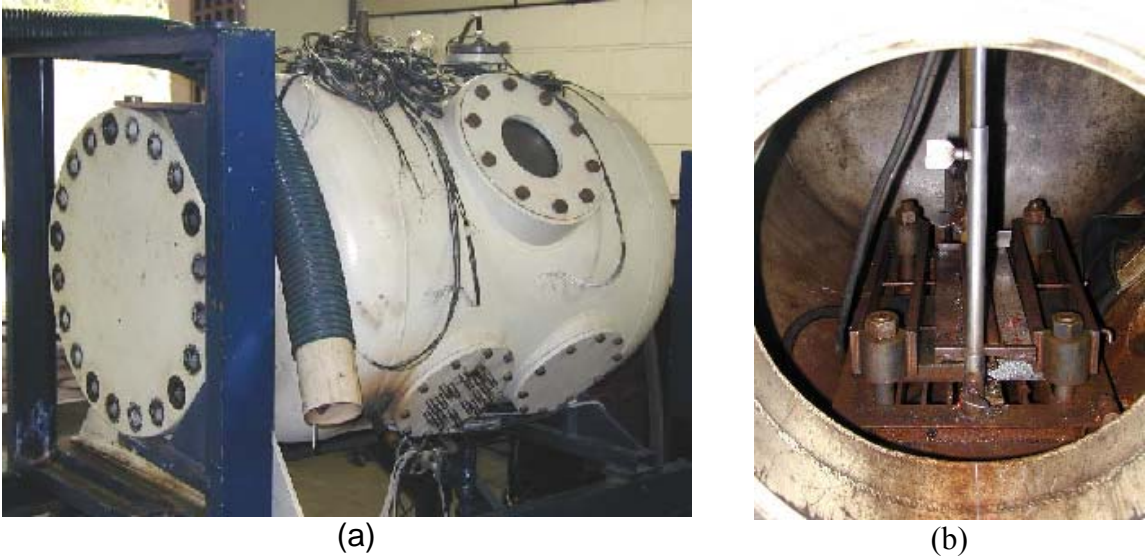


Figure 2.1.2. (a) Hyperbaric chamber used to perform the wet welds and (b) gravity welder inside the chamber.

The welding cycle in the hyperbaric chamber using the gravity welder is as follows:

- a) Place the steel plate and electrode in the gravity welder inside the chamber
- b) Close the chamber and tighten the nuts to the right torque
- c) Fill the chamber with fresh water
- d) Pressurize the chamber with compressed air to the desired pressure
- e) Start the arc
- f) Record arc signals
- g) Disconnect the power after arc extinguishes
- h) Release the air pressure
- i) Pump out the water
- j) Open the chamber
- k) Extract the welding fumes
- l) Remove the plate and clean the weld

2.1.3 Results

As expected wet welds deposited at 150 m water depth exhibited more porosity than weld made at shallower water depths using the same electrode grades and steel plates. Porosity ranged from 7.3 to 23.5 percent reducing the tensile strength to less than 50 percent the tensile strength of the base metal.

Despite the difficulties in depositing the wet welds at this water depth, three multipass V-groove welds were successfully made using E6013 and E7024 grade electrodes, see Figures 2.1.3a, 2.1.4a, and 2.1.5a. However, these welds had rough bead surfaces with considerable number of pinholes and pores on the bead surface. Radiographic images of the multipass welds in Figure 2.1.3b, 2.1.4b, and 2.1.5b showed very large pores at the beginning of the welds. The number and the size of the pores decreased as the welds progressed.

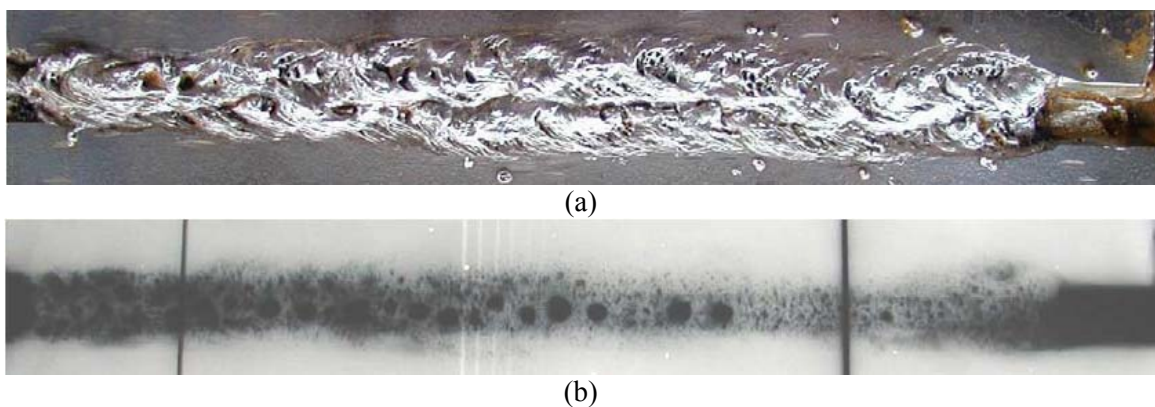


Figure 2.1.3. (a) Multipass V-groove wet weld deposited with E6013 electrodes on A36 steel plates at 150 m and (b) its radiographic image. The weld passes started at the left-hand side.

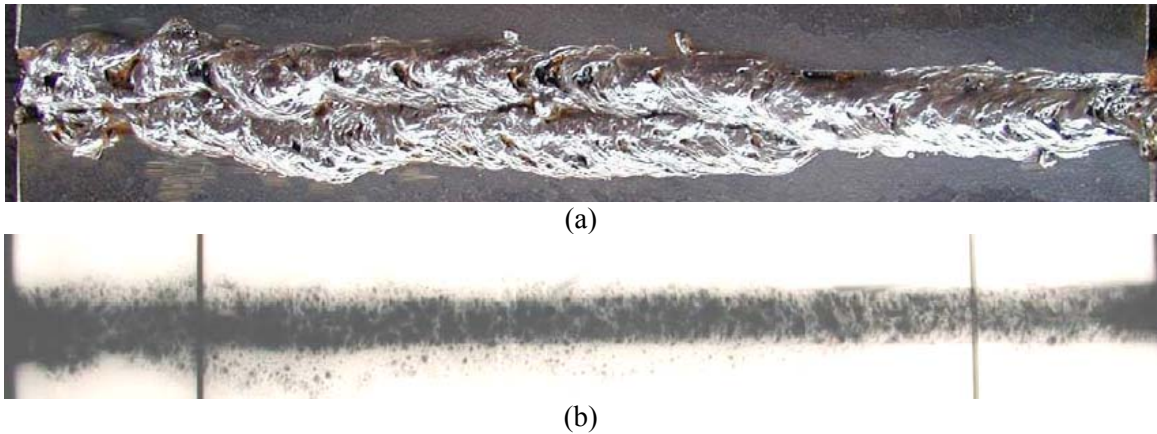


Figure 2.1.4. (a) Multipass V-groove wet weld deposited with E7024 electrodes on A36 steel plates at 150 m and (b) its radiographic image. The weld passes started at the left-hand side.

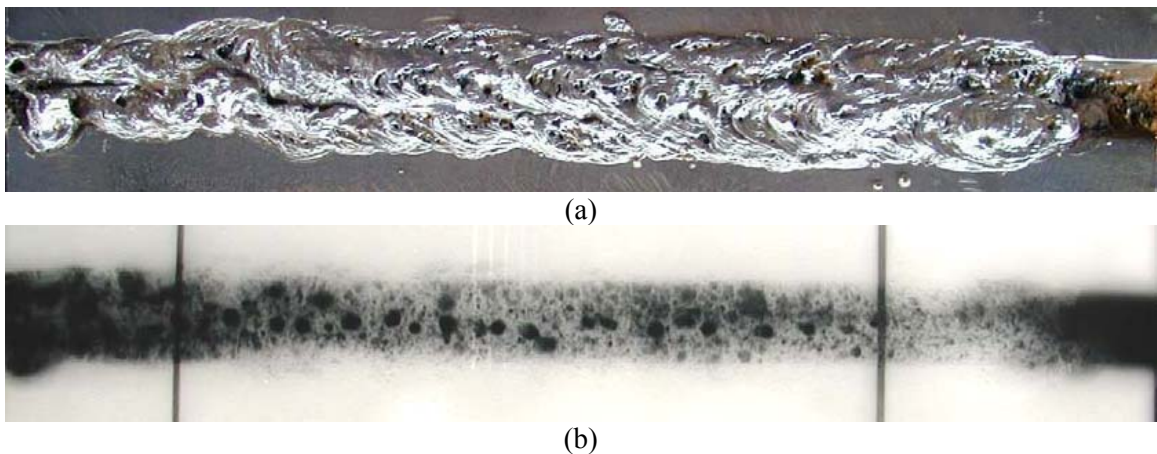


Figure 2.1.5. (a) Multipass V-groove wet weld deposited with E6013 electrodes on API 5L Gr. B steel plates at 150 m and (b) its radiographic image. The weld passes started at the left-hand side.

Arc voltage and current signals were acquired during welding to identify metal transfer modes and arc stability. Figures 2.1.6 and 2.1.7 show voltage signals recorded during wet welding with E6013 and E7024 grade electrode on A36 steel. The average voltages were 35.5 and 60.0 V with standard deviations of 5.5 and 8.7 V for the E6013 and E7024 grade electrode, respectively. Note the very high arc voltage when welding with E7024 grade electrodes. Arc length is directly related to the average welding voltage and depends on the flux coating composition and thickness (the thicker the flux coating, the longer the arc length). Since E6013 electrodes have thinner flux coating, the arc length is expected to be shorter. Conversely, the thicker coating E7024 electrode will have longer welding arc. The metal transfer mode associated with both electrode grades at 150 m was globular, indicated by the large voltage variations and large standard deviations. Comparing the two electrodes, E6013 electrode produced small droplet sizes than E7024 electrode.

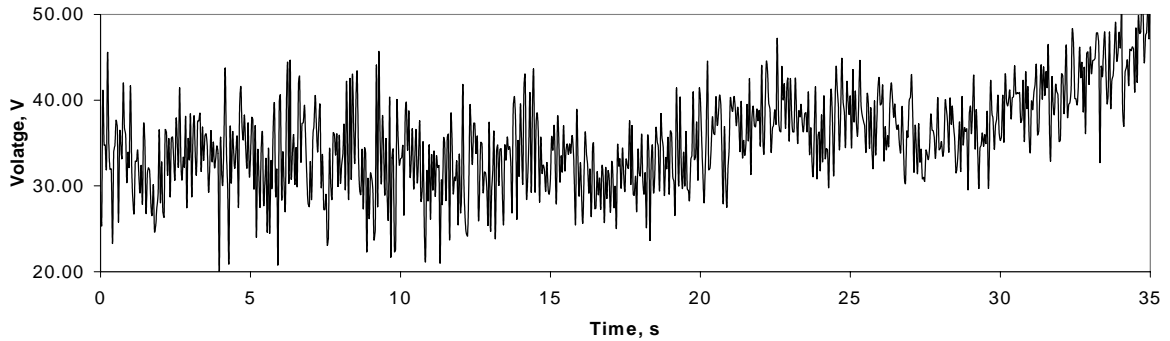


Figure 2.1.6. Arc voltage signal acquired during wet welding with E6013 electrode on A36 steel. The average and standard deviation are 35.5 and 5.5 V, respectively.

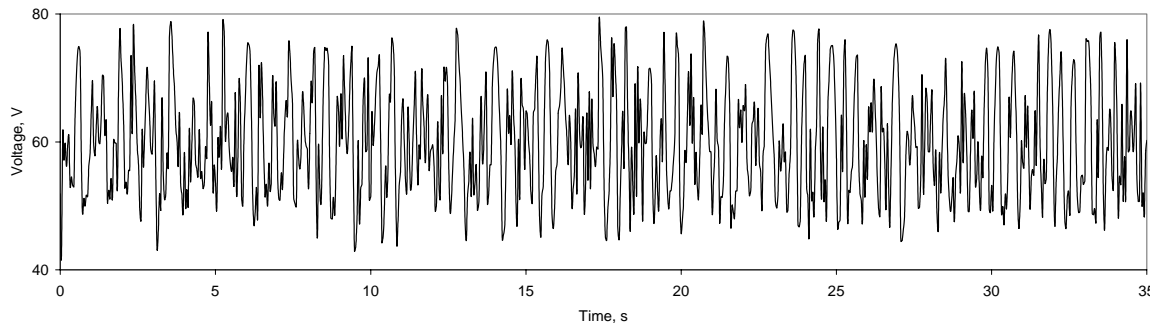


Figure 2.1.7. Arc voltage signal acquired during wet welding with E7024 electrode on A36 steel. The average and standard deviation are 60.0 and 8.7 V, respectively.

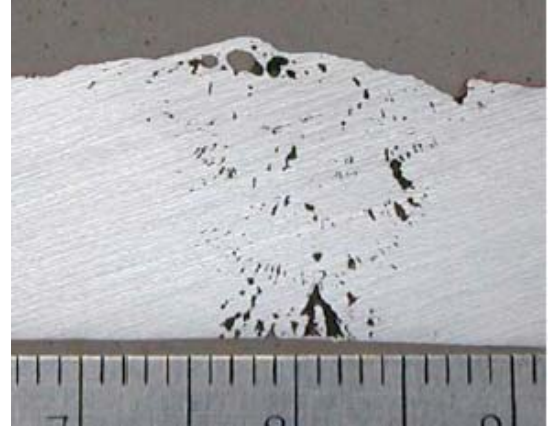
Two transverse cross-section macrographs were taken from each multipass wet weld to examine the soundness of the weld metal. Figures 2.1.8a, 2.1.9a, and 2.1.10a present macrographs taken from the beginning side of the welds and Figures 2.1.8b, 2.1.9b, and 2.1.10b present macrographs taken from the end side of the welds. As can be seen, porosity percentages were higher at the beginning side of the weld, ranging from 15.8 to 23.5 %. On the end side of the welds, the porosity measured from 7.3 to 16.7 %. Porosity variation along the length of the weld is an important finding since it can indicate changes in the arc regarding chemical equilibrium, electrode temperature, or metal transfer mode. For example, porosity variation has been attributed to temperature changes of the electrode (being cold in the beginning and hotter at the end) which change the droplet sizes and metal transfer modes.

Note the two large weld beads located at the top side of the multipass weld and shown in Figure 2.1.10a, the large pores open to the surface of the welds. It can be inferred that smaller electrode diameters will produce smaller weld beads and smaller pore sizes. Consequently, lower porosity is expected.

Regarding types of electrodes, E6013 electrode reported less porosity than the E7024 electrode grade.



(a) 15.8 % at the beginning side of the weld.



(b) 7.3% at end side of the weld.

Figure 2.1.8. Cross-section macrographs showing porosity of the V-groove deposited with E6013 electrode on A36 steel at 150 m (the scale is in millimeters).

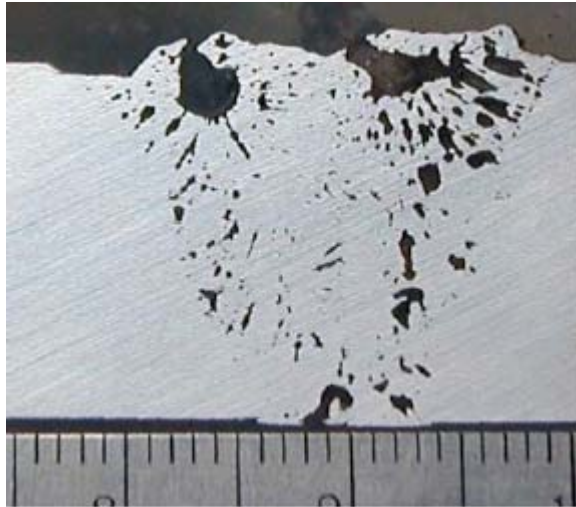


(a) 23.5 % at the beginning side of the weld.

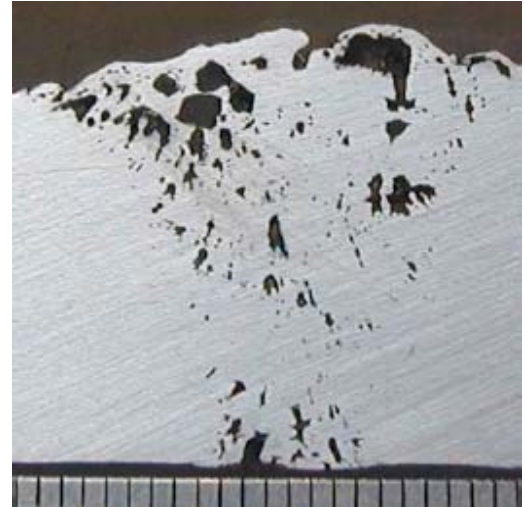


(b) 16.7 % at end side of the weld.

Figure 2.1.9. Cross-section macrographs showing porosity of the V-groove wet welds deposited with E7024 electrode on A36 steel at 150 m (the scale is in millimeters).



(a) 16.6 % at the beginning side of the weld.



(b) 13.6 % at end side of the weld.

Figure 2.1.10. Cross-section macrographs showing porosity of the V-groove wet welds deposited with E6013 electrode on API 5L Gr. B steel at 150 m (the scale is in millimeters).

The large porosity percentages measured in the transverse cross-section macrographs clearly suggest poor mechanical properties of the welds. Tensile specimens were machined from the multipass welds according to Figure 2.1.11 and the tensile test results are presented in Table 2.1.3. As expected, the tensile strengths are approximately 50% the strength of the base metals (60 ksi) and the decrease in strength can be attributed to the presence of porosity.

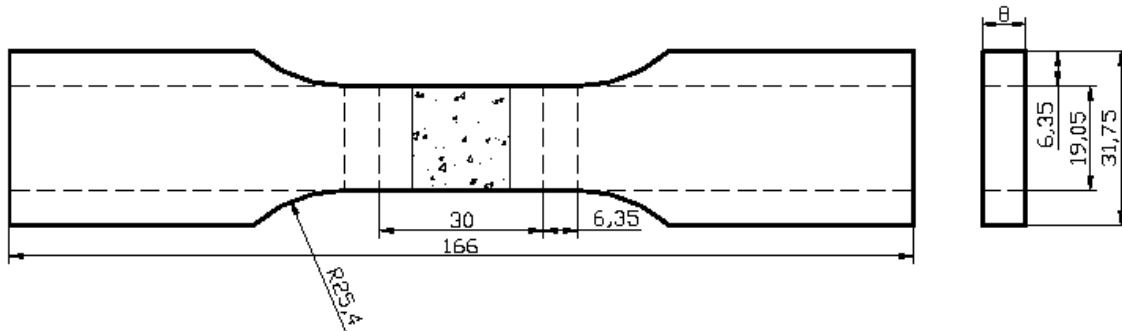
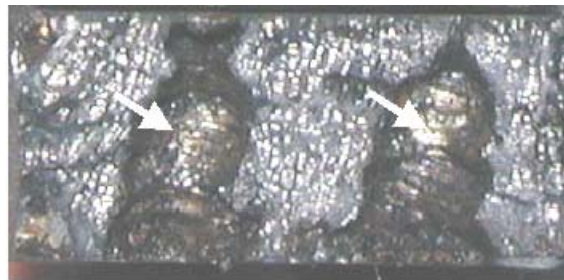


Figure 2.1.11. Shape and dimensions of the tensile specimens extracted from the wet welds deposited at 150 m.

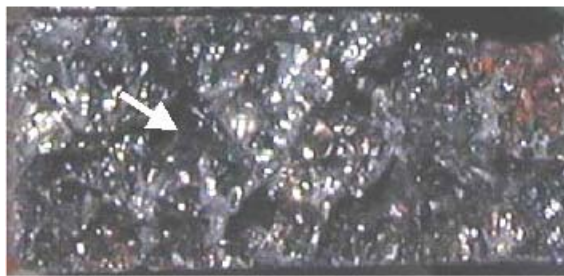
Table 2.1.3. Tensile test results of the wet welds deposited at 150 m.

Electrode	Steel plates	Tensile strength		
		Avg. (ksi)	Min. (ksi)	Max. (ksi)
E6013	A36	32.4	31.0	33.8
	API 5L Gr. B	30.8	24.6	37.1
E7024	A36	25.0	22.9	37.1

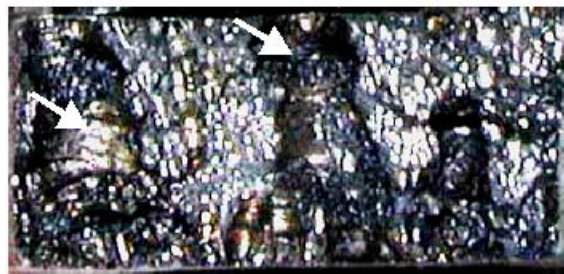
Figure 2.1.12 shows the fracture surfaces of some of the tested specimens where large communicating pores (darker area pointed with arrows) considerably reduce the cross-sectional area of the weld metal. The pores represent approximately 50 % the weld metal cross-sectional area. The ripples found on the surface of the pores show clear evidence of gas pressure and pore growth during solidification.



(a)



(b)



(c)

Figure 2.1.12. Fracture surfaces of wet weld made with (a) E6013 electrodes on A36 steel, (b) E7024 electrodes on A36 steel, and (c) E6013 electrodes on API 5L Gr. B steel. Arrows are pointing to communicating pores (the width is 19 mm and the high is 8 mm).

2.1.4 Conclusions

- Porosity clearly limits wet welding at 150 m water depth to non-critical components and represents the main problem to be overcome in wet welding.
- Porosity in wet welds made at 150 m water depth ranged from 7.3 to 23.5 pct. and reduced considerably the tensile strength of the wet welds.
- Wet welds deposited with E6013 electrodes presented the lowest level of porosity and the highest tensile strength.
- The tensile strength of the weld metal was approximately 50% that of the base metal.
- Better arc stability was observed with the E6013 grade electrodes.
- Large electrode diameter increased the deposition rate producing large weld beads and large pores.

2.2 Performance of cellulosic electrodes

2.2.1 Introduction

Although different electrodes have been tested underwater, not all the results obtained have been completely satisfactory. For example, rutile-grade electrodes exhibit good performance underwater; the arc can be readily started and remains stable. However, the welds deposited with these electrodes do not usually meet stringent strength requirements because of excessive porosity and loss of alloying elements. Based on the performance of commercial electrodes, new electrodes have been developed (Rowe (1999) to reduce some of the problems reported. For example, adding proper amounts of alloying elements to the flux covering has improved the mechanical properties of the wet welds. The porosity problem in some cases has also been reduced considerably.

Results from previous experimental projects also reported that as the water depth increased the contents of alloying elements decreased except carbon, oxygen and porosity, which increased. When the still hot weld metal is exposed to the high cooling rates of the surrounding water environment, hard microstructures resulted that when combined with the defects in the weld metal reduced the ductility of the weld steel.

The main goal of this task was to characterize the performance of E6010 grade electrodes in wet welding conditions to verify if the above-mentioned problems would be mitigated.

To study the performance of E6010 electrodes it was necessary to deposit bead-on-plate (BOP) welds made in wet and dry conditions (for reference) and BOP wet welds at different simulated water depths. Welding parameters recommended by the electrode manufacturer were used. The arc current, and voltage signals were acquired for analysis. V-groove wet welds were produced to extract specimens for mechanical testing at two water depths, 0.3 and 50 m. Charpy impact tests at two temperatures 32 and 77°F were performed on the specimens fabricated from the multipass V-groove welds. Also tensile tests were done on all-weld metal specimens.

In terms of welding behavior, experiments were conducted to examine arc start and arc extinction, spatter, noise, and bead morphology. Cross-sections of the BOP wet welds were prepared for macro- and microscopic analyses. Macrographic analyses served to characterize weld bead morphology and weld defects such as porosity, macro and micro-cracking. Weld defects and microstructures were examined using light microscopy. Chemical analyses on the BOP welds were correlated with the mechanical properties and microstructures observed.

2.2.2 Experimental procedure

Direct current electrode positive (DCEP) was used to deposit BOP and V-groove wet welds on A-36 steel plates. BOP wet welds were made at five water depths, 0.3, 14, 28, 42, and 50 m. V-groove multipass welds were made at two depths, 0.3 and 50m, using a gravity welding system. All welds were made inside a hyperbaric chamber, which is shown in Figure 2.2.1.



Figure 2.2.1. Hyperbaric chamber at the Colorado School of Mines for underwater wet welding where different water depths can be simulated (maximum pressure 300 psig).

The AWS E6010 grade electrodes used in this experimental work were 4.8 mm (3/16") in diameter and 356 mm (14") in length. To avoid water absorption by the flux covering the electrodes were waterproofed with commercial varnish.

For each BOP wet weld, the steel plate and the electrode were placed in the gravity welder inside the chamber. After partially filled with tap water, the chamber would be pressurized with air to simulate the desired water depth. The welding cables were properly connected to the tank before starting the welding machine to initiate the arc. A mildly conductive flux paste placed between the electrode tip and the plate was used to initiate the arc. The angle between the electrode and the plate was kept constant at 51°. This angle and the selected welding parameters determined the welding speed and melting rate of the electrode.

Arc current and voltage signals were collected with a data acquisition system at a rate of 1200 Hz for further analysis.

ASTM A-36 steel plates of dimension 12.7 mm x 127 mm x 250 mm (1/2 x 5 x 10 in) were used to deposit the BOP welds and for the V-groove multipass welds.

2.2.3 Results Performance

The E6010 grade electrodes performed well in wet conditions with a powerful arc that was significantly noisier and produced more spatter than rutile-grade electrodes. The cellulose in the flux covering decomposed in the arc and the hydrogen generated fuels the arc column during welding resulting in a powerful arc that was able to penetrate deep into the base metal. The arc readily started with proper setting of welding current. Otherwise, the electrodes easily short-circuited onto the base plate. Once the arc started, it did not extinguish during welding, except when encountering irregularities on the plate surface or the surface of previous weld passes.

Figure 2.2.2 shows photographs of some of the BOP wet welds deposited with the E6010 grade electrodes. The deep craters in the dry welds and wet welds made at 0.3 m water depth demonstrate the strong arc force produced by these electrodes. Surface roughness observed in the wet welds was probably due to molten droplet explosion and the release of gases from the liquid metal, and the quenching effect of water that froze the weld metal.



a) Made at surface in dry conditions



b) Deposited underwater at 0.3m



c) Made at 50m

Figure 2.2.2. Bead-on-plate wet welds deposited with E6010 electrode type. The welds were sandblast cleaned.

According to the electrode manufacturer, the range of welding current is between 140 to 225A for surface dry welding. However, for the underwater environment, the proper welding parameters also depend on the welding equipment setup. Non-insulated electrical connections in water within the welding tank are prone to current losses. The length-to-diameter ratio of the cables is also important in delivering current with minimum losses. Table 2.2.1 shows the welding parameters selected to make the BOP wet welds with the E6010 grade electrodes

Table 2.2.1. Welding parameters selected to deposit the bead-on-plate welds with E6010 electrodes.

Welding conditions	Current Amperes
Dry at surface	150
Wet at 0.3m	150
Wet at 14 m	168
Wet at 28 m	180
Wet at 42 m	180
Wet at 50 m	180-220

The spatter observed on the weld beads made at 50 m of water depth was substantially larger than that observed in welds deposited at 0.3 m. As mentioned before, spatter probably occurred due to the

explosion of large droplets in flight from the electrode to the weld pool. Figure 2.2.3 shows a picture of the V-groove weld deposited at 50m of water depth with the E6010 grade electrodes. In this figure, one can see the spatter on the plate. Because of the spatter loss, this V-groove weld needed more electrodes to complete the weld than the V-groove wet weld made at 0.30m.



Figure 2.2.3. V-groove multipass wet weld after a weld pass. Note the amount of spatter on the weld and plate.

Figure 2.2.4. Shows the V-groove wet weld being deposited inside the hyperbaric chamber at 50m with the E6010 electrodes.



Figure 2.2.4. V-groove multipass wet weld inside the hyperbaric chamber.

Arc Signals

Welding current and voltage signals acquired during welding at a rate of 1200 Hz were analyzed. Figure 2.2.5(a) shows the voltage signals acquired during wet welding at the depth of 0.3m. Only a few voltage drops were observed. The voltage fluctuations were approximately 10V, with the largest droplets reaching values close to 5 V, which were associated with short-circuiting. On the other hand, Figure 2.2.5 (b) shows the voltage signal acquire during wet welding at 50 m, with variations of approximately 20 V. In this case, a considerably large number of voltage drops reached values close to zero volts. Large voltage variations correspond to large droplet sizes. Metal transfer mode with this

electrode type at 0.3 m water depth is mainly globular, and as the water depth increases short-circuit becomes dominant. At 50 m water depth, the mean short circuit metal transfer frequency was 10 Hz, as shown in Figure 2.2.5(c), which means that large droplets are transferred through the arc at a rate of 10 droplets per second.

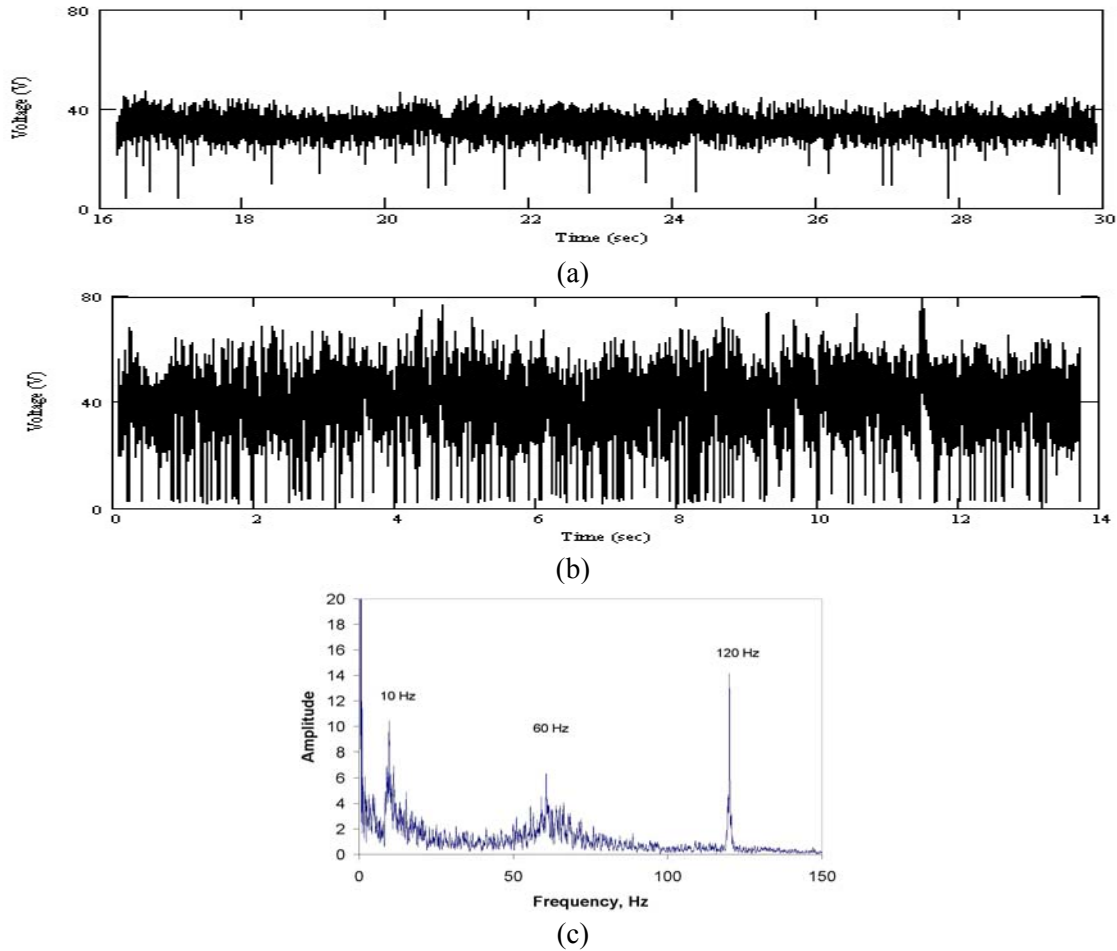


Figure 2.2.5. Voltage signals acquired during welding at depths of (a) 0.3 and (b) 50 m, and (c) power spectrum density of a voltage signal acquired during wet welding at 50m.

The average welding current value used to deposit the welds at 0.3m was 150 A, the arc voltage was 32 volts, and the welding speed 3.3 mm/s (7.7 in/min). For the V-groove weld made at 50 m, the average welding current was 169 A, the averaged voltage was 38.6 V, and the welding speed was 3.8 mm/s (8.9 in/min).

Bead morphologies

The BOP wet welds were cross-sectioned for macrographic analysis. Figure 2.2.6 shows the BOP cross-sections, where one can see the differences in shape with increasing water depth. It was observed that the width and penetration of the weld beads decreased with increasing water depth, as shown in Figure 2.2.7. As water pressure or depth increased, more gases were generated from the decomposition

of water vapor and the electrode flux covering to form large bubbles. When escaping to the surface of the weld pool, the gas bubbles extracted heat from the arc, resulting in shallower welds.

The average width of the 50m BOP wet welds decreased 2 mm with respect to the BOP welds made at 0.3m. The average penetration of the 50 m wet welds decreased by a factor of two with respect to those made at 0.3m.

Using E6010 electrodes, the penetration at 50 m was 2.5 mm, approximately two times deeper than that obtained with rutile-grade electrodes at the same water pressure. In multipass wet welds, the greater penetration achieved by the E6010 grade electrodes represents an advantage over the rutile-grade electrodes because more pores and slag entrapped between passes can be “re-melted” (Bracarense, 2003) and removed by subsequent weld passes.

The penetration of BOP wet welds deposited with E6013 electrode was only 1.3 mm, but the width was 12.2 mm, greater than the width of BOP welds made with E6010 electrodes. These findings clearly demonstrate the relationship between weld characteristics and flux properties.

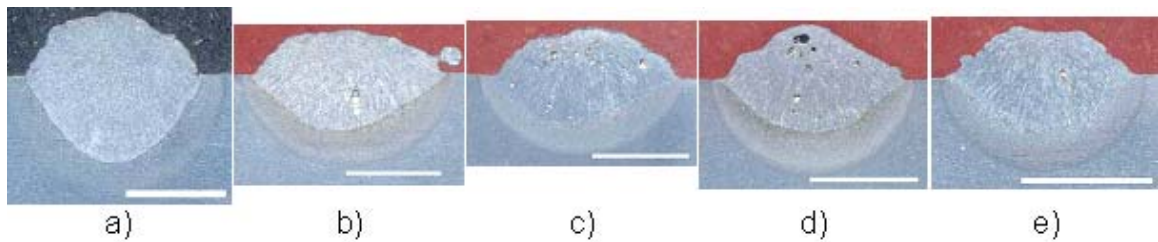


Figure 2.2.6. Cross-section macrographs of the BOP weld deposited with the E6010 electrode at water depths of (a) 0.30m, (b) 14m, (c) 28m, (d) 42m, and (e) 50 m. The dimension of the white scale is 6 mm.

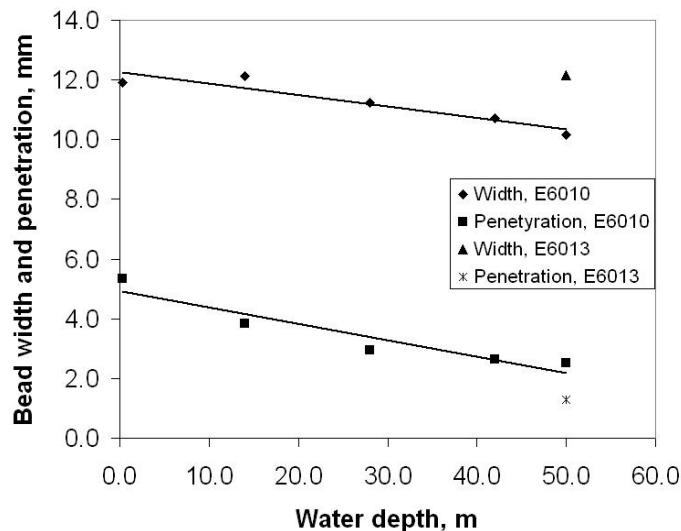


Figure 2.2.7. Variation of width and penetration with water depth of the weld beads deposited with E6010 electrodes. The width and penetration of a wet weld made with E6013 electrode at 50 m are given for comparison.

Fast cooling rate experienced by the heat-affected zone (HAZ) of the welds produced hard microstructures such as martensite, becoming susceptible to hydrogen cracking. This problem was observed in the central region of the BOP wet welds, where the crack in the HAZ followed the fusion line. The length of the cracks shown in Figure 2.2.8(a) and 2.2.8(b) is 8 mm (0.31 in) and 4 mm (0.15 in), respectively. The BOP welds were deposited at 14 and 50m.

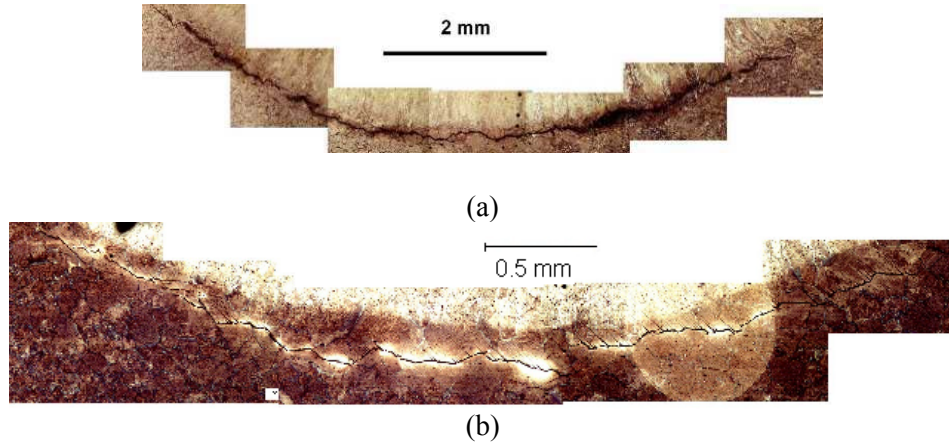


Figure 2.2.8. Cracking at the fusion line of a bead-on-plate wet welds deposited at (a) 14 m and (b) 50 m water depth (Note the differences in scale).

Porosity

It is well known that porosity increases with increasing water depth. Suga and Hasui (1986) reported that porosity increased linearly from 0 to 8% when the water pressure increased from 0 to 6 kg/cm² (85 psi). Due to the increase in pressure, more gas in the arc column is expected to enter the liquid metal. Therefore, hollowed droplets are typically observed. The gas that enters the weld metal droplet does not escape from the liquid metal and are entrapped to form pores in the solidified weld metal. The entrapped gas bubbles can coalesce with other gas bubbles from the following weld passes to form wormhole porosity or large pores.

Three transverse cross-sections were extracted from each BOP weld to measure porosity, one cross-section at the center and two at 25 mm (1 in) away from the beginning and end of the BOP welds. Figure 2.2.9 shows some of the cross-sections from the BOP welds deposited with E6010 grade electrodes where porosity measurements were taken.

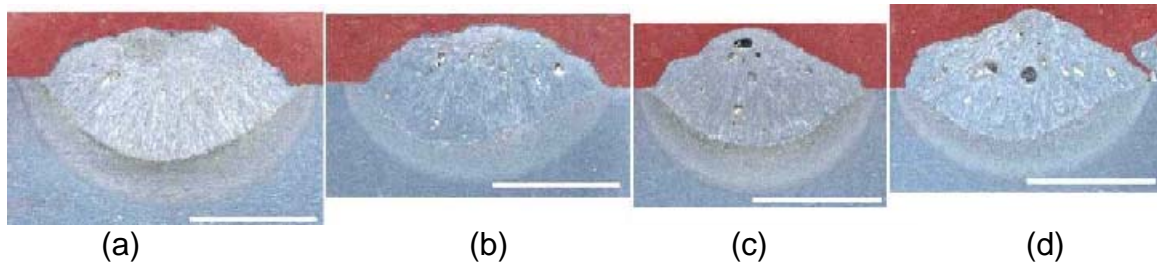


Figure 2.2.9. Cross-section macrographs of the bead-on-plate wet welds deposited at four water depths, (a) 14 m, (b) 28 m, (c) 42 m, and (d) 50m. The dimension of scale is 6 mm.

The averaged percentages of porosity of welds made using E6010 electrodes (as estimated from transverse micrographs) are presented in Figure 2.2.10 as function of water depth. Porosity increased from 0 to 4 pct. when the water depth varied from 0.3 to 50 m.

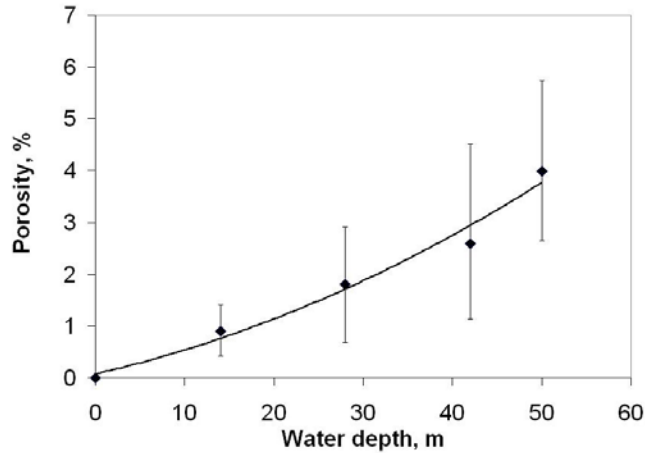


Figure 2.2.10. Porosity percent versus water depth from the cross-section macrographs of the BOP welds.

The weld reinforcement of the BOP welds was machined flush to the base plate as illustrated in Figure 2.2.11(a) also to quantify porosity. Figures 2.2.11(b), (c), (d) and (e) show the areas of the BOP welds made at 14, 28, 42, and 50m, respectively. One can see how porosity increased with increasing water depth. The porosity percentages are shown in Figure 2.2.12. No significant differences exist between the porosity values given in Figures 2.2.10 and Figure 2.2.12.

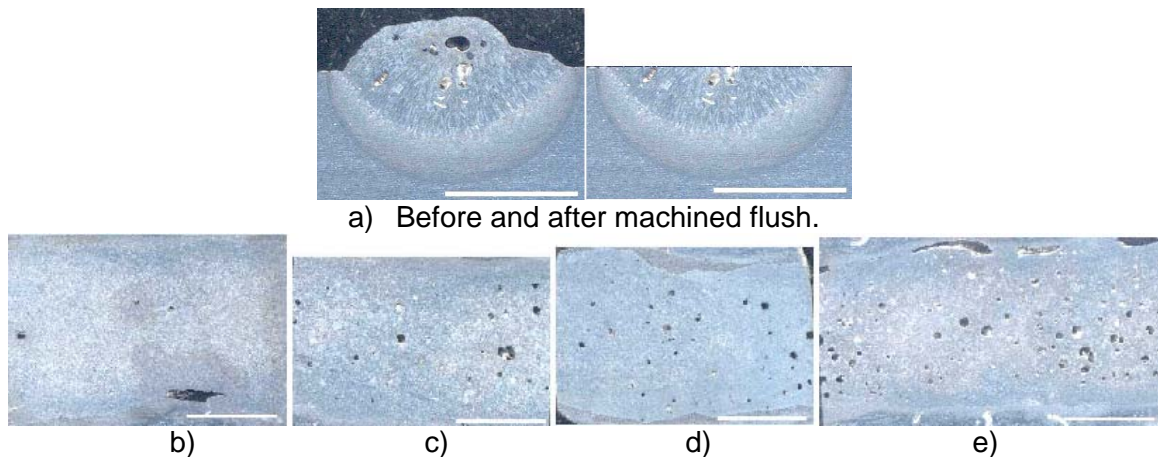


Figure 2.2.11. Cross-section macrographs parallel to the top surface of the plate showing the porosity in the weld metal. The welds were deposited at (b) 14m, (c) 28m, (d) 42 and (e) 50m of water depth. The white scale represents 6 mm.

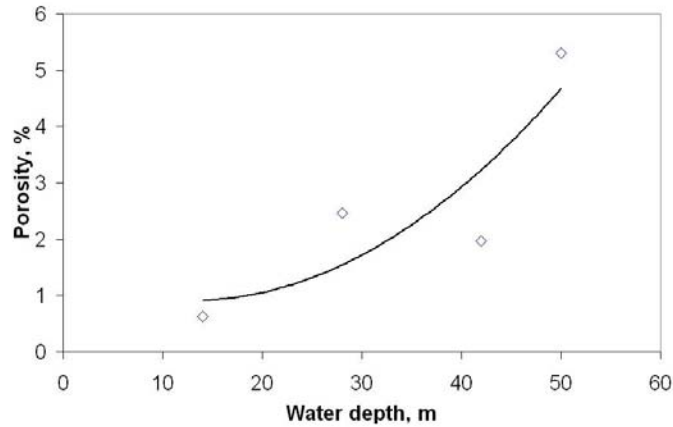


Figure 2.2.12. Porosity variation as a function of water depth. From the cross-section macrographs shown in Figure 2.2.11.

As shown in Figure 2.2.9 there are pores very closed to the top surface of the BOP welds. In a multipass weld the top of a bead and the pores there located can be “re-melted” (Bracarense (2003) by a subsequent bead, thus resulting in a weld with overall lower porosity. Figure 2.2.13 presents a transverse cross-section macrograph of the V-groove multipass weld made with E6010 grade electrodes at 50m water depth. The porosity percent of this weld is 1.79, less than the corresponding value given in Figure 2.2.10 for this water depth. Note the absence of large pores and defects such as slag entrapment in the weld metal. The light slag and the deeper penetration obtained with the E6010 grade electrodes were found to minimize defects in wet welds and reduce porosity.



Figure 2.2.13. Cross-section macrograph of the V-groove wet weld deposited at 50 m of water depth with E6010 electrodes.

Chemical composition

Chemical analyses were carried out on the weld metal of the BOP welds. Four plots show the variations of manganese, silicon, carbon, and oxygen as a function of water depth. Results for welds made with E6010 grade electrodes were never reported in the literature.

As one can see in Figure 2.2.14 the manganese wt. pct. dropped from 0.71 to 0.2 wt, pct. when water depth increased from 0.3 to 28 m, and remained at 0.2 wt. pct. from 28 to 50m. This loss of manganese is similar to those reported in the literature for welds made using rutile-grade electrodes, where manganese decreased quickly from 0.55 wt. pct. (at surface) to 0.25 wt. pct. at 33 m; deeper than 90 m, manganese remained constant at approximately 0.15 wt. pct. (Ibarra (1988) and Liu (1994)). The manganese content in the weld metal depends primarily on the manganese content of the electrode and

base metal. In the presence of oxygen, which increases with water depth, manganese forms manganese oxides that could be transported into the slag or retained in the weld metal as inclusions.

Despite the small number of silicon analysis conducted in this work, the decreasing trend of silicon concentration with increasing water depth substantiated earlier finding of Liu (1994). However, in this earlier work, the silicon content decreased from 0.09 wt. pct. at surface to approximately 0.06 wt. pct. at 33 m, then remained constant with increasing depth, see Figure 2.2.15.

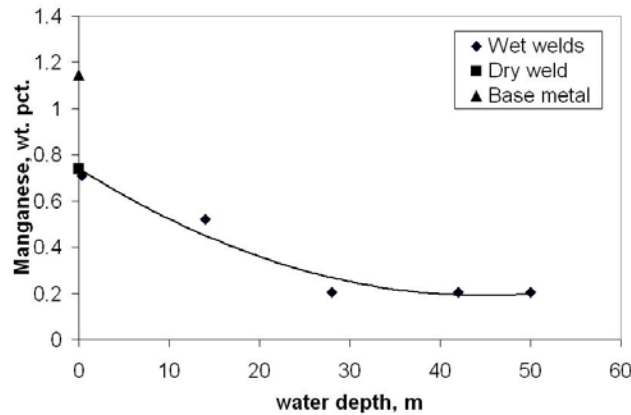


Figure 2.2.14. Manganese content as a function of water depth In the weld metal of the welds deposited with E6010 electrodes.

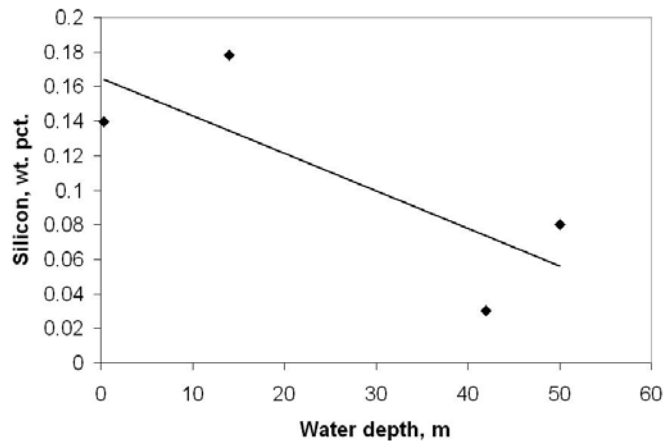


Figure 2.2.15. Silicon content as a function of water depth in the weld metal deposited with E6010 electrodes.

In the case of carbon content, Figure 2.2.16 shows a decrease from 0.18 to 0.10 wt. pct. with increasing water depth from 0.3 to 50m. This behavior is different from that reported in the literature (Ibarra (1988) and Liu (1994)) in which carbon content increased with increasing water depth. The difference in behavior could be attributed to the type of electrodes used in the different research programs rutile-grade versus cellulosic-grade. It is plausible that the carbon in the weld system could react with oxygen to form carbon monoxide or carbon dioxide, which could escape from the weld metal. However, no direct evidence could be found to support the above-mentioned mechanism.

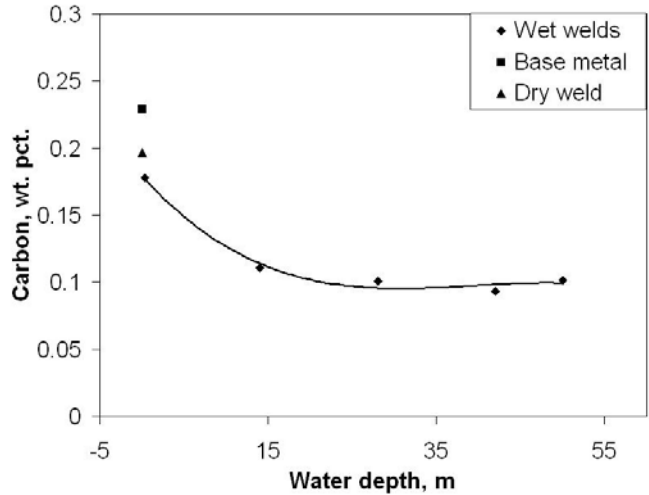


Figure 2.2.16. Carbon content as a function of water depth in the weld metal of the welds deposited with E6010 electrodes.

Figure 2.2.17 presents the oxygen content as a function of water depth. The oxygen content varied linearly from 0.05 to 0.2 wt. pct. in the water depth range from 0 to 30 m. In the literature, Ibarra (1988) and Liu (1994) reported more rapid increases, going from 0.09 to 0.19 wt. pct. for water depths ranging from 0 to 18 m. The oxygen content then decreased slightly to around 0.15 wt. pct. at 75 m where it remained constant for welds made at deeper water depths. Liu and Pope (1994) observed a similar trend using oxidizing electrodes with the maximum oxygen content at deep waters, around 0.23 wt. pct. The maximum oxygen content obtained in this work was 0.25 wt. pct., larger those values reported by Ibarra (1988) and Liu (1994), but comparable to that found by Liu and Pope (1994). As mentioned earlier, the oxygen increase and alloying element loss could be attributed to the large arc voltage fluctuations. Long arc lengths would also increase the volume of the steam bubbles and the likelihood of water vapor decomposing into hydrogen and oxygen.

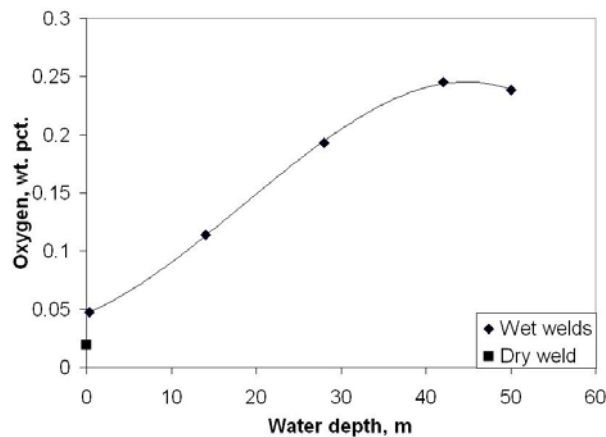


Figure 2.2.17. Oxygen content as a function of water depth in the weld metal of the welds deposited with E6010 electrodes.

The product of oxidation of manganese, silicon and other alloying elements is oxide inclusions. Figure 2.2.18 shows several oxide inclusions observed under a light microscope. The largest inclusion in the transverse cross-section of a BOP wet weld measured 39 μm , however small inclusions were observed all over the weld metal as shown in Figure 2.2.18 b.

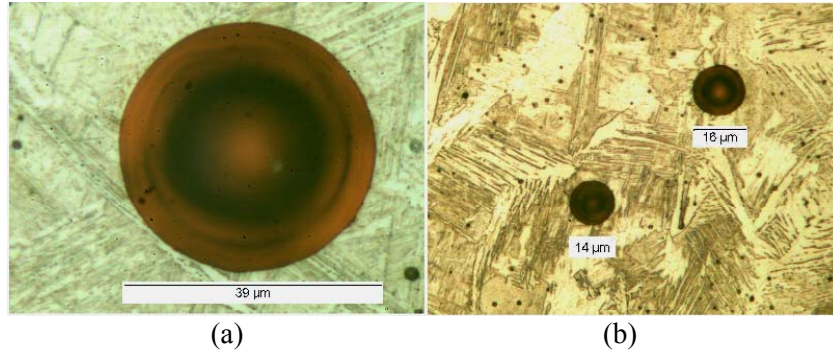
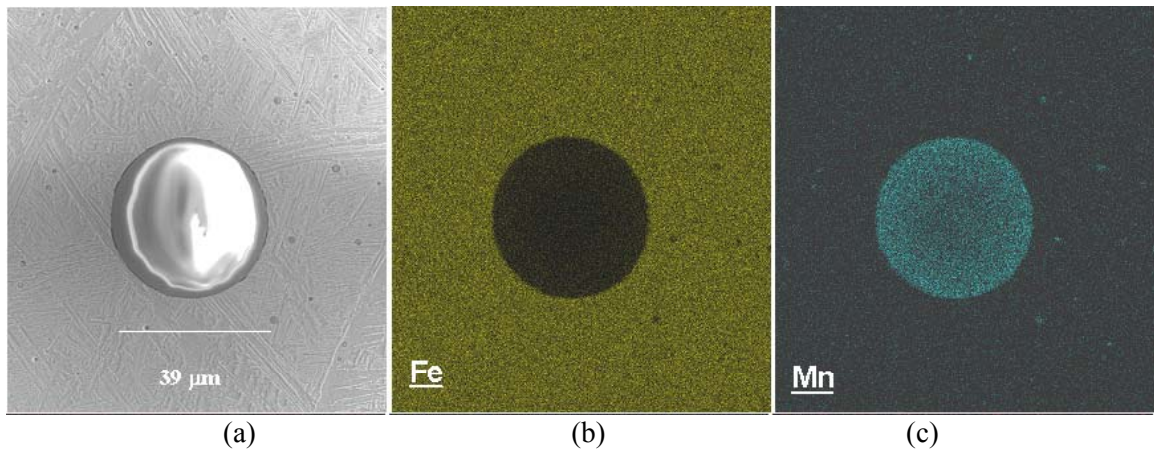


Figure 2.2.18. Micrographs showing oxide inclusions in a wet weld deposited at 50 m water depth with E6010 electrode. (a) Large oxide inclusion with 39 μm in diameter and (b) two smaller oxide inclusions with 14 and 16 μm in diameter. Note also the inclusions with diameters around 1 μm in diameter.

Electron dot mapping shows the distribution of elements such as iron, manganese, oxygen, silicon, and titanium in the weld metal and inclusions deposited at 50 m water depth. Figures 2.2.19 and 2.2.20 show that the inclusion contained high amounts of manganese, silicon and oxygen, clearly indicating that it is a manganese silicate particle. Titanium mainly remained in the weld metal but a small quantity can be found in the inclusion.



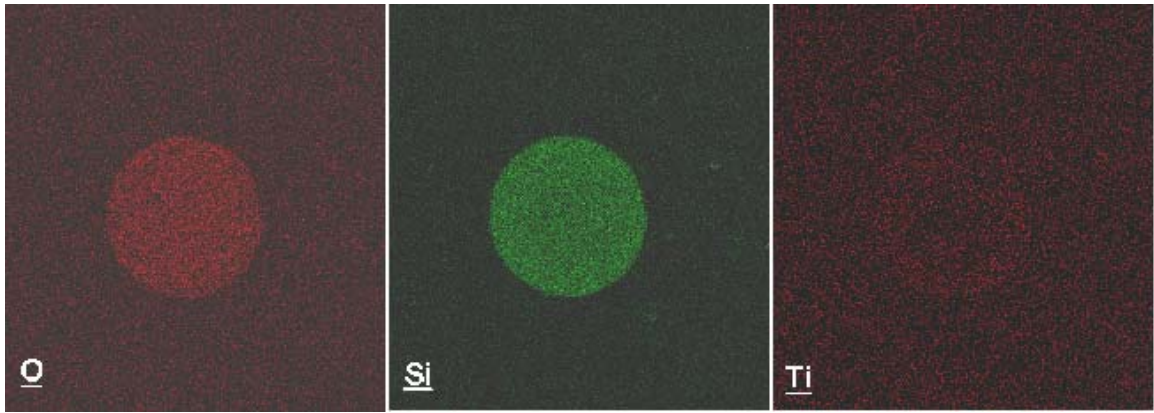


Figure 2.2.19. (a) SEM micrograph and electron dot maps of a large inclusion, (b) iron, (c) manganese, (d) oxygen, (e) silicon, and (f) titanium distribution in the weld metal.

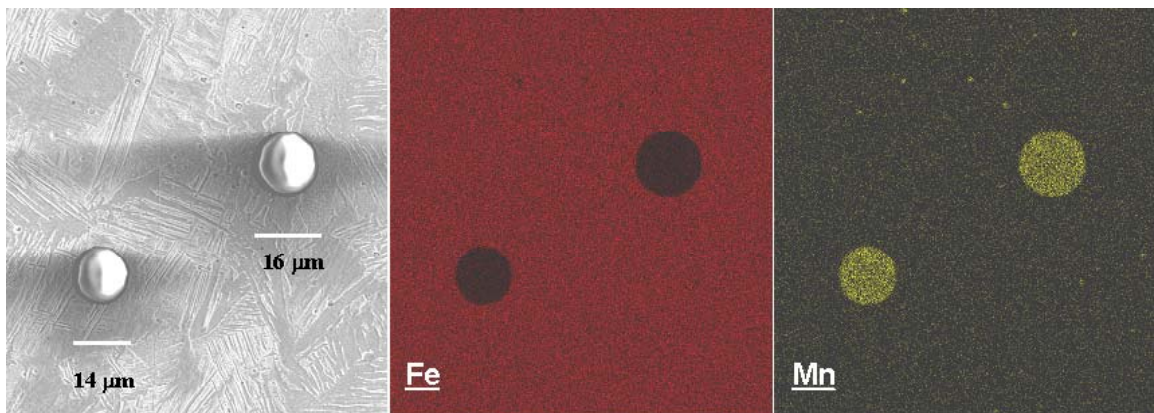


Figure 2.2.20. (a) SEM micrograph of the EDS mapped region showing two inclusions, (b) iron, (c) manganese, (d) oxygen, (e) silicon, and (f) titanium distribution in the weld metal.

Based on the microanalysis results, it can be concluded that much of the alloying elements actually exist in the combined form as oxide inclusions. Since alloying elements are added to the iron matrix to improve the mechanical properties of the steel weld deposits, their presence in the inclusions indicates deterioration of microstructures and properties. Alloying elements need to be replenished by reformulating the flux coatings for specific ranges of water depth.

Microstructures

The transverse cross-sections of the BOP welds were etched with 2 pct. nital solution for microstructural development. In the welds deposited at surface (0m water depth) in dry conditions, acicular ferrite was found to be the dominant microstructure, as shown in Figures 2.2.21(a) and (b). Micrographs from the BOP welds deposited at 0.3 m shown in Figures 2.2.21(c) and (d) show martensite (M) and acicular ferrite (AF) as the major phases. Martensite formed because of the high quench in water. Note also the presence of fine grain boundary ferrite (GBF), which is a softer microstructure. Ferrite and martensite microstructures are responsible for the large variations in hardness (210 to 470 on the Vickers scale, respectively).

The welds made at 50m also showed martensitic microstructure as shown in Figures 2.2.21(e) and (f). Figure 2.2.22 also shows a comparison of microstructures between wet welds made at 0.3 m and 50 m. One can see the presence of martensite, acicular ferrite, fine grain boundary ferrite and ferrite with aligned second phases microstructures in the surface wet weld. On the other hand the wet weld made at 50m shows considerable less martensite, no acicular ferrite, wider grain boundary ferrite and more ferrite with aligned second phases.

Taking into account the chemical composition differences between the welds from the two water depths, the 50m water welds are softer than the welds made at 0.3 m, as shown in Figure 2.2.23.

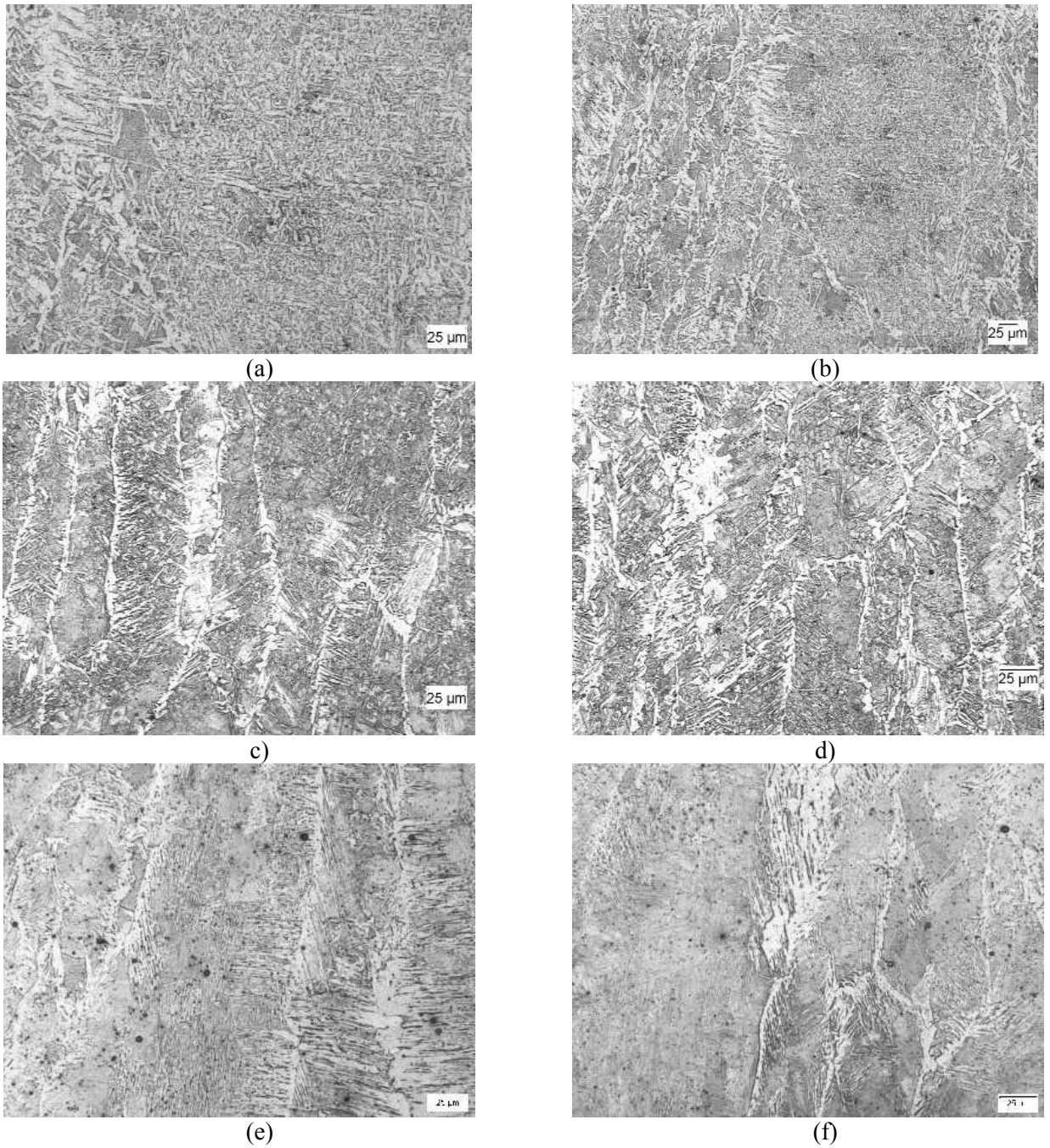


Figure 2.2.21. Micrographs from the bead-on-plated wet weld deposited with E6010 electrodes (a) and (b) at surface in dry conditions, (c) and (d) at 0.3 m, and (e) and (f) at 50m (the scale box represents 25 μm).

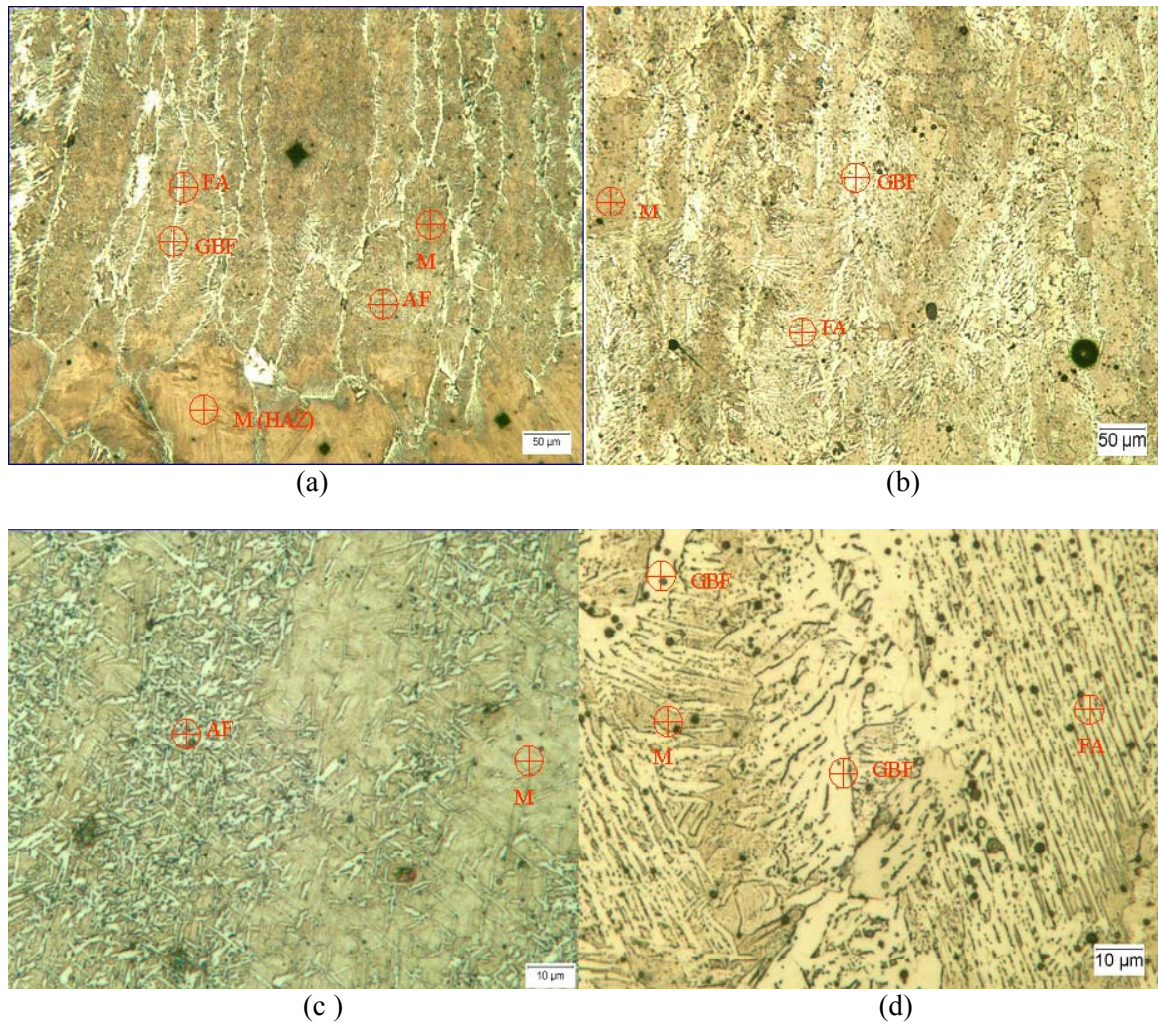


Figure 2.2.22. Additional micrographs from bead-on-plate wet welds deposited at (a) surface and (b) 50 m water depth; (c) and (d) are high magnification views from (a) and (b) respectively.

Hardness

Diamond pyramid hardness (DPH) or Vickers hardness (HV) measurements were taken along the centerline of the BOP cross-sections. As expected, the hardness of the wet welds deposited with the E6010 type electrodes decreased with increasing water depth, from 320 to 210 HV. Figure 2.2.23 shows the variation of DPH as a function of water depth. The loss of alloying elements discussed earlier play an important role in the softening of the microstructure.

In the heat-affected zone of the BOP wet welds the hardness varied from 400 to 500 Vickers with an average value of approximately 450 Vickers. The chemical composition of the base metal and fast cooling rates in the HAZ produced hard martensitic microstructures.

In the multipass V-groove weld made with E6010 grade electrodes at 50 m of water depth, the average hardness was 194 HV as compared to 165 HV for a similar weld made with E6013 type electrodes, as shown in Figure 2.2.24. These differences in hardness could be associated with differences in the chemical composition of the weld metal and differences in the heat input of the welds.

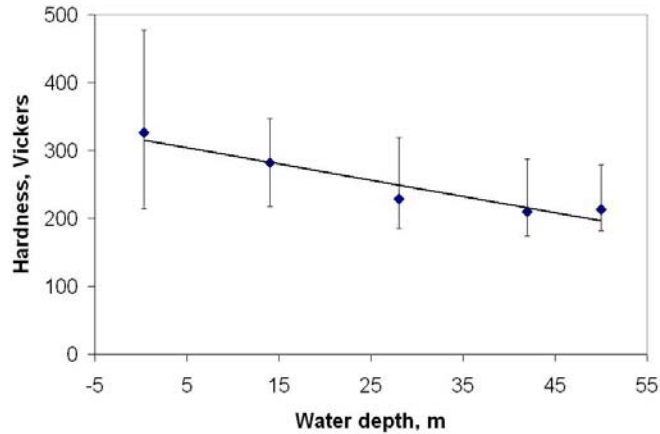


Figure 2.2.23. Diamond pyramid hardness or Vickers Hardness (500 g load) from the bead-on-plate wet welds.

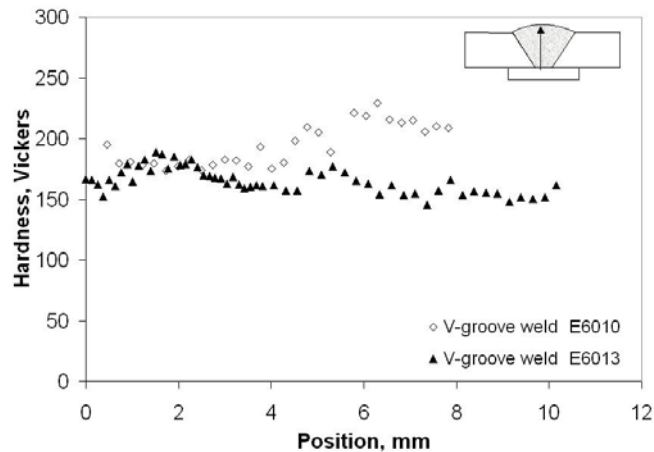


Figure 2.2.24. Diamond pyramid hardness or Vickers hardness (500 g load) from V-groove wet welds made with E6010 and E6013 electrodes at 50 m.

Impact testing

Standard size Charpy V-notch (CVN) specimens were machined from the V-groove wet welds made at two water depths, 0.3 and 50 m. The specimens were tested at two temperatures, 32 and 77 F (0 and 25°C). Figure 2.2.25 presents the average CVN values; also in this figure the average CVN values of similar specimens made from V-groove wet weld deposited with E6013 grade electrodes at 50 and 100 m were included for comparison.

The toughness decreased with increasing water depth, from 38 to 19 ft-lb. (51.5 to 25.8 J) at 77 F and from 32 to 17 ft-lb. (43.6 to 22.6 J) at 32 F for water depths of 0.3m and 50m, respectively. The averaged toughness of the weld deposited with E6013 electrodes at 50m was 27 and 24 ft-lb. (36.6 and 31.9 J) at 77 and 32 F, respectively. Hence the E6013 electrodes produced welds with high toughness values in this research. However, much lower CVN values had been reported for E6013 type welds in the literature. Bracarene (2004) reported 18.2 ft-lb. (24.7 J) for wet welds made at 50m with E6013

electrodes. Defects in the welds deposited with E6013 electrodes as well as chemical composition could be the reason for different values.

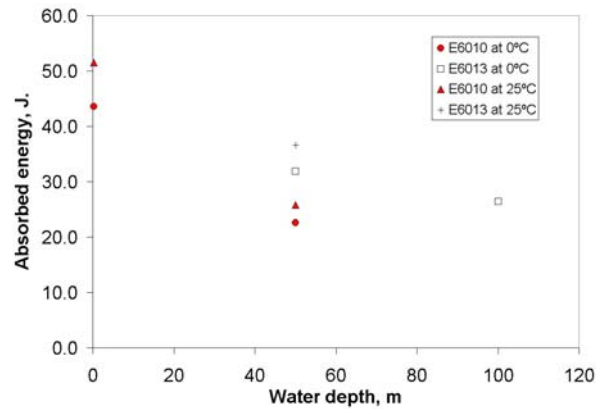


Figure 2.2.25. Toughness of wet welds deposited with E6010 grade and rutile-type electrodes tested at two temperatures.

Tensile testing

All-weld-metal reduced-section tensile specimens were made from the V-groove wet welds deposited with E6010 type electrodes at, 0.3 m and 50 m and with E6013 grade electrodes at 50m. Although the weld made with the rutile electrodes showed more porosity and inclusions, it gave slightly higher strength and ductility values at 50m, which agrees with the DPH and the CVN values previously reported, see results in Table 2.2.2.

Table 2.2.2. Tensile testing results from all weld metal specimens.

Electrode-Depth	Yield Strength (ksi)	Ultimate Tensile Strength (ksi)	Elongation %
E6010-0.3m	56	70	2.9
E6010-50m	52	57	5.1
E6013-50m	55	61	5.4
E6013-50m (Bracarense 2004)		65	

The information presented above shows consistency between the chemical composition of the wet welds, porosity content, microstructure, and mechanical properties with increasing water depth. As water depth increases, alloying content decreases but porosity increases. In general, weld metal microstructures become deteriorated with increasing water depth, leading to poor mechanical properties (hardness, toughness, and tensile strength).

2.2.4 Conclusions

Based on the conditions under which this experimental work was carried out, the conclusions are as follows:

- The AWS E6010 type electrodes performed well underwater. At 50m water depth, a two-fold increase in the weld penetration was obtained when compared with welds deposited with E6013 electrodes.
- The light slag produced was easily removed, without slag entrapment problem.
- Macro-cracks were observed along the fusion line of the BOP weld, however only a few micro-cracks were observed in the multipass welds made at 0.3 m and 50 m.
- In the V-groove welds, the average porosity was only 1.8 pct. due to the re-melting effect, which represents a 50% reduction from the BOP welds deposited at 50m.
- Carbon decreases with increasing water depth.
- Most alloying elements in the wet welds are in the form of oxide inclusions.
- Toughness and tensile strength decrease with increasing water depth.

2.3 Out-of-position welding

2.3.1 Introduction

In actual repairs with wet welding, most of the welds are deposited out-of-position (e.g. vertical down) with only small sections of the whole weld being deposited in flat or overhead positions, see Figure 2.3.1, which is a side view of part of a tubular structure (e.g. an offshore rig). In this illustration, one can see that the wet welds (multipass fillet welds) are deposited in nearly vertical position (b and c) with small sections in flat (a) and overhead (d) positions.

However, because of its simplicity, most of the experimental work in wet welding has been carried out in the flat position. Therefore, there is a need to investigate out-of-position welding so that actual problems or difficulties associated with welding position can be identified and measures to correct the problems determined. This task consists of depositing experimental wet welds using a specially designed gravity feed system to study out-of-position (vertical-down and vertical-up) welding.

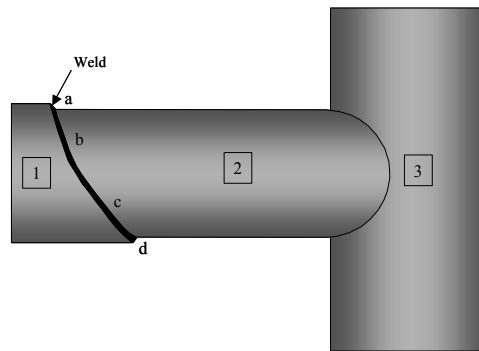


Figure 2.3. 1. Schematic illustration of the replacement of part of a damaged structural member (2), which is welded to a main column (3). A slightly large diameter sleeve (1) is wet welded to the remaining end of the damaged member.

2.3.2 Experimental procedures

Two gravity welding system were designed and built for vertical-up and vertical-down welding, as shown in Figure 2.3.2. For vertical-down, the electrode holder slides down by gravity maintaining the electrode in contact with the base plate. For the vertical-up position, the electrode is pulled upwards by a string-pulley-counterweight system. In both systems, the required length of the weld bead determines the angle between the sliding bar and the base plate. In both welding positions, the base plate is placed in vertical position. Depending on the welding polarity, the positive or negative welding cable is directly connected to the electrode holder.

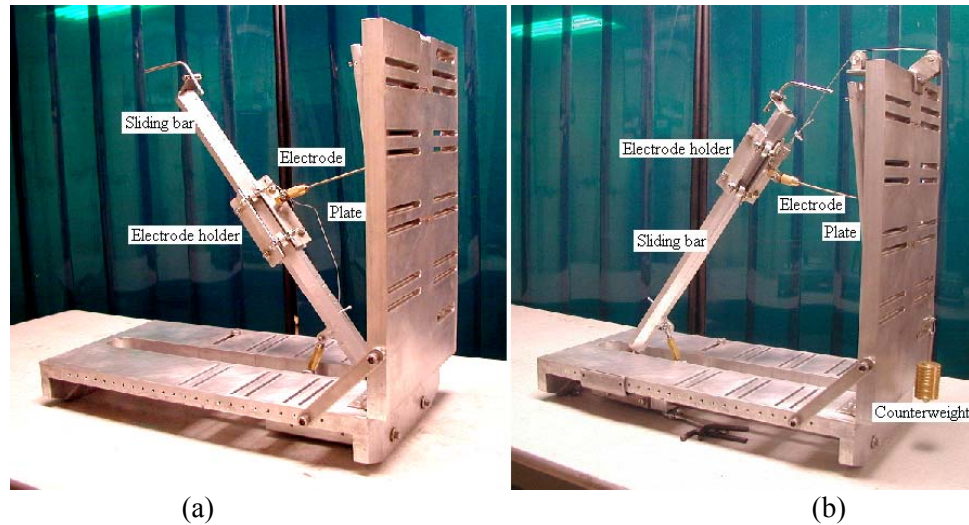


Figure 2.3. 2. Gravity feed system for out-of-position welding (a) vertical-down and (b) vertical-up.

Experimental matrix

The proposed experimental matrix is presented in Table 2.3.1. As can be seen, three electrode grades, three steels and three water depths were originally included. However, based on the results obtained in Phase I and initial results from this task, the experimental matrix has been reduced.

The three water depths initially considered are 50, 100, and 150 m. The out-of-position welding experiments at 150 m were eliminated based on the results reported in Task 2.1. In order to test the welding equipment and procedures an additional water depth was considered, which is the 0.5 m.

Table 2.3.1. Experimental matrix for out-of-position wet welding at three water depths (0.5, 50 and 100 m).

Steels	Electrodes		
	E6013	E7018	E6010
ASTM A36	√	√	√
ASTM A572 Gr. 50	√	√	√
API 5L Gr. B	√	√	√

The gravity welding system was placed inside a small water tank for initial testing as shown in Figure 2.3.3. Bead-on-plate wet welds were deposited at a shallow water depth to determine suitable welding current values for each type of electrode. Adjustments to the counterweight, electrode-plate angle, and travel speed were made to the gravity welder.



Figure 2.3. 3. Vertical-down gravity welding system inside a water tank for initial tests.

As in the other tasks, the water depths are simulated in the hyperbaric chamber shown in Figure 2.1.2.

Figure 2.3.4 shows the dimensions of the plates used for the bead-on-plate, out-of-position wet welds. Figure 2.3.5 shows a photograph of the covered electrodes used in these experiments. The electrodes were waterproofed with varnish to protect the flux coating from water absorption.

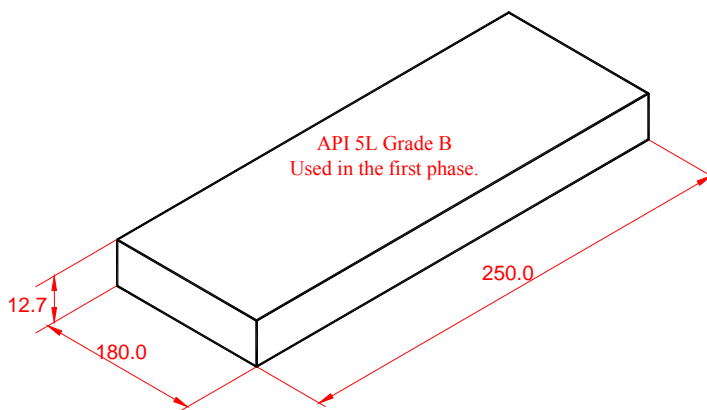


Figure 2.3. 4. Steel plates to deposit bead-on-plate wet weld in vertical position.



Figure 2.3. 5. Flux-covered electrodes E6010, E7018 and E6013 (from top to bottom).

Three cross-section macrographs were extracted from each BOP wet weld, as shown in Figure 2.3.6 for bead morphologies and porosity measurement.

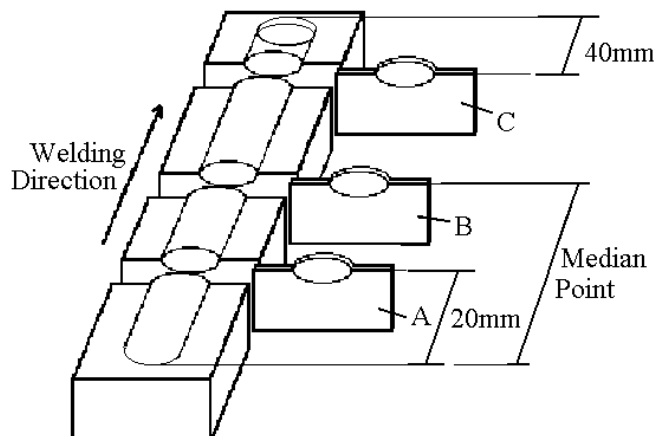


Figure 2.3. 6. Location and identification of cross-sections extracted from the dead on plate-wet-welds.

2.3.3 Results

Initial welds in vertical-down position at 0.5 m

In order to identify proper welding current values for each electrode type and diameter, wet welds were deposited using several welding current values as plotted in Figure 2.3.7. Welding current values that produced the best arc stability and acceptable bead morphologies were selected for further experiments.

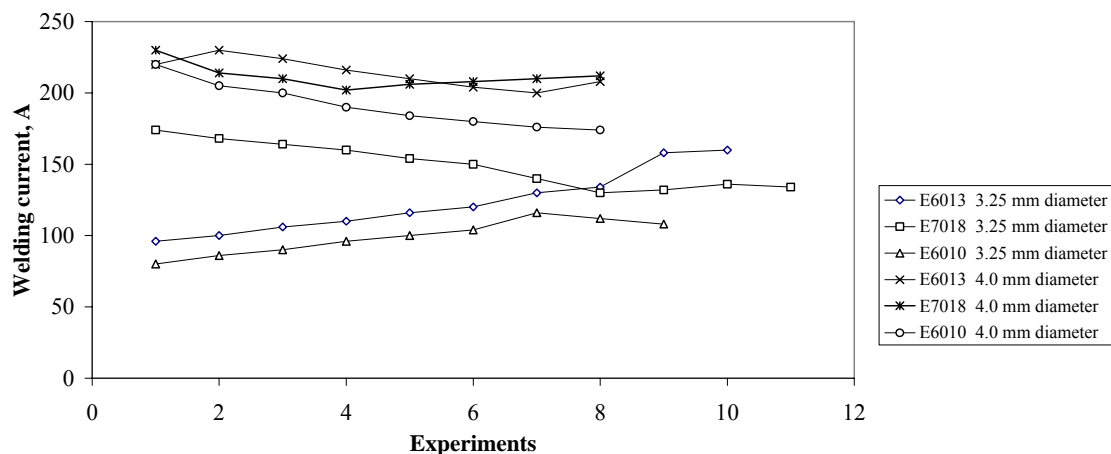


Figure 2.3. 7. Welding current values tested in the vertical-down position with two electrode diameters.

The actual current values used for electrode types and diameters are given in Table 2.3.2. The flux coating thickness is one of the parameters that determine the arc voltage. As such, with similar flux coating thickness in the different electrodes, the measured voltage values are very similar.

Although for each water depth, an adjustment in the welding current values is required for optimum results. The values presented in Table 2.3.2 can be considered the starting point for adjustments.

Table 2.3.2. Welding parameters for the 3.2 mm electrode diameter.

Electrode Grade (diameter, mm)	Selected current (amperes)	Voltage measured (Volts)	Weld bead length (L _i)	Complete bead
E6013 (3.25)	160	32	145	Yes
	160	32	145	No ⁽¹⁾
	160	32	145	Yes
E7018 (3.25)	134	31	145	Yes
	134	30	146	Yes
E6010 (3.25)	108	31	150	Yes
	108	31	150	Yes
E6013 (4.0)	208	31	150	Yes
	208	31	150	Yes
E7018 (4.0)	212	32	146	Yes
	212	32	146	Yes
E6010 (4.0)	174	32	150	Yes
	174	32	150	Yes

Note: 1. The arc extinguished before melting the whole electrode.

Using the selected welding current values, BOP wet welds were deposited with the out-of-position welding systems at surface conditions. Figure 2.3.8 presents photographs of the wet welds deposited with three electrodes grades and two electrode diameters.



(a) Electrode diameter 3.3 mm



(b) Electrode diameter 4.0 mm

Figure 2.3. 8. Bead-on-plate wet welds deposited in vertical-down position with E6010, E7018, and E6013 electrode on API 5L Gr. B steel plates.

During wet welding in the vertical-down position, the pressure of the arc supported the liquid weld metal as illustrated in Figure 2.3.9 and produced acceptable wet welds.

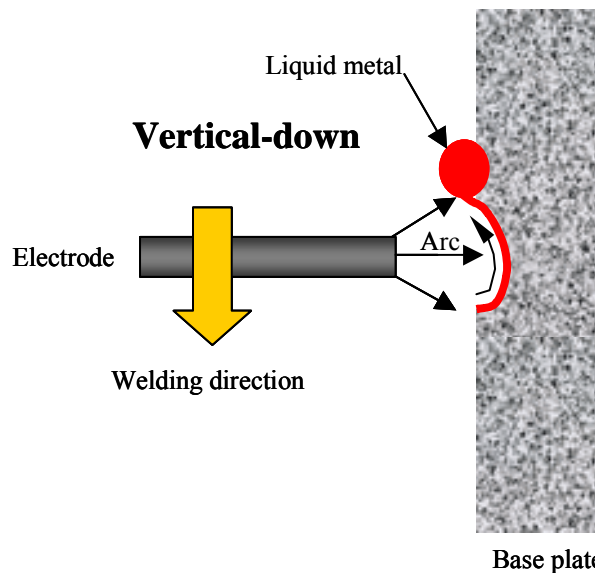


Figure 2.3. 9. Weld liquid metal with vertical support.

Cross-sections from the BOP wet welds were extracted for weld bead measurements, which are shown in Figures 2.3.10 and 2.3.11. Undercutting is observed in Figure 2.3.10a and c, and 2.3.11c,

which indicate that further adjustments of welding current and/or travel speed may be required to correct this problem.

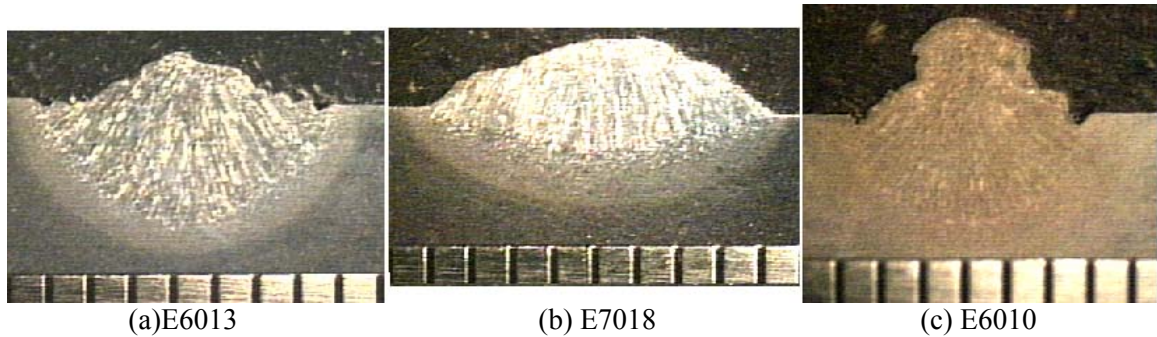


Figure 2.3. 10. Cross-section macrographs of the bead-on-plate wet weld deposited using electrodes with 3.3 mm in diameter.

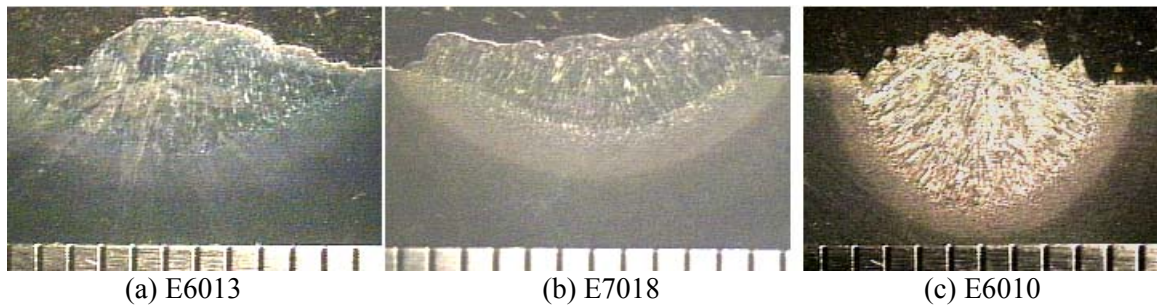


Figure 2.3. 11. Cross-section macrographs of the bead-on-plate wet weld deposited using electrodes with 4 mm in diameter.

Table 2.3.3 reports the width, penetration and reinforcement values measured from the cross-section macrographs. As expected narrower weld beads were produced with smaller electrode diameters.

Table 2.3.3. Weld bead morphologies.

Electrode Type (diameter)	Width (mm)	Penetration (mm)	Reinforcement (mm)
E6013 (3.25 mm)	7.1	3	1.2
E7018 (3.25 mm)	8.3	1	2.7
E6010 (3.25 mm)	5.6	2.5	2.3
E6013 (4.0 mm)	10.9	2.6	1.7
E7018 (4.0 mm)	9.7	1.9	1.1
E6010 (4.0 mm)	7.5	3.8	1.6

Arc voltage and current signals recorded during welding are shown in Figures 2.3.12 and 2.3.13. Globular with a few short-circuiting, Short-circuiting, and Globular are the predominant metal transfer modes observed for the E6013, E7018 and E6010 grade electrodes, respectively. Since voltage

variations are associated with droplet size, the smallest droplet sizes obtained with E6013 grade electrodes could be related to the more uniform voltage signals. Larger droplet sizes were produced with E6010 type electrodes and E7018 electrodes produced the largest droplets during transfer.

Arc stability can be calculated as the ratio of maximum current value over minimum current value, $Arc\ Stability\ Index = \frac{I_{max}}{I_{min}}$, more stable arcs are those with arc stability index values close to 1.0.

For the conditions tested, the three electrodes exhibited similar arc stability index values.

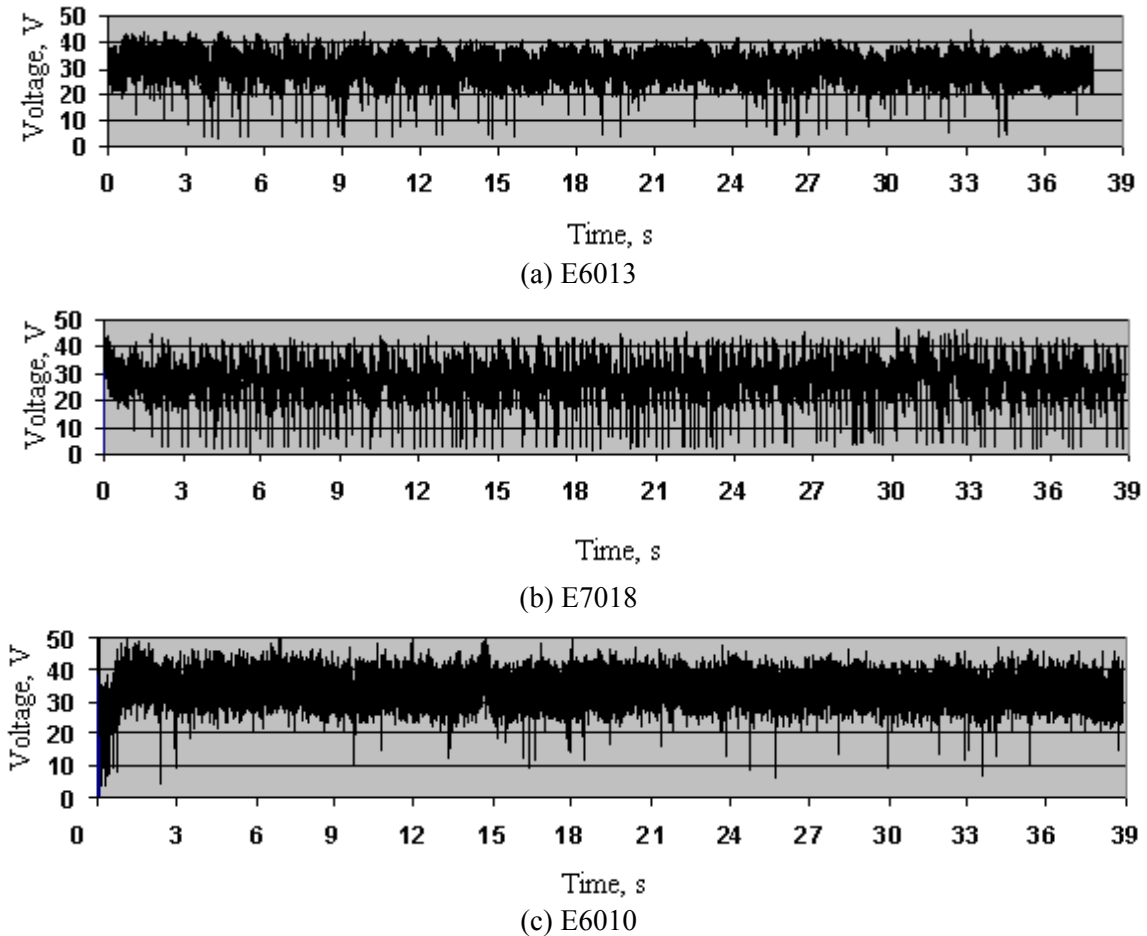
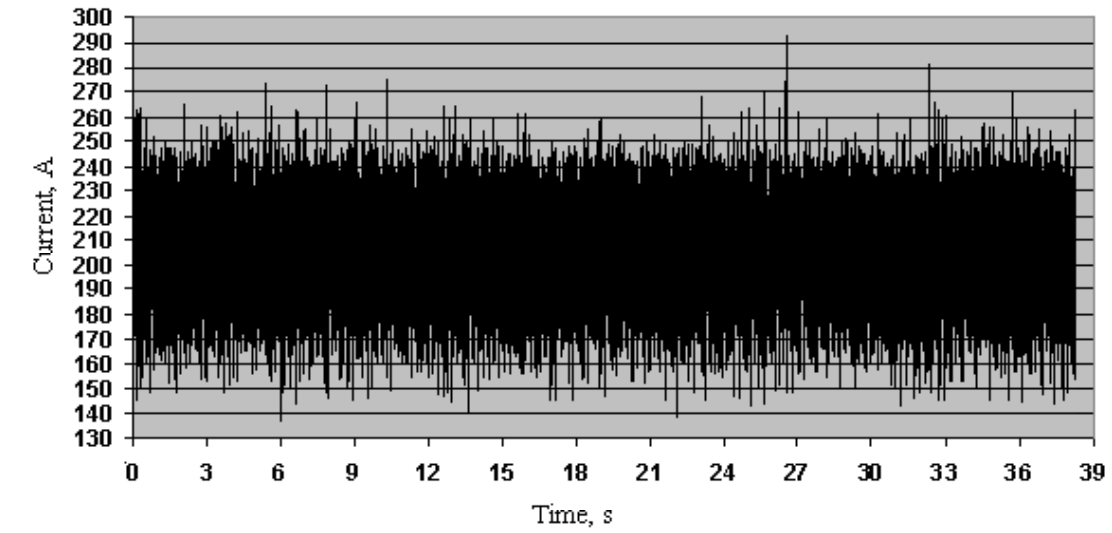
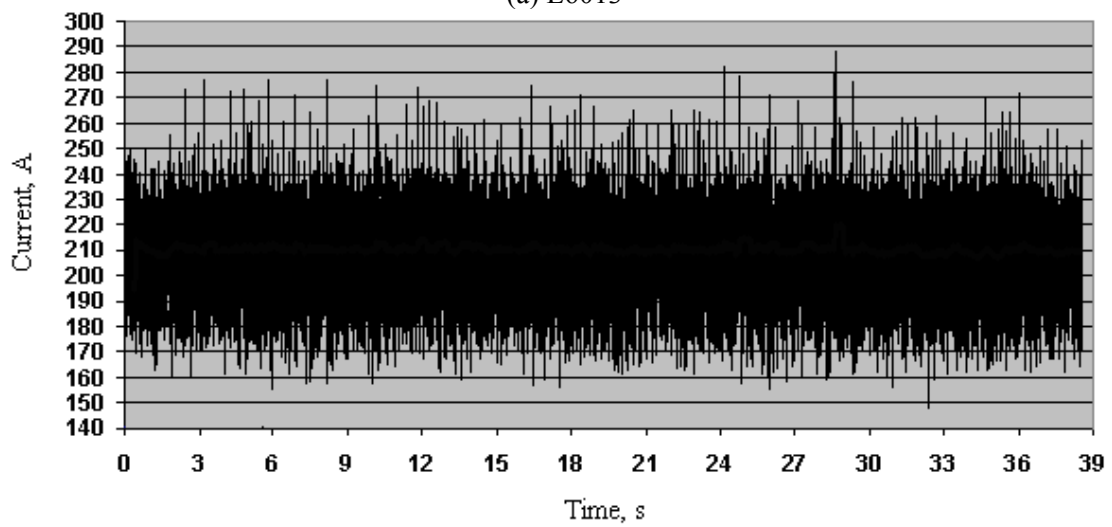


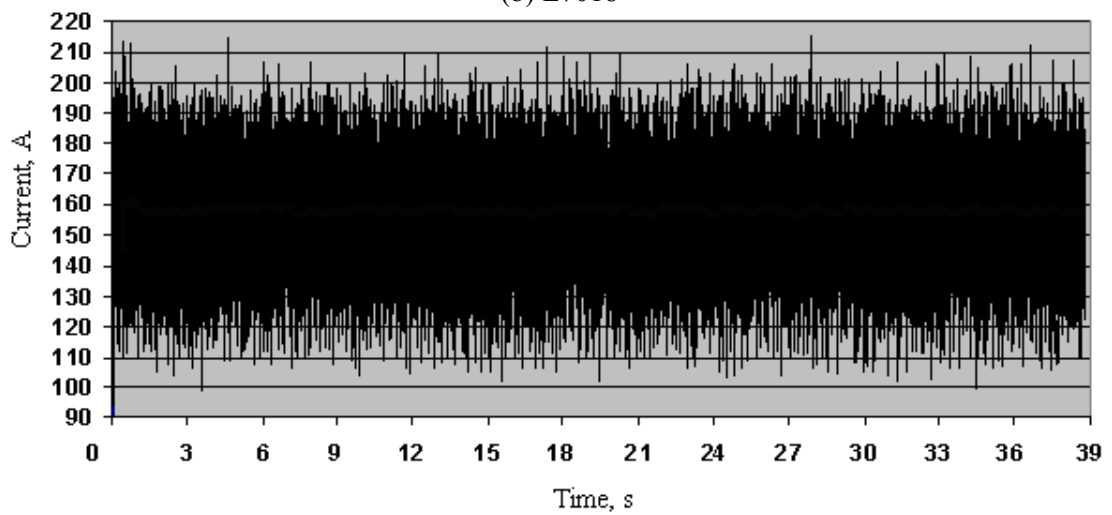
Figure 2.3. 12. Arc voltage signals recorded for the three electrode types.



(a) E6013



(b) E7018



(c) E6010

Figure 2.3. 13. Arc current signals recorded for the three electrode types.

Vertical-down at 0.5 m with E7024 electrodes

Initially the E7024 electrode grade was selected for out-of-position welding based on the good performance observed in the flat position. However, in the vertical-down position its performance was not accepted. This electrode grade has thick flux coating that contains iron powder to increase the deposition rate. In order to completely melt the electrode high welding current values are required resulting large weld beads. During wet welding the weight of the large volume of liquid metal usually pushed to the backside of the weld pool could exceed the supporting force of the arc flooding the weld pool and extinguishing the arc. Excellent arc initiation and arc stability were the main characteristics of this electrode type in the flat position, but the arc was difficult to initiate and maintain in out-of-position wet welding. For this reason the E7018 electrode grade previously tested in the flat position was tested in out-of-position wet welding.

Vertical-down at 0.5 m with E6013 electrodes

Three BOP wet welds were made with E6013 electrodes at this water depth on A-36 steel plates. The selected welding current for this depth was 130A and the welding speed of 3.5 mm/s. The diameter of the steel rod of the electrode was 3.25 mm. The BOP welds are shown in Figure 2.3.14. Irregular beads were obtained with some defects such as high reinforcement, undercuts, and insufficient weld metal filling of the weld cavity at the beginning side of the welds.

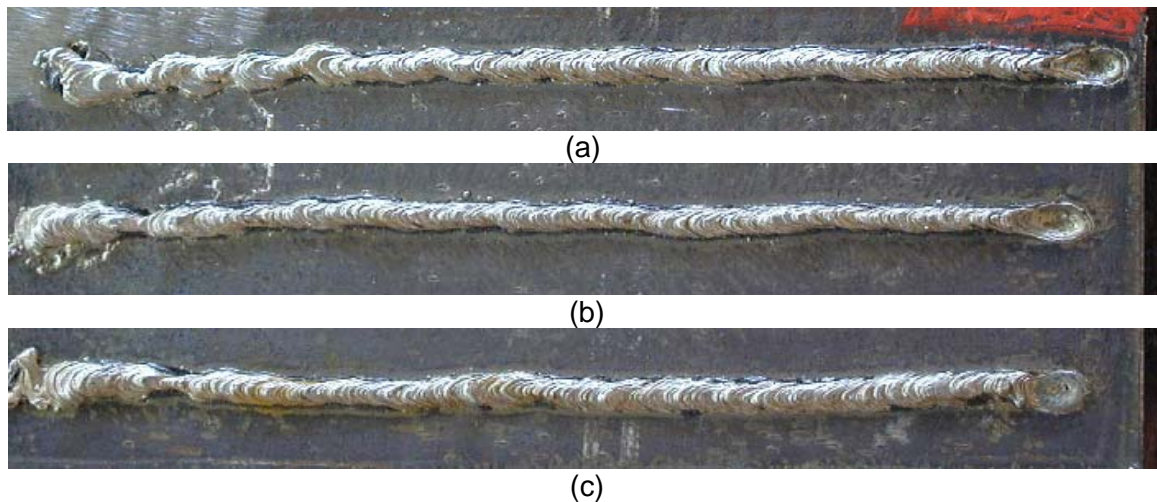


Figure 2.3. 14. Three BOP wet welds deposited in the vertical-down position with E6013 electrodes at 0.5 m water depth.

Cross-sections of the BOP welds were extracted for bead morphology measurements, which are presented in Figure 2.3.15. One can see good weld penetration, high reinforcement on some cross-sections, and undercuts.

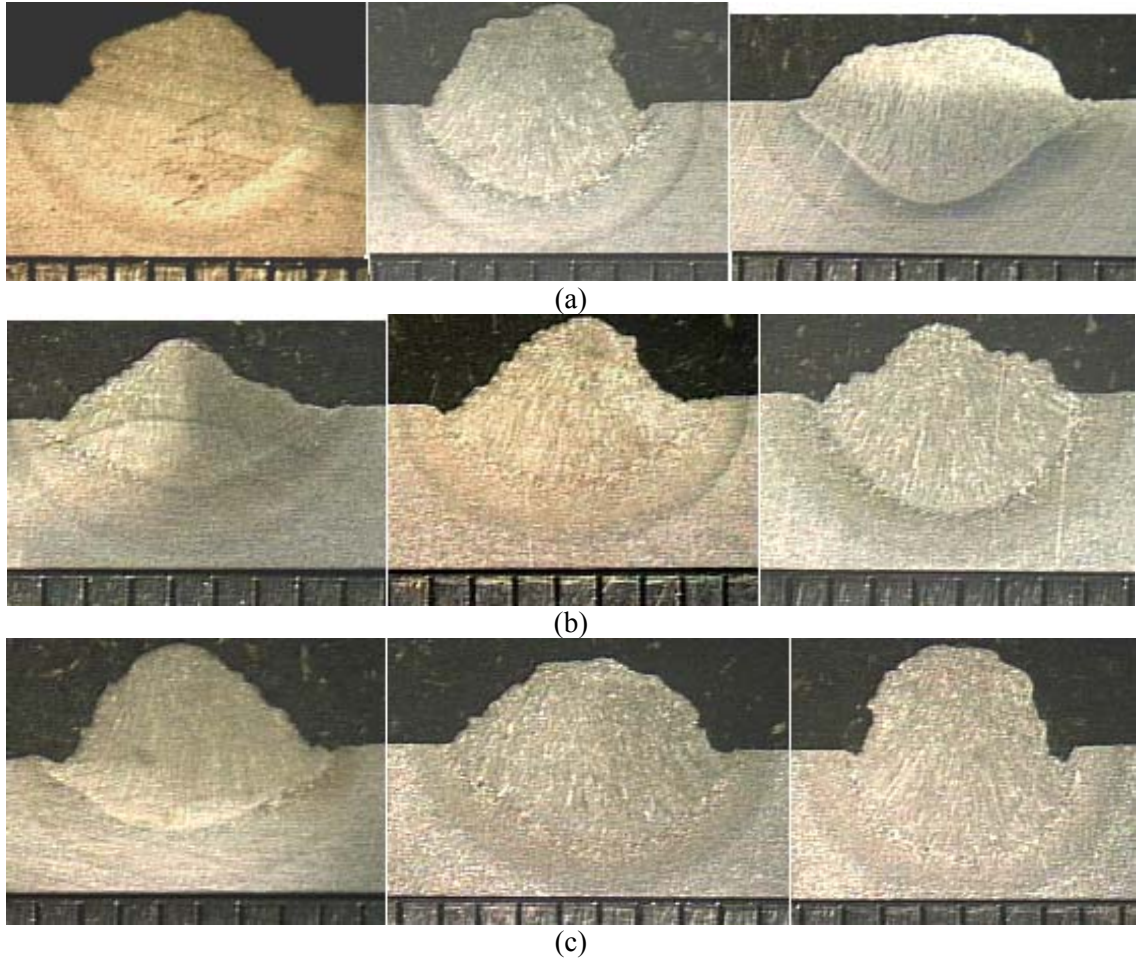


Figure 2.3. 15. Cross-sections from the bead-on-plate wet welds deposited with E6013 electrodes at 0.5 in the vertical-down position. The scales are in millimeters.

Table 2.3.4 presents the width, penetration and reinforcement of these BOP, which averaged values are 6.8, 2.3 and 2.2 mm, respectively.

Table 2.3. 4. Bead morphologies of the bead-on-plate wet welds.

Cross-section	Width (mm)	Penetration (mm)	Reinforcement (mm)
BOP 1 – a	6.8	2.4	2.4
BOP 1 – b	5.9	2.3	2.5
BOP 1 – c	7.8	2.5	1.7
BOP 2 – a	6.9	1.6	1.8
BOP 2 – b	6.7	1.7	2.0
BOP 2 – c	6.5	2.8	1.7
BOP 3 – a	7.2	1.9	2.8
BOP 3 – b	7.4	2.4	2.2
BOP 3 – c	5.7	2.7	2.6
Avg.	6.8	2.3	2.2

Vertical-down at 0.5 m with E6010 electrodes

Three BOP wet welds were made with E6010 electrodes at this water depth on A-36 steel plates. The selected welding current for this depth was 122A and 3.5 mm/s as the welding speed. The diameter of the steel rod of the electrode was 3.25 mm. The BOP welds are shown in Figure 2.3.16. Weld discontinuities, high weld reinforcements, and deep undercuts are observed in the weld beads deposited with this electrode type.

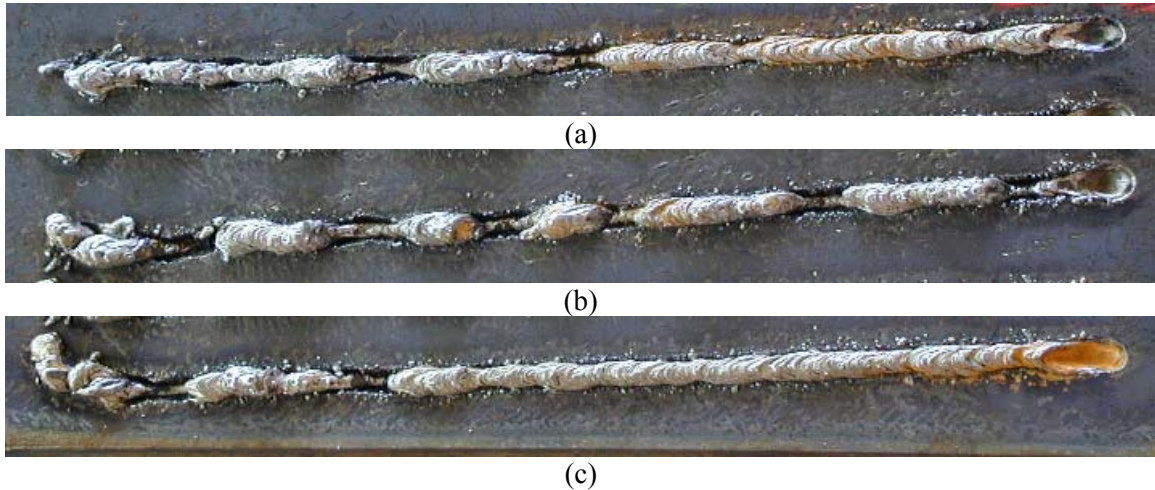
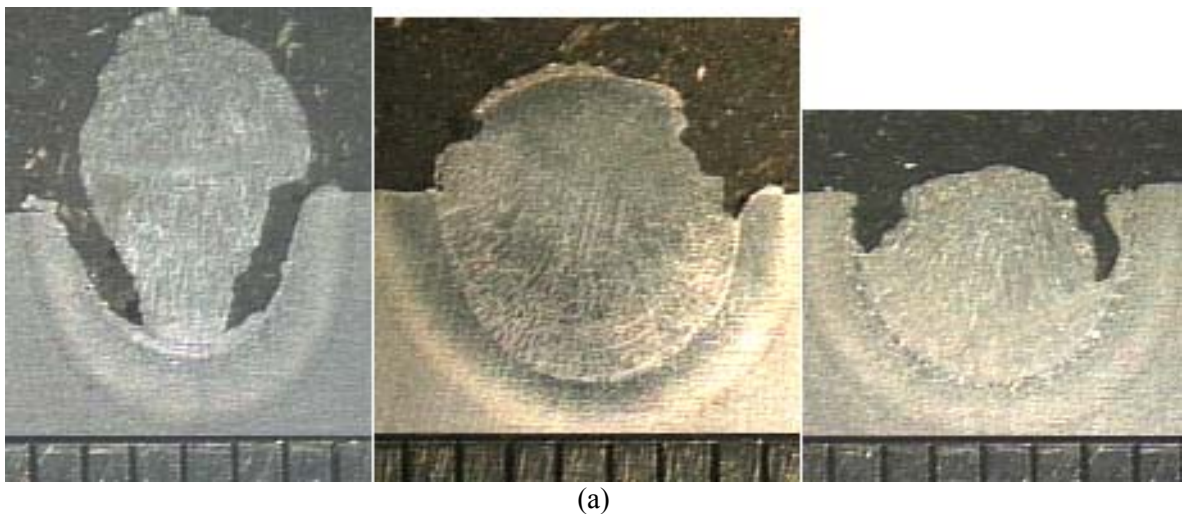
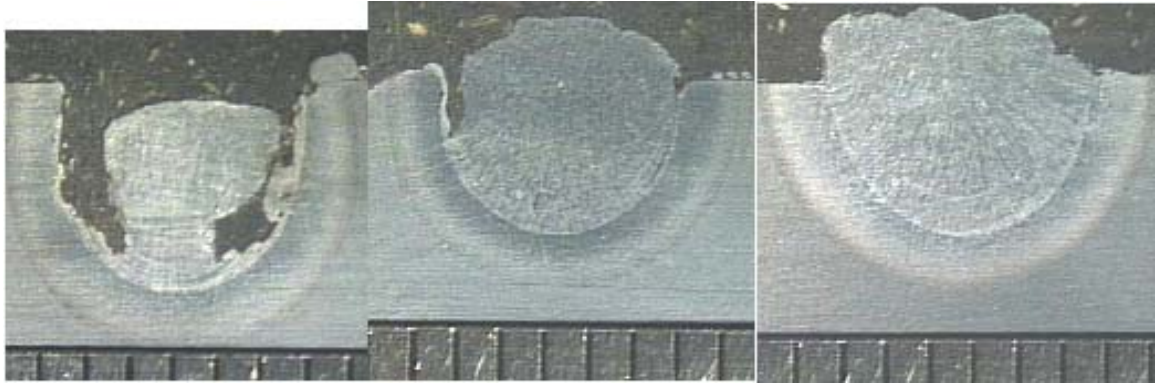


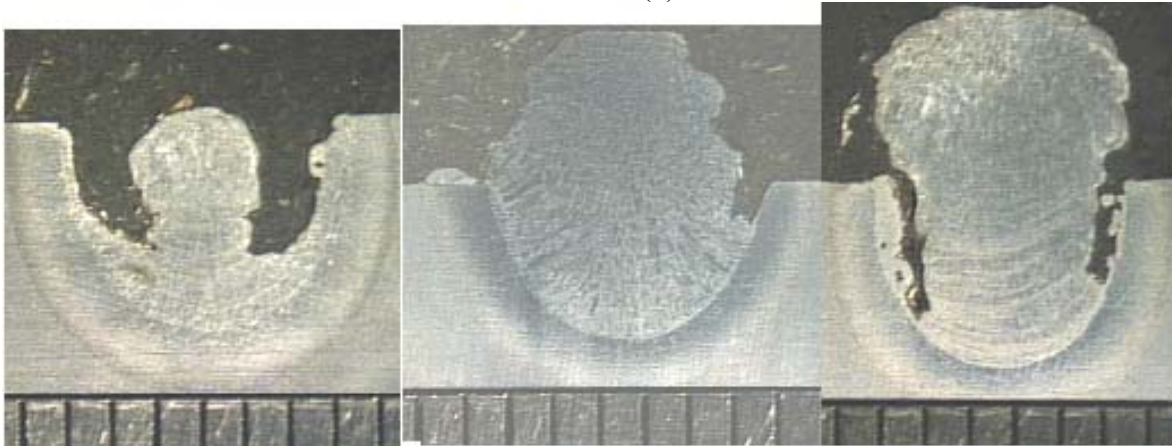
Figure 2.3. 16. Three BOP wet welds deposited in the vertical-down position with E6010 electrodes at 0.5 m water depth.

Cross-sections of the BOP welds were extracted for bead morphology measurements, which are presented in Figure 2.3.17. One can see the deep weld penetration, which is one of the main characteristics of the cellulosic electrodes. The main problems observed in the cross-section macrographs are deep undercutting, insufficient filling of the weld crater, and high reinforcement.





(b)



(c)

Figure 2.3. 17. Cross-sections from the bead-on-plate wet welds deposited with E6010 electrodes at 0.5 in the vertical-down position.

Table 2.3.5 presents the width, penetration and reinforcement of these BOP, which averaged values are 5.6, 3.8 and 1.8 mm, respectively. Narrower weld beads with deeper penetration were obtained with the E6010 electrode grade.

Table 2.3. 5. Bead morphologies of the bead-on-plate wet welds.

Cross-section	Width (mm)	Penetration (mm)	Reinforcement (mm)
BOP 1 – a	5.1	3.0	3.5
BOP 1 – b	6.1	3.9	2.2
BOP 1 – c	5.1	3.8	0.5
BOP 2 – a	5.1	4.5	0.0
BOP 2 – b	5.5	3.5	1.2
BOP 2 – c	6.1	3.5	1.8
BOP 3 – a	6.0	4.5	0.0
BOP 3 – b	6.1	3.5	3.3
BOP 3 – c	5.5	4.2	3.9
Avg.	5.6	3.8	1.8

Vertical-down at 0.5 m with E7018 electrodes

Three BOP wet welds were made with E7018 electrodes at 0.5 m water depth on A-36 steel plates. The selected welding current for this depth was 140A and 3.6 mm/s as the welding speed. The diameter of the steel rod of the electrode was 3.25 mm. The BOP welds are shown in Figure 2.3.18. Good bead morphologies were produced with this electrode type.

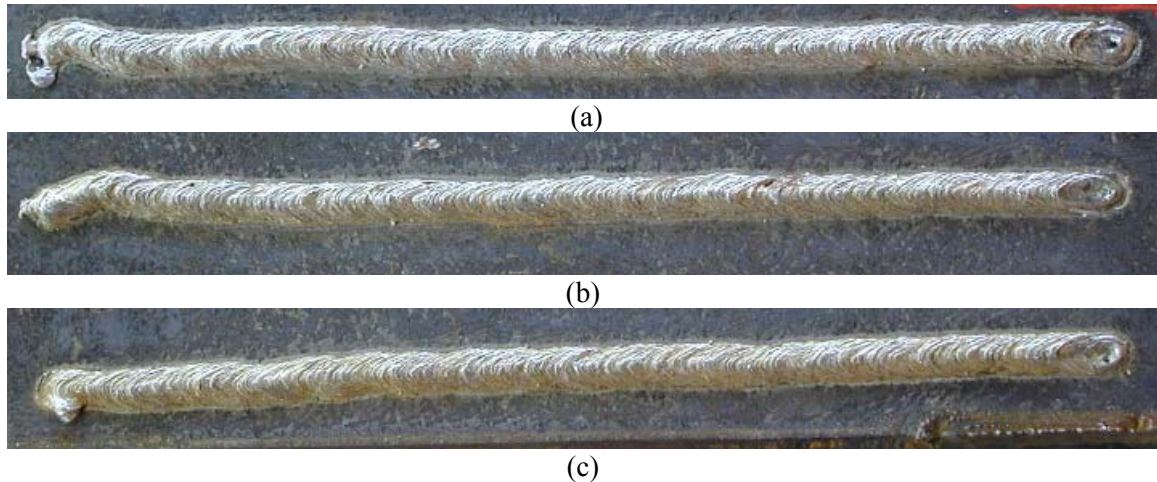
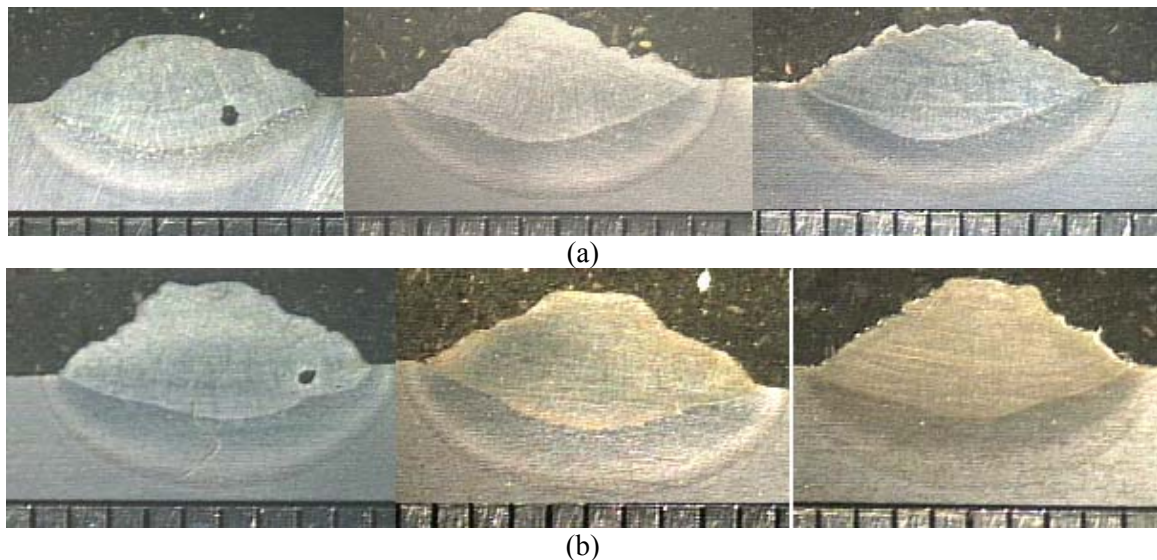


Figure 2.3. 18. Three BOP wet welds deposited in the vertical-down position with E7018 electrodes at 0.5 m water depth.

Cross-sections of the BOP welds were extracted for bead morphology measurements, which are presented in Figure 2.3.19. Although good cross-sections macrographs are observed note the presence of porosity at this water depth.





(c)

Figure 2.3. 19. Cross-sections from the bead-on-plate wet welds deposited with E7018 electrodes at 0.5 in the vertical-down position.

Table 2.3.6 presents the width, penetration and reinforcement of these BOP, which averaged values are 8.9, 1.5 and 2.2 mm, respectively. Wider and shallower weld bead were produced with this electrodes grade.

Table 2.3. 6. Bead morphologies of the bead-on-plate wet welds.

Cross-section	Width (mm)	Penetration (mm)	Reinforcement (mm)
BOP 1 – a	8.3	1.5	1.9
BOP 1 – b	9.2	1.6	2.3
BOP 1 – c	8.9	1.6	1.9
BOP 2 – a	8.4	1.3	2.3
BOP 2 – b	8.9	1.5	2.1
BOP 2 – c	8.7	1.3	2.4
BOP 3 – a	9.2	1.6	2.4
BOP 3 – b	9.2	1.6	2.2
BOP 3 – c	8.9	1.3	2.1
Avg.	8.9	1.5	2.2

Vertical-down at 50 m with E6013 electrodes

Three BOP wet welds were made with E6013 electrodes on A-36 steel plates at 50 m. The steel rod diameter of the flux-covered electrodes was 3.25 mm. The selected welding current was 180 A and welding speed of 4 mm/s. Figure 2.3.20 shows the BOP wet welds, where one can see the weld surface defects such as porosity and discontinuous weld beads.



(a)



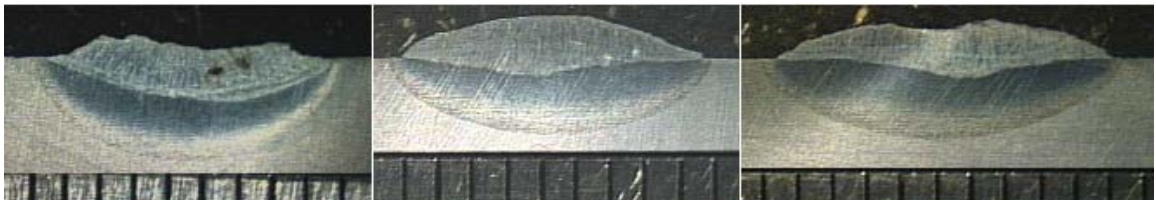
(b)



(c)

Figure 2.3. 20. Three BOP wet welds deposited in the vertical-down position with E6013 electrodes at 50 m water depth.

Cross-sections macrographs extracted from the BOP wet welds are shown in Figure 2.3.21. With respect to the welds deposited at 0.5 m one can see wider weld beads with shallower penetration and reinforcement. The reinforcement of the welds deposited at 50 m is not as high as that of the ones deposited at 0.5 m with the same electrode grade. This observation seems to suggest less efficient transfer of weld metal at 50 m.



(a)



(b)



(c)

Figure 2.3. 21. Cross-sections from the bead-on-plate wet welds deposited with E6013 electrodes at 50 in the vertical-down position.

Table 2.3.7 presents the width, penetration, and reinforcement of the BOP wet welds deposited with E6013 electrodes at 50 in the vertical-down position. Weld beads deposited at 0.5 m presented narrower welds bead than the ones deposited at 50 m. A possible reason for wider weld beads is higher arc pressure, since the arc pressure increases with increasing water depth or pressure.

Table 2.3. 7. Bead morphologies of the bead-on-plate wet welds.

Cross-section	Width (mm)	Penetration (mm)	Reinforcement (mm)
BOP 1 – a	8.4	1.3	0.6
BOP 1 – b	8.8	0.5	1.2
BOP 1 – c	9.8	0.6	1.1
BOP 2 – a	8.1	0.8	0.7
BOP 2 – b	7.7	1.5	0.8
BOP 2 – c	7.8	1.2	0.6
BOP 3 – a	7.8	1.3	0.3
BOP 3 – b	8.9	1.4	0.6
BOP 3 – c	8.6	1.0	1.1
Avg.	8.4	1.1	0.8

Weld metal porosity was measured on the cross-section of the BOP welds; the results are presented in Table 2.3.8. The average porosity measured is 0.6 pct., which is less than the 1.2 pct. previously reported for flat welding position. It is important to mention that porosity varied along the weld as previously reported, but it also varied with the cross-section. At this point the porosity difference between welding positions cannot be determined. More precise porosity measurements techniques are required.

Table 2.3. 8. Weld metal porosity measured on the cross-sections.

Cross-section	Weld metal porosity, vol. pct.
BOP 1 – a	2.2
BOP 1 – b	0.4
BOP 1 – c	0.2
BOP 2 – a	0.5
BOP 2 – b	1.1
BOP 2 – c	0.3
BOP 3 – a	0.5
BOP 3 – b	0.1
BOP 3 – c	0.3
Avg.	0.6

Vertical-down at 100 m with E6013 electrodes

At this water depth, three BOP wet welds were made with E6013 electrodes on A-36 steel plates. The steel rod diameter of the flux-covered electrodes is 3.25 mm. The selected welding current was 184 A that is very closed to the value selected for the 50 m water depth and welding speed of 4.2 mm/s. Figure 2.3.22 shows the BOP wet welds. Rough weld surfaces and more porosity is observed in the welds deposited at this depth.

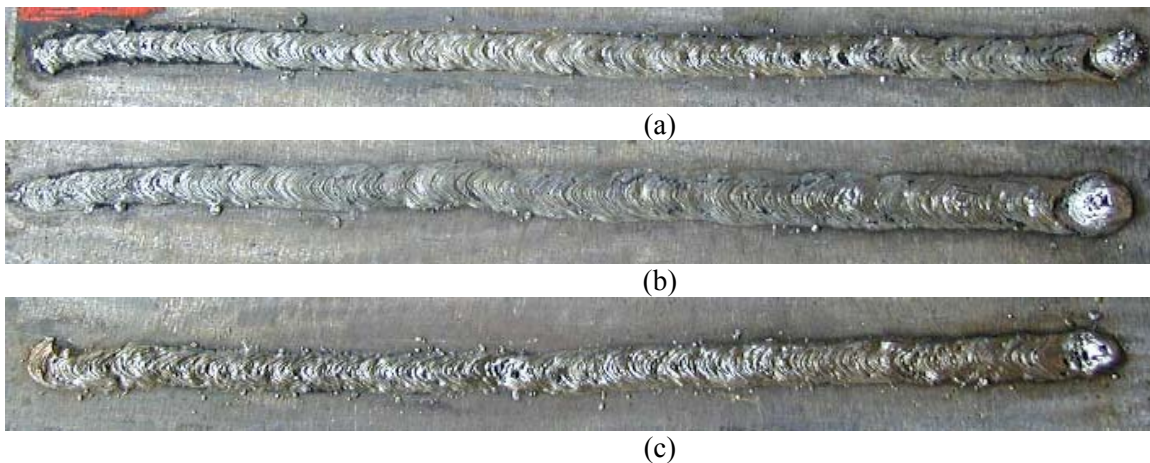


Figure 2.3. 22. Three BOP wet welds deposited in the vertical-down position with E6013 electrodes at 100 m water depth.

Cross-sections macrographs extracted from the BOP wet welds are shown in Figure 2.3.23. Once again with respect to the welds deposited at 0.5 m one can see wider weld beads with shallower penetration and reinforcement.

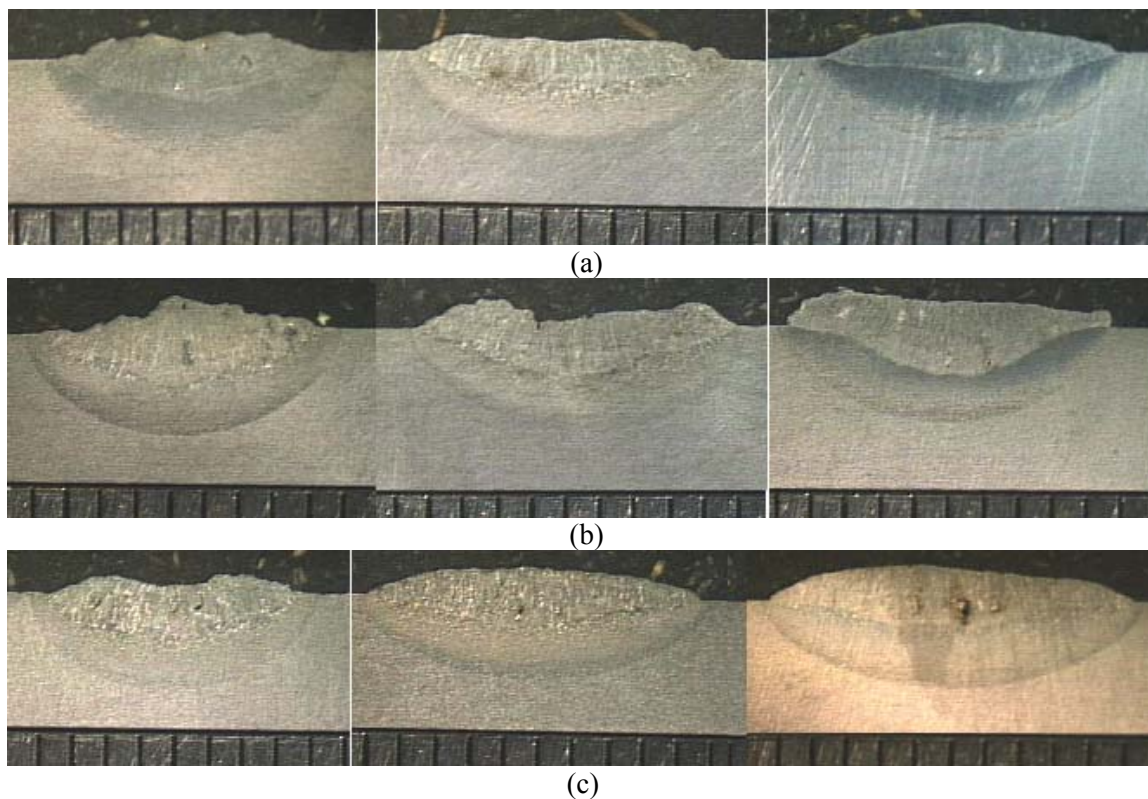


Figure 2.3. 23. Cross-sections from the bead-on-plate wet welds deposited with E6013 electrodes at 100 in the vertical-down position.

The bead morphologies of these wet welds are given in Table 2.3.9, which are very similar to the ones measured on welds deposited at 50 m. Note the slightly wider weld beads produced at this depth.

Table 2.3. 9. Bead morphologies of the bead-on-plate wet welds.

Cross-section	Width (mm)	Penetration (mm)	Reinforcement (mm)
BOP 1 – a	7.6	1.1	0.7
BOP 1 – b	9.0	0.9	0.5
BOP 1 – c	8.8	0.8	0.9
BOP 2 – a	8.6	1.5	1.0
BOP 2 – b	9.4	1.3	0.8
BOP 2 – c	9.3	1.0	1.4
BOP 3 – a	7.5	1.1	0.5
BOP 3 – b	9.7	0.8	0.9
BOP 3 – c	10.7	0.9	1.0
Avg.	9.0	1.0	0.9

Table 2.3.10 presents the porosity values measured on the cross-sections of the wet welds. The average porosity is 1.7 pct., which is very low compared to the 8.4 pct. measured on BOP welds deposited at 100m in the flat position. It is important to mention that the electrode diameter (steel rod diameter 3.25 mm) used for the wet welds deposited out-of- position is smaller than the electrodes used in the flat welding position (steel rod diameter 5.0 mm). This electrode diameter difference must contribute to the porosity difference mentioned. Also as stated above, a more precise method is required to more precisely determine the porosity difference between welding positions.

Table 2.3. 10. Weld metal porosity measured on the cross-sections.

Cross-section	Weld metal porosity, pct.
BOP 1 – a	1.4
BOP 1 – b	0.6
BOP 1 – c	0.4
BOP 2 – a	2.3
BOP 2 – b	0.8
BOP 2 – c	1.0
BOP 3 – a	2.9
BOP 3 – b	4.2
BOP 3 – c	1.8
Avg.	1.7

In order to estimate the loss of weld metal in the welds deposited at 50 and 100 m with respect to the welds deposited at 0.5 m, the volume of the weld reinforcement was calculated. Table 2.3.11 presents the average values of weld reinforcement. With respect to the welds deposited at 0.5 m, these welds measured only about 40 pct. of the shallow water weld metals.

Table 2.3. 11. Reinforcement volume of the wet welds deposited at 0.5, 50, and 100 m water depth with E6013 electrodes.

Weld and water depth	Volume (mm ³)
BOP-1 at 0.5 m	2.2
BOP-2 at 0.5 m	1.4
BOP-3 at 0.5 m	2.3
Avg.	2.0
BOP-1 at 50 m	1.5
BOP-2 at 50 m	0.8
BOP-3 at 50 m	0.9
Avg.	1.1
BOP-1 at 100 m	1.1
BOP-2 at 100 m	1.2
BOP-3 at 100m	1.2
Avg.	1.2

An accumulation of metal droplets was observed at the bottom of the chamber after depositing the welds, which agrees with the above presented. Weld metal runs away down from the weld pool when the gravitational force of the liquid metal becomes greater than the supporting force provided by the arc. A balance of forces is required to reduce the loss of weld metal.

Vertical-down at 50 m and 100 m with E7018 and E6010 electrodes

As shown previously, the performance of the E7018 electrode type at 0.5 m was good. However similar problems to the ones reported for the flat position at 50 m were experienced in the vertical down position at 50 m. Porosity, arc instability, and arc extinction were the observed problems. Figure 2.3.24 shows a BOP wet weld deposited with E7018 electrode grade at 50 m, porosity is observed along the weld bead.

As shown in Figures 2.3.16 and 2.3.17, the weld beads made with E6010 electrodes at 0.5 m show discontinuities, deep penetration, deep undercuts, and no reinforcement in some sections.

Based on the above reasons the experimental matrix was completed and therefore this report does not include the performance of the E7018 and E6010 electrode grades at 50 and 100 m water depths in the vertical-down position.



Figure 2.3. 24. Wet weld made with E7018 electrode type at 50 m.

Vertical-up at 0.5 m water depth

During wet welding in the vertical-up position, the liquid metal is expected to run away from the weld pool by gravity, making it difficult to produce acceptable weld beads. Figure 2.3.25 illustrates this effect and Figure 2.3.26 shows actual BOP wet welds made with E6013, E6010, and E7018 electrodes at 0.5 m water depth. Discontinuous wet welds and undercutting are the main problems in the vertical-up direction. As illustrated by the weld craters, the weld pool cavity created by the arc would not be completely filled by liquid weld metal. Deep undercuts could also be observed on both sides of the wet weld.

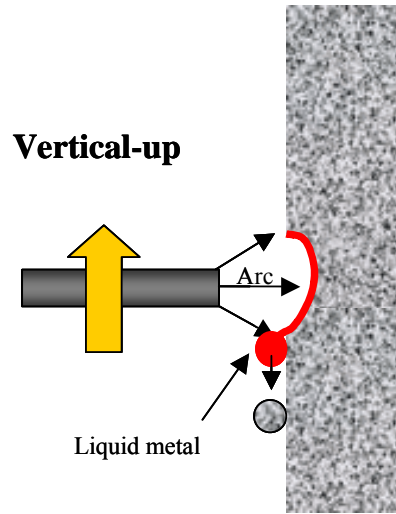


Figure 2.3. 25. Weld liquid metal without vertical support.



Figure 2.3. 26. Bead-on-plate wet welds deposited in the vertical-up position at 0.5 m using E6013, E6010 and E7018 electrodes, respectively.

Vertical-up at 50 and 100 m water depths

Since poor results were obtained at 0.5 m water depth, wet welds in the vertical-up position were not deposited at these two water depths.

2.3.4 Conclusions

Based on the results above presented for out-of position wet welding, the following conclusions can be given:

Vertical-down welding position

- E6013 grade electrodes produced the most stable arc and smallest droplets of the three electrodes tested at 0.5m water depth. E7018 electrodes produced the largest droplets with largest fluctuations in arc voltage.
- Wet welds deposited with E6010 electrodes produce discontinuous welds at 0.5 m water depth.
- Vertical-down wet welds were deposited with the specially designed gravity welder system at three water depths (0.5, 50, and 100m) using the E6013 electrode grade.
- The E6010 was not tested at 50 and 100 m due to the poor results obtained at 0.5 m.
- Porosity and arc instability were the main problems with the E7018 electrode at 50 m, thereafter no more tests were made at this depth or at 100 m.
- A “loss” of weld metal (likely due to erratic transfer) close to 50% was observed in welds deposited at 50 and 100 m with respect to the ones made at 0.5 m.

- Further work is needed to minimize the loss of weld metal in wet welds at 50 and 100 m water depth.
- Less porosity was measured on the wet welds deposited in the vertical-down welding position with respect to previous results reported for the flat welding position. However, it is important to consider the difference in the reinforcements of the welds.

Vertical-up welding position

- Due to the lack of support of the molten weld pool, vertical-up wet welds were discontinuous and exhibited deep undercuts on both sides of the welds at 0.5 m water depth.
- Wet welds were not deposited at 50m or 100 m water depths due to the poor results obtained at 0.5 m.

2.4 Performance of rutile electrodes with nickel additions

2.4.1 Introduction

Wet welds deposited at one foot water with oxidizing electrodes with nickel additions exhibited toughness improvements with nickel contents between 2 to 3 wt. pct. tested at 32°F, Pope (1994). Wet welds deposited with rutile-grade electrodes with nickel additions at approximately 2.3 wt. pct. also showed toughness improvements, Perez (2003). Figure 2.4.1 plots the toughness improvements obtained with nickel additions to rutile and oxidizing electrodes. The improvement could be attributed to grain refinement because of nickel.

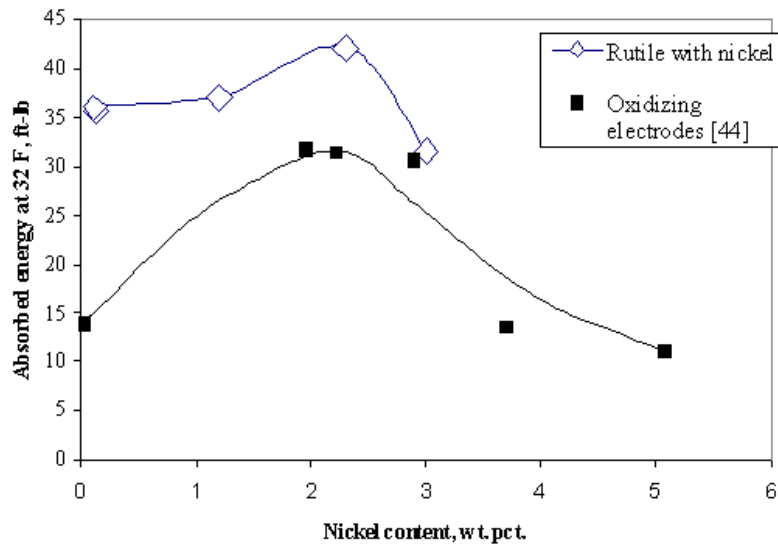


Figure 2.4.1. Effect of nickel on impact toughness of wet welds deposited with rutile and oxidizing electrodes at 32 F, Perez (2003).

In Figure 2.4.2, Charpy V-notch absorbed energy was plotted as function of nickel content. Note that at high testing temperatures, nickel additions demonstrated little effect on impact toughness. At cryogenic testing temperatures, however, the effect of nickel became evident. With approximately 3.0 wt. pct. nickel addition, an impact toughness of 35 ft-lb at -58°F was observed. These test specimens exhibited ductile behavior, with dimples on the fracture surface. At lower nickel contents, the Charpy specimens failed in a brittle manner, with cleavage fracture, as shown in Figure 2.4.3.

Similar effects could be expected from wet welds deposited at water depths beyond one or two feet. Thus, experimental rutile-grade electrodes with nickel additions were extruded at CSM to deposit multipass wet welds at 50 m water depth.

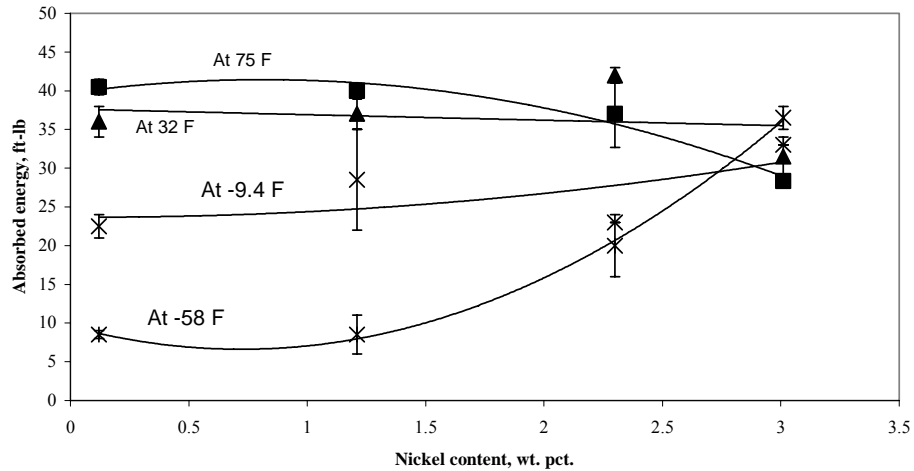
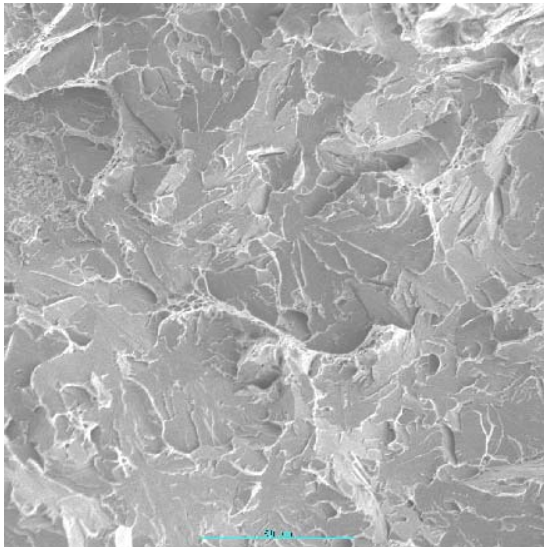
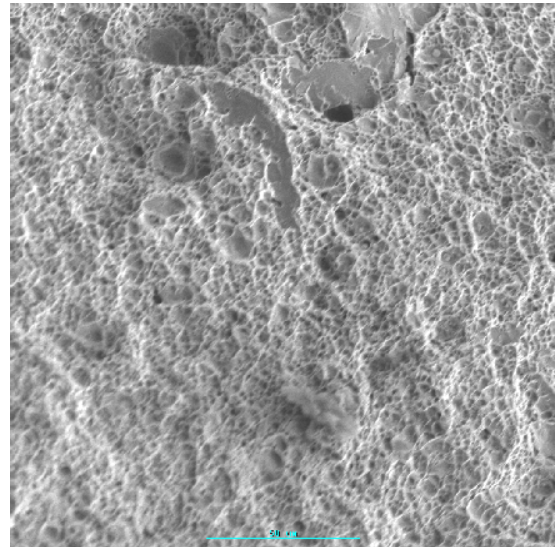


Figure 2.4.2. Impact toughness versus nickel content tested at different temperatures – Surface welds Perez (2003).



(a) 2.3 wt. pct. Nickel



(b) 3.0 wt. pct. Nickel

Figure 2.4.3. Fracture surfaces of Charpy V-notch specimens tested at -58 F.

2.4.2 Experimental Procedures

Experimental electrodes were extruded at CSM using the extrusion press shown in Figure 2.4.4 and the flux formulation given in Table 2.4.1. Three batches of experimental rutile-grade electrodes with nickel additions were extruded. Nickel was added at the expense of rutile as presented in Table 2.4.1. The electrodes were dried at room temperature for 24 hours followed by baking at 302°F for 3 hours. Low carbon steel rods of 355×4 mm in length and diameter were used to extrude the electrodes; flux thickness was 0.8 mm. Similarly, the electrodes were waterproofed with commercial varnish.

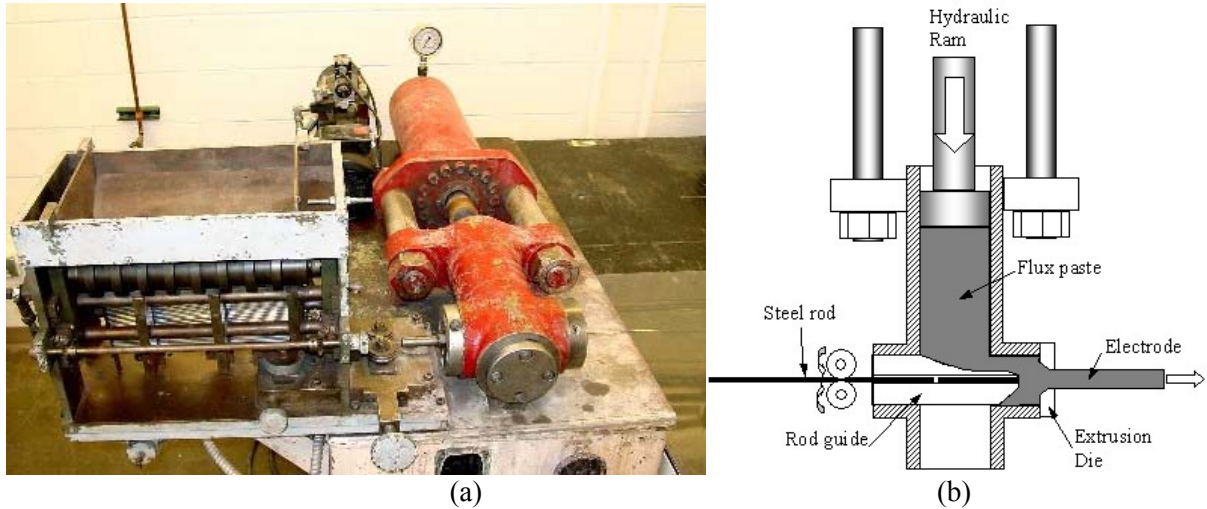


Figure 2.4.4. (a) Electrode extruder at CSM and (b) extruder illustration, Perez (2003).

Table 2.4.1. Main ingredients used for experimental rutile-grade electrode with nickel addition.

Mineral	Batch 1, %	Batch 1, %	Batch 1, %
Cellulose	12	12	12
Calcium carbonate	5	5	5
Titanium dioxide	51	47	43
Ferromanganese	10	10	10
Nickel	4	8	12

Three multipass wet welds were deposited in the hyperbaric chamber shown in Figure 2.2.1 at 50 m water depth in fresh water. A constant voltage power source, electrode positive was used instead of the normal constant current process.

Standard Charpy specimens were extracted from the multipass wet welds for impact testing as shown in Figure 2.4.5.

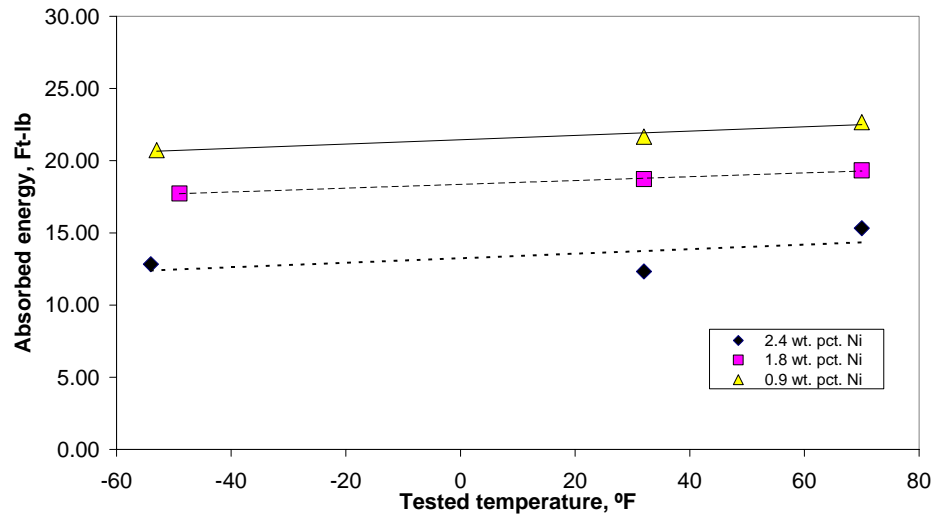


Figure 2.4.5. Set of standard Charpy V-notch specimens made from a multipass wet weld deposited at 50 m with rutile electrodes with nickel additions. These specimens show the bottom side of the multipass weld.

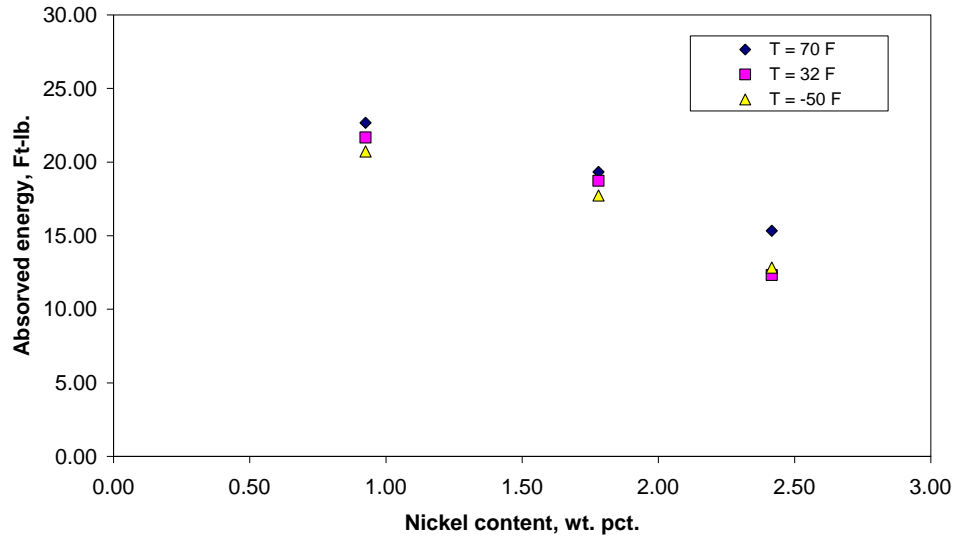
2.4.3 Results

As mentioned earlier, the loss of alloying elements and porosity increased with increasing water depth. At 50 m water depth, the weld metal porosity was approximately 5 % and most of the manganese and silicon would already be oxidized. Additionally, the rutile-grade electrodes did not exhibit as good penetration as the cellulosic electrodes increasing the susceptibility of slag entrapment between weld passes in a multipass weld. Therefore, the mechanical properties of these welds deposited at 50 m. would be lower than the wet welds deposited at surface.

Figure 2.4.6 shows the average impact toughness results of the multipass wet welds made with rutile electrodes with nickel additions. The effect of testing temperature was as expected. Higher absorbed energy was measured at higher testing temperatures, albeit the differences were small. The toughness values between 12 to 22 ft-lb were lower than those obtained in the surface wet welds, from 8 to 42 ft-lb. Differences in toughness values between the maximum and minimum testing temperatures were 2.5, 1.5 and 2 ft-lb for the 2.4, 1.8 and 0.9 wt. pct. nickel additions, respectively. As nickel increased from 0.9 to 2.4 wt. pct. impact toughness decreased from 21 to 13 ft-lb. This observation is unexpected since the highest toughness values were expected at approximately 2.4 wt. pct. nickel at 70°F.



(a) Absorbed energy vs. testing temperature.

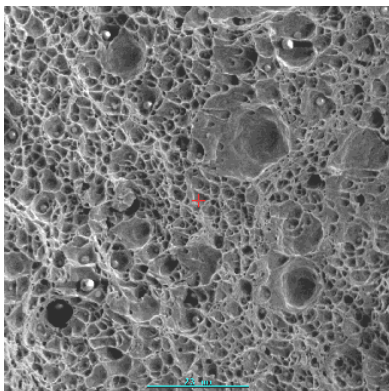


(b) Absorbed energy vs. nickel content.

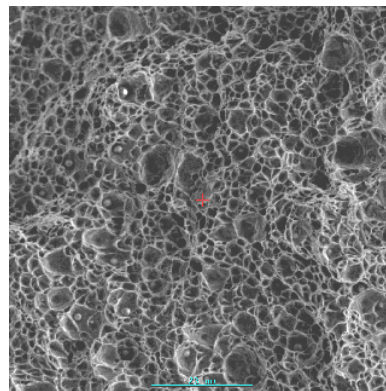
Figure 2.4.6. Average impact toughness of the three multipass wet welds made with rutile electrodes and nickel additions.

The weld with 0.9 wt. pct. nickel exhibited the highest toughness in these tests. At -50°F , the impact energy was 23 ft-lb. considering that these welds were made at 50 m water depth, the impact toughness found was quite reasonable.

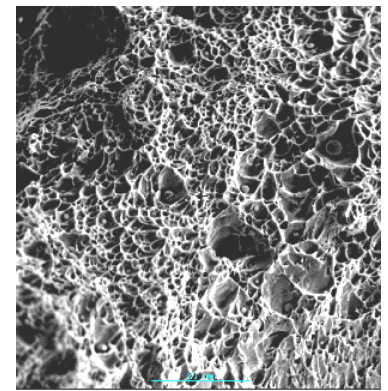
Outside the pores, the fractures surfaces of all the tested specimens showed microvoids or dimples, typical features of ductile failure, Figure 2.4.7. Specimens tested at -58°F also showed small areas with typical cleavage facets associated with brittle transgranular fracture (Figure 2.4.8a). Note the presence of the inclusions. A mixture of cleavage and microvoids is shown in Figure 2.4.8b of a specimen tested at -58°F .



10, (a) 2.4 wt. Pct. Ni 70 F



(b) 2.4 wt. Pct. Ni 32 F



(c) 2.4 wt. Pct. Ni -58°F

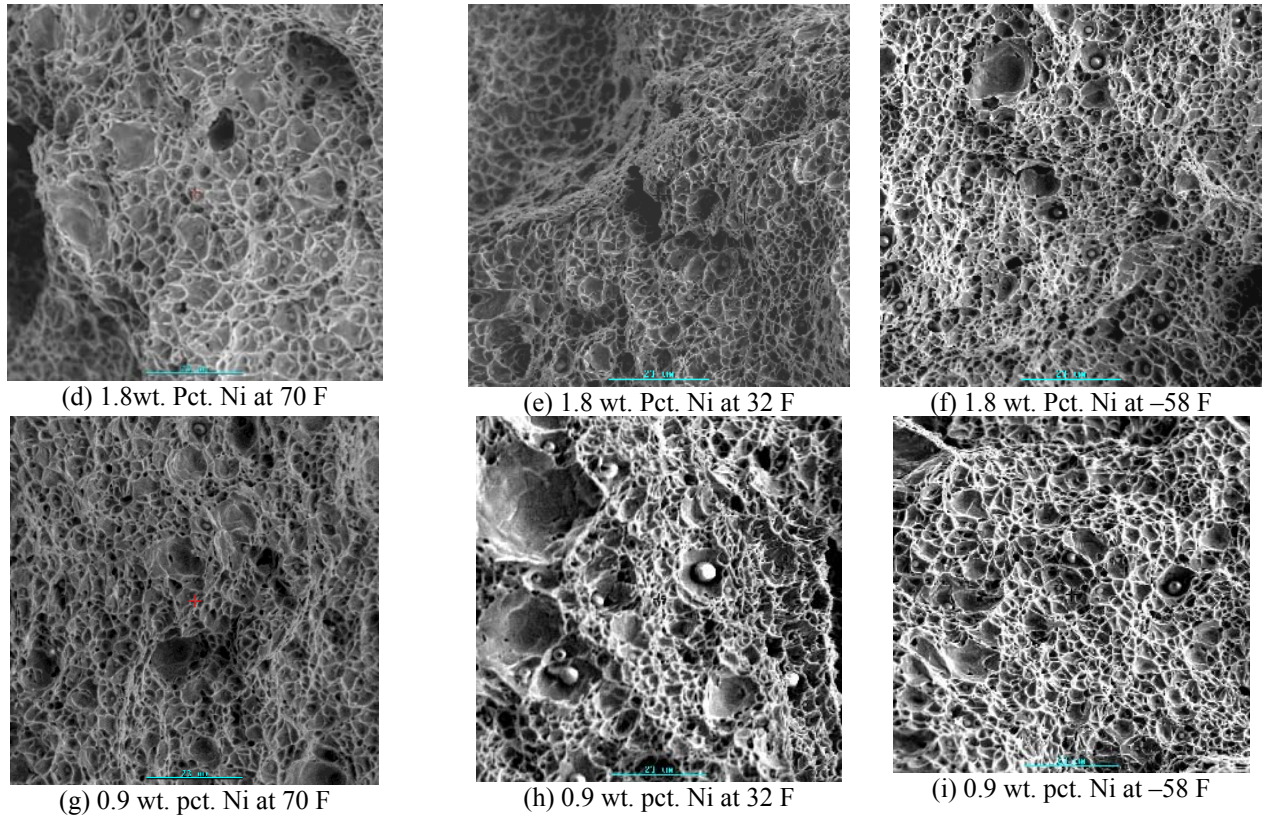


Figure 2.4.7. SEM photographs taken from the fracture surfaces showing dimples, the scale bar indicates 23 μm

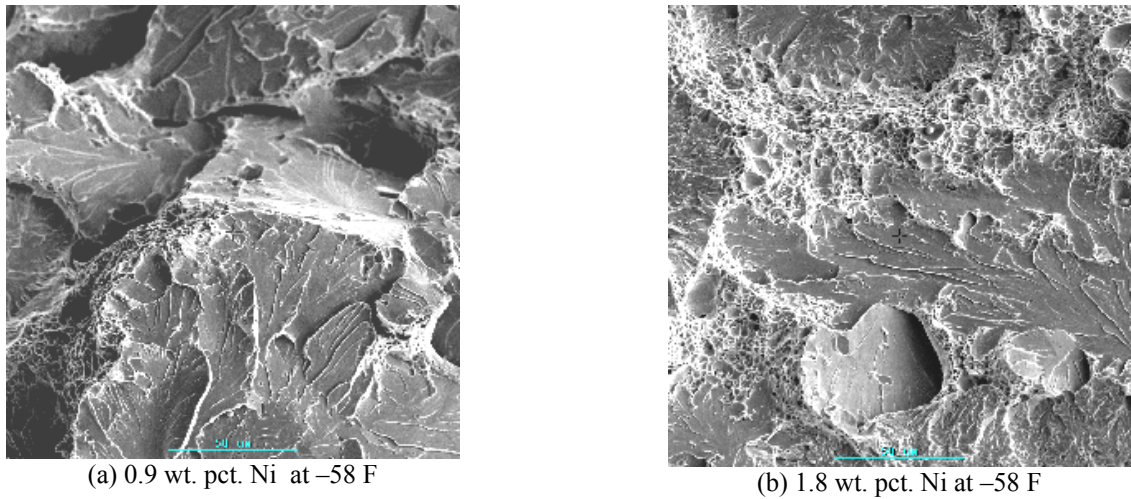


Figure 2.4.8. SEM photographs taken from the fracture surfaces showing (a) cleavage fracture and (b) a mixture of dimples and cleavage facets, the scale bar indicates 50 μm .

Although ductility was observed in the fracture surfaces the absorbed energy was not large due to the weld defects mentioned earlier. Figure 2.4.9 shows SEM macrographs from the fracture surface of the Charpy V-notch specimens where one can see porosity and slag entrapment in the dark areas.

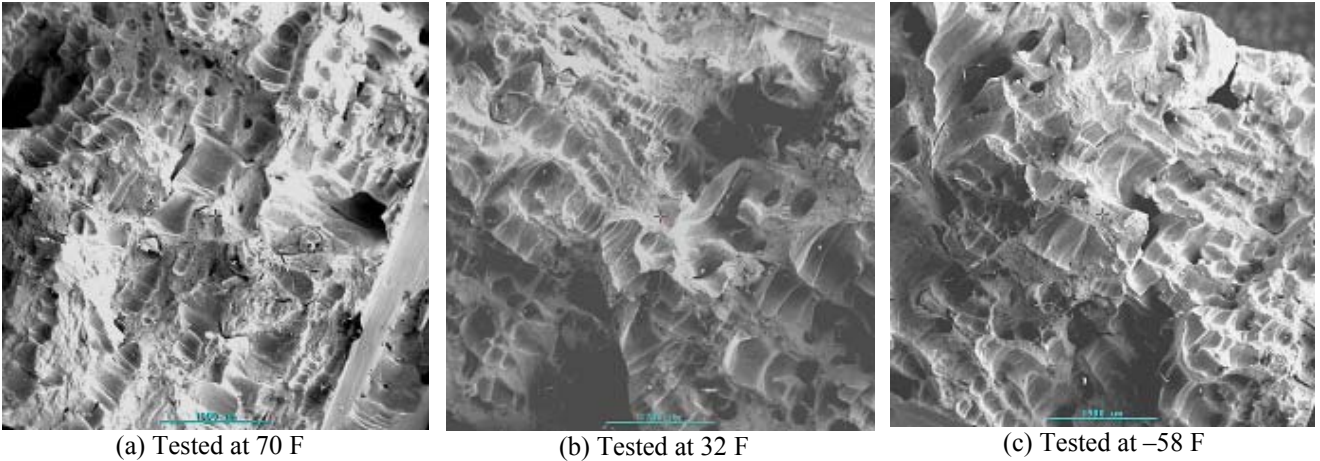


Figure 2.4.9. Fracture surface of Charpy V-notch specimens made from the multipass wet weld with 2.4 wt. pct. nickel showing defects such as porosity and slag entrapment.

Finally, Figure 2.4.10 presents micrographs that show grain refinement observed in the multipass wet welds with an average grain size of less than 4 μm . It is well established that steels with fine grain microstructures exhibit better mechanical properties than steels with coarse grains. However, even with fine grain microstructures, these wet welds did not exhibit good mechanical properties due to the weld defects.

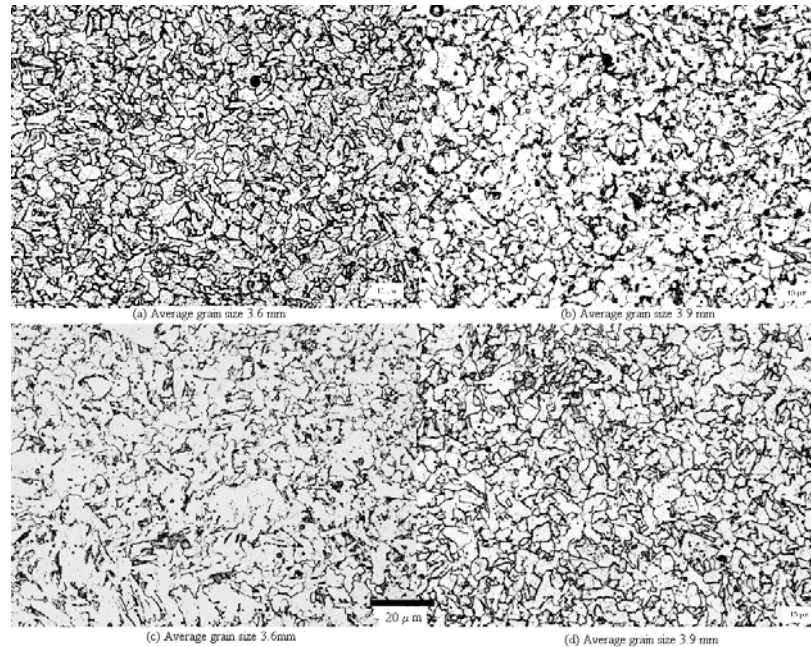


Figure 2.4.10. Micrographs taken from the Charpy V-notch specimens extracted from the multipass wet welds showing the fine grains in the reheated zone

2.4.4 Conclusions

- Different from the surface and shallow water wet welds, higher nickel content did not improve the impact toughness.
- The 50 m water depth welds had impact toughness ranging from 21 to 13 ft-lb (0.9 and 2.4 wt. pct. nickel, respectively).
- Ductile fracture was observed outside the pores. Thus, weld defects instead of the microstructure affected more significantly the mechanical behavior of these welds.

2.5 Mitigation of porosity

2.5.1 Introduction

It is well established that porosity, amounts of alloying elements loss and other welding defects increase with increasing water depth. Thus wet welds will typically exhibit mechanical properties that are inferior to reference dry welds. Section 2.1 clearly showed the effects of very large pores in welds deposited at 150 m water depth. These discontinuities significantly reduced the strength of the weld metal.

To obtain quality wet welds that would meet stringent requirements for critical applications, mechanisms of porosity formation must be characterized. An additional objective of this task is also to recommend mitigating measures to reduce porosity of wet welds.

Literature review

It has been reported in the literature that droplets detached from flux-covered electrodes are hollowed as can be seen in Figure 2.5.1a and b. In the welding arc, the decomposition of ingredients in the flux coating produces gaseous species that may become trapped in the liquid droplet formed at the electrode tip.

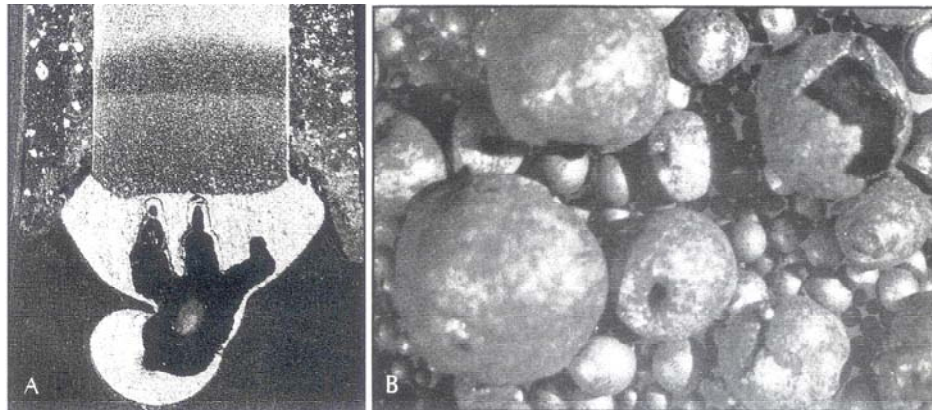


Figure 2.5.1. (a) Droplet attached to the tip of the electrode and (b) collected droplets (Brandt, S., Taniguchi C. and Liu S. (1991)).

Droplets detached from three different electrodes were collected to determine their apparent porosity. These values are reported in Table 2.5.1. As can be seen, E6013 and 7018 electrodes produced droplets that passed US Sieve number 5, i.e. 5 mesh - 5 particles per square inch and approximately 4 mm diameter. These droplets also exhibited large porosity percentages, e.g. 50 to 60%. As droplet size decreased, the porosity percentage also decreased. Droplets that measured 18 mesh showed 4 to 5% porosity. Considering the relationship between droplet size and porosity percent, it appears that by controlling the droplet size, porosity can also be lowered.

Table 2.5.1. Porosity of droplets collected during welding in dry conditions (Brandi, S., Taniguchi C. and Liu S. (1991)).

USA Sieves Series Number	Mean apparent porosity %		
	E6011	E6013	E7018
5	-	62.09	51.15
7	27.10	44.91	38.55
10	14.12	23.16	17.43
14	6.87	7.51	7.25
18	5.22	4.96	4.83

According to the international Institute of Welding (IIW), metal transfer modes can be free flight, bridging and flux wall guided type. For flux-covered electrodes, metal droplets typically transfer by free flight (globular and explosive) and bridging type (short-circuiting). In globular and short-circuiting transfer, the relatively large droplets hanging from the tip of the electrode would be subjected to several forces that include:

- Surface tension
- Gravitational
- Drag
- Electromagnetic
- Vapor

As its name indicates, explosive transfer involves the breaking up of larger droplets into smaller ones. Pressure build-up because of the entrapment of gaseous products is often attributed as the cause of explosive transfer.

Surface tension forces, which depend on the liquid metal surface tension and contact area of the droplet with the electrode rod, keep the droplet attached to the electrode tip. The larger the electrode rod diameter, the larger will the pendant droplets be. In flat position, gravitational force on the droplet acts against the surface tension force to promote faster detachment. Drag force is associated with the arc plasma acting in favor of droplet detachment. Particularly in the gas metal arc welding process, shielding gas flow provides the major part of the drag force. Electromagnetic (or Lorentz) force is associated with the current flow, which promoted droplet detachment by the “pinch effect”. Vapor force originates from the vaporization of atoms from the surface of the metal droplet. It is a recoil force that under normal circumstances acts against droplet detachment. The interaction of these forces will determine the size of the droplets to be transferred as well as the frequency of this transfer. Depending on whether the gaseous products can be readily eliminated from the droplets, the pore within each droplet may be transferred into the weld pool.

It is clearly shown by the authors of this report and Suga and Hasui (1986) that as water depth or pressure increases weld metal porosity increases, Figures 2.2.10 and 2.2.12 and Figure 2.5.2.

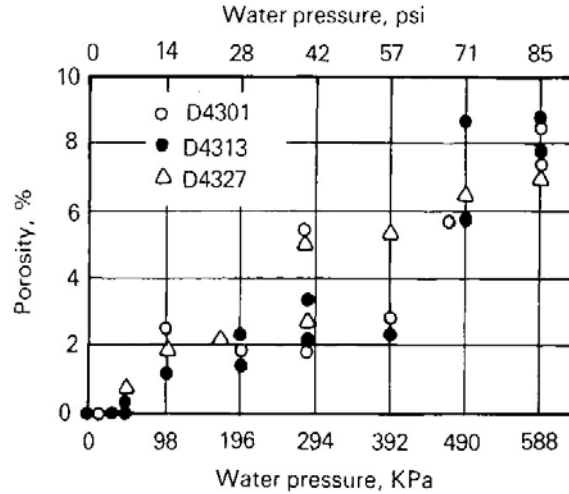


Figure 2.5.2. Weld metal porosity as a function of water pressure, by Suga and Hasui (1986).

An opposite view was offered by Ibarra (1995) that as water depth or pressure increases, porosity should be reduced because a gas bubble nucleus must overcome larger external pressure to form. In fact, pressure inert gas metal arc (PIGMA) process is used in aluminum welding to reduce weld metal porosity. Pressure as high as two or three atmospheres are typically used. The two opposing views led to the conclusion that the amount of gas products in the droplet is likely more important than pressure alone in the determination of final weld porosity.

Hydrogen has been reported in the literature to be the main gas measured in the pores, Sanchez-Osio (1995). Table 2.5.2 presents results of pore gaseous species reported by three authors.

Table 2.5.2. Gaseous species detected in pores, Sanchez-Osio (1995).

Source	Gaseous species			
	H ₂	CO	CO ₂	Other
Suga and Hasui (1986)	96	0.4	0.06	
Chew (1973)	62-82	11-24	4-6	
Sapiro (1973)	45	43	8	4

2.5.2 Experimental procedures

Underwater wet welds were deposited in the hyperbaric chambers shown in Figures 2.1.2 and 2.2.1 with gravity welders as shown in Figure 2.2.4. Since direct observation of the arc in wet welding is not easily implemented, measurements of the arc voltage and current can provide information to better understand the welding process and its associated problems. Arc voltage signals acquired during wet welding with different electrodes grades (E6013, E7018, E7024, and E6010) were carefully analyzed and compared.

Bead-on-plate wet welds made with pulsed currents (in an attempt to control metal droplet size) were deposited on A36 steel plates using E6010 type electrodes at 50 and 75 m water depth. The electrodes were waterproofed with commercial varnish to protect the flux coating from water absorption.

2.5.3 Results

Results from the arc voltage signals collected during wet welding with different electrodes showed interesting information. The E7018 grade electrodes presented short-circuiting metal transfer modes as shown in Figure 2.5.3. The signals acquired at 100 m exhibited more short-circuiting events than those at 50m. Considering that the electrode size and welding time were similar, having more short-circuiting events at 100 m indicates more droplets being transferred across the arc. The first 10 s of the voltage signals shown in Figure 2.5.3 has 24 and 35 short-circuiting events (droplets) at 50 and 100 m respectively. If the total mass deposited in the two conditions were approximately the same it becomes apparent that at 50 m the droplets had more mass that at 100 m. Consequently, the droplets detached at 100 m had less mass and more gas than those at 50 m.

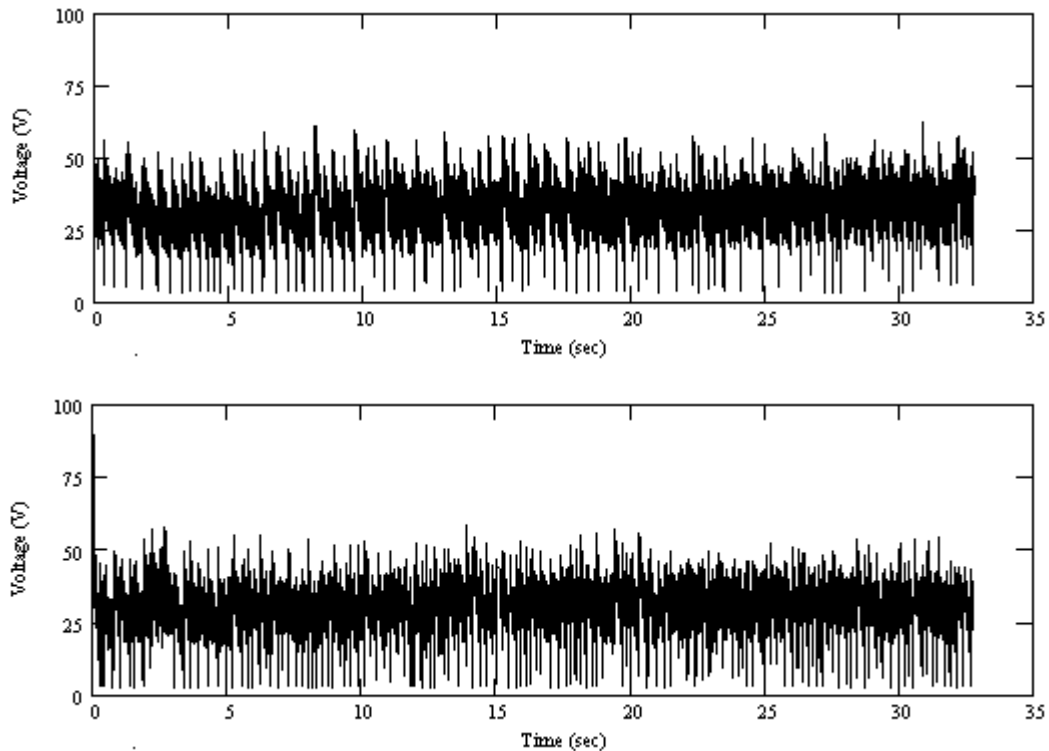


Figure 2.5.3. Arc voltage signals acquired during wet welding at 50 m (top) and 100 m (bottom) water depths.

Porosity increase with increasing pressure – Proposed Model

As a consequence of this latest observation that the porosity/droplet mass ratio increased with water depth, it becomes important to understand how this increase occurred. A possible mechanism of gas entrapment in the droplet is described in the following. Partial pressures of the different gases generated in the arc increase with water depth. As molten droplets grow in hydrogen-rich arcs, the high temperature and pressure gradients cause hydrogen to diffuse into the pendant droplet, increasing its

volume. Since the pressure of the water head is approximately 5 and 10 kg/cm² for 50 and 100 m water depth, respectively and that the arc pressure must be equal or greater than the external pressures, hydrogen diffusion into the droplets is expected to readily occur. Therefore, the droplets transferred at 100 m will have less mass and more gas than those transferred during wet welding at 50 m resulting in higher weld metal porosity. Electrochemical effect, i.e. the electrode polarity (DCEP or DCEN) contribution, is not discussed in this work but may contribute to the hydrogen pick-up in the droplets.

Further examination of droplets collected in dry welds shown in Figure 2.5.1b showed that even at low hydrogen environments, large porosity could occur. The findings of Brandi et al. (1991) suggest that an additional mechanism must be identified together with hydrogen diffusion to explain porosity formation in wet welds.

This second mechanism could be mechanical entrapment of gas during droplet formation in both dry and wet welding. Pressure, temperature, and surface tension gradients interact in a complex manner and together with fluid dynamics play a fundamental role in the droplet formation process.

During welding, the arc length is determined by the flux cone formed at the tip of the electrode and the crater on the base metal. The thicker the flux coating and the deeper the weld crater, the longer the arc will be. In wet welding, experimental or actual fabrication, one side of the flux cone actually drags on the base metal.

Although droplets formed at the tip of the electrode are covered liquid with slag, the slag may not completely cover the bottom side of the droplet where gas can diffuse into the droplet. Ascending water vapor against drop detachment could play an important role on gas porosity.

After the droplet detaches hydrogen, carbon monoxide or carbon dioxide (now in molecular form) cannot easily diffuse out of the droplet. The detached droplet(s) is incorporated into a shallow layer of liquid metal that is pushed to the backside of the weld pool. The gas pore now incorporated in the weld pool will not easily escape because of the fast solidification of the weld metal. Vapor of alloying elements may also be part of the gas pore. Droplet formation and growth, gas diffusion into the droplet, and porosity in wet welding can be seen in Figure 2.5.4.

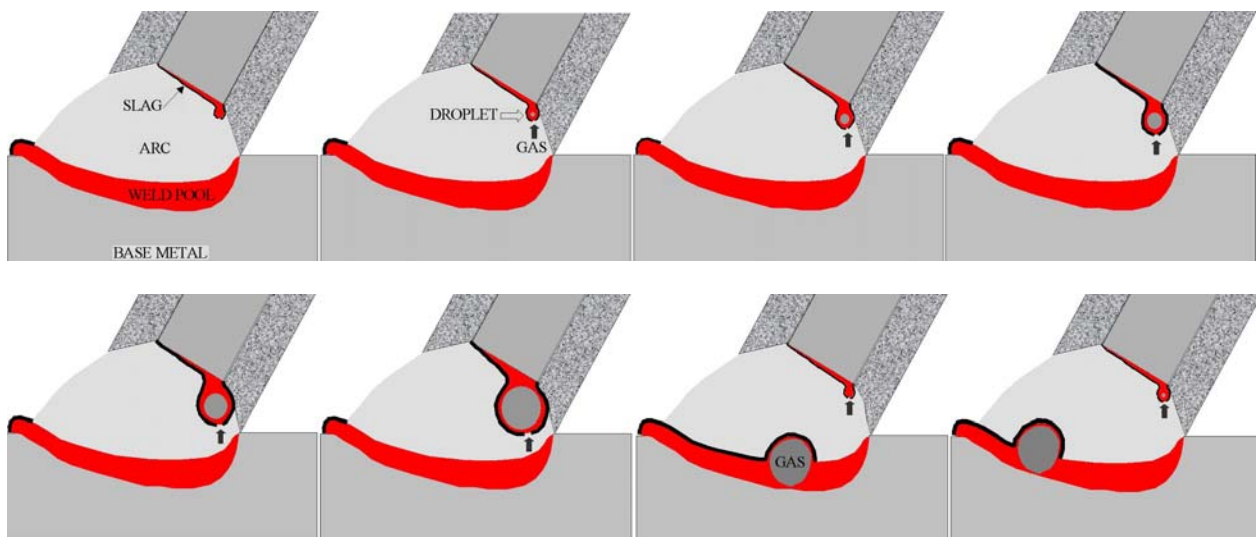


Figure 2.5.4. Illustrations of droplet formation and growth at the electrode tip, gas diffusion, and gas entrapment in the weld metal.

In dry welding conditions, gas porosity is significantly lower because of the lower hydrogen content in the arc and because of the lower system pressure (mainly arc pressure and hydrostatic pressure). In wet welding, the system pressure is much higher because of the water head and this pressure acting on the weld surface becomes a strong obstacle for the escape of the gas bubbles. This model explains the observation that wet welds deposited with E7018 grade electrodes at 100 m exhibited more porosity than wet weld made at 50 m because of the pressure difference. The effect of hydrogen content would be evident when comparing dry to wet welds.

Porosity reduction

Electrode diameter. If porosity is a function of the droplet sizes transferred during wet welding, smaller droplets are expected to result in reduced porosity. Smaller electrode diameter typically produces shorter arc length and smaller droplet during welding than larger electrodes in short-circuiting metal transfer. Also smaller electrode diameter implies smaller droplet contact area at the electrode tip that will reduce the surface tension force that supports the droplet. However, using smaller electrode diameters decreases the weld metal deposition rate requiring more weld passes thus more time to complete a multipass wet weld. The decrease in productivity during fabrication makes this a less attractive alternative in controlling porosity.

Pulsed current. It is typically used with the gas metal arc welding (GMAW) process to control the metal transfer modes. The several parameters in pulsed current process that can be used to control droplet transfer are listed in the following.

- Background current
- Peak current
- Peak time (time at peak current)
- Peak voltage
- Pulsed per second (frequency)
- Waveform

The background current level is the minimum current required to maintain the arc and depends on the wire size. The peak current, time at peak current, and peak voltage are the parameters that form and detach one droplet (per current pulse), These parameters also depend on the wire diameter. The pulses per second depends on the wire size and peak time and will give the droplet rate if one droplet is detached per current pulse. Typical waveforms are square or triangular (saw tooth). Other forms can exist depending on the power source capabilities.

Pulsed current is also used in the gas tungsten arc welding (GTAW) process to improve the weld bead morphology and other properties.

In order to test the effects of pulsed current on droplet detachment and porosity level, wet welds were deposited at 50 m water depth with E6010 grade electrodes. The power source used has very limited pulsing capabilities and current output. The output waveform is the square type with very low frequency (≈ 5 Hz) and low current output (max. 300A). One can see in Figure 2.2.5c that for E6010 electrodes at 50 m (non-pulsing conditions) the metal transfer mode was short-circuiting at a rate of 10 cycles per second. Therefore, the rate of droplet detachments has to be greater than 10 Hz to produce smaller droplets and affect gas pore transport.

Figure 2.5.5 shows a top view of a BOP wet weld deposited with E6010 grade electrodes at 50 m. the reinforcement of the weld was ground flush to the base plate surface. The left-hand side of the weld was made with constant current at 220 A and the right-hand side was made with the limited pulsing current capabilities of the power source. Definite decrease in porosity could be observed. Smaller pore size and lower density resulted in the pulsed current welding condition (right-hand side).

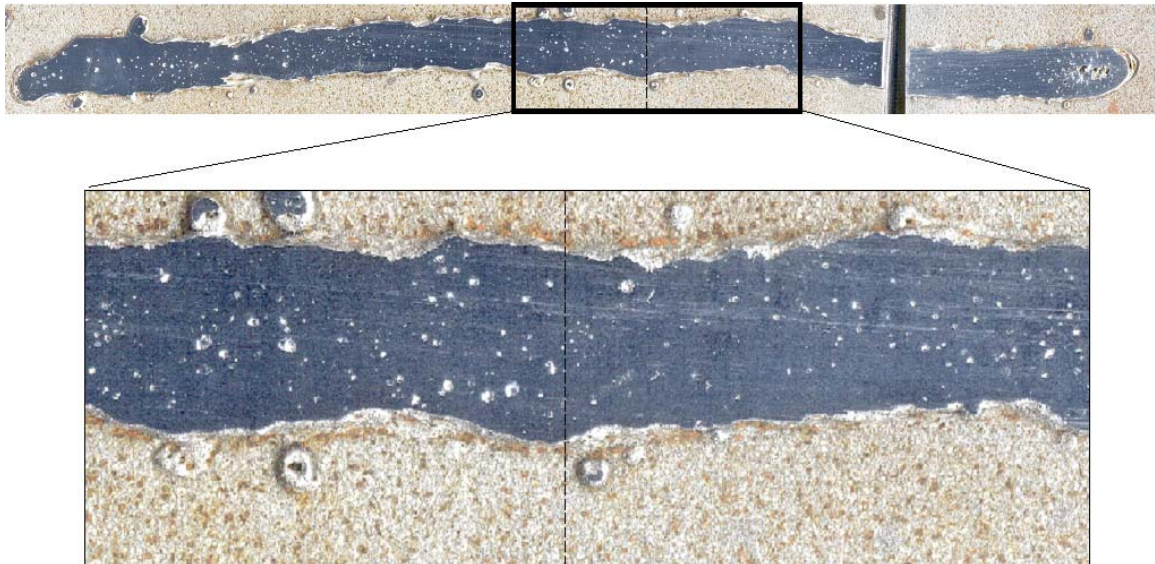


Figure 2.5.5. Top view of a bead-on-plate wet weld deposited with E6010 electrode at 50 m.

In order to have more clear porosity differences between constant and pulsed current, wet welds were made at 75 m water depth where porosity becomes larger. Figure 2.5.6 shows a longitudinal section of the BOP wet weld made with constant current that clearly illustrates the size of the pores and its uniform distribution. Figure 2.5.7 shows a longitudinal section of the BOP wet weld made with pulsed current. A sizeable porosity-free region was obtained and the 10.3 % porosity (constant current) decreased to 3.2 % (pulsed current).



Figure 2.5.6. Longitudinal section from a bead-on-plate wet weld deposited with E6010 electrode at 75 m water depth using constant current. The porosity percentage measured is 10.3 %.



Figure 2.5.7. Longitudinal section from a bead-on-plate wet weld deposited with E6010 electrode at 75 m water depth using constant current. The porosity percentage measured is 3.2 %.

More experimental work has been conducted with pulsed current; however the power sources used were designed for processes other than wet welding. For example, a power source with an external current pulser capable of producing a wide range of pulse frequencies designed for the GTAW was used. The experiment was unsuccessful because when the power source detected short-circuiting the current would be adjusted to low values, insufficient to break the short-circuiting events need to transfer the droplets in SMAW process. This current adjustment is used in the GTAW process to protect the tungsten electrode from melting.

Experimental work is in progress using the Pulsed GMAW process with flux-covered electrodes. Initial experiments conducted in dry conditions showed promising results.

2.5.4 Conclusions

- Larger porosity percentages are associated with larger droplets detached from the electrode tip.
- Hollowed droplets carry gas into the weld metal to result in weld porosity.
- As water pressure increases the external pressure (arc pressure + hydrostatic pressure) acting on the weld metal also increases making it more difficult for the gas bubbles to escape.
- Mechanical gas entrapment in the droplet during droplet formation contributes significantly to weld porosity alongside with hydrogen diffusion.
- A wet weld deposited with pulsed current at 75 m water depth showed 3 pct. porosity compared to the 10.3 pct. porosity in a wet weld deposited at the same water depth with constant current.

2.6 Welding with covered electrodes using a constant voltage power source

2.6.1 Introduction

Arc welding processes are well established with respect to the type of power sources and consumables to be used. For example, GMAW uses constant voltage power sources and metal-cored or solid wires with external shielding gases. Flux covered electrodes, on the other hand, are used with SMAW, which is a constant current process. However, it has been explored at the Colorado School of Mines to combine flux-covered electrodes with constant voltage power sources and no shielding gas. This combination offered several advantages when depositing welds with a mechanical system or robot. The main advantage is the ability to start the arc by electrical contact between the electrode and base metal. Another advantage is being able to control better the arc length and metal transfer modes. Also, a better bead appearance could be obtained when welding parameters are properly selected. The main disadvantage, however, is the high current values used to break short-circuiting events.

Hevia-Garcia (2005) used the constant voltage process with flux-covered electrodes to improve bead morphologies of wet welds. His experimental work using a gravity welder and a constant current power source resulted in wavy beads, undercuts, and humping defects. Switching to a constant voltage power source and adjusting the welding parameters, eliminated these defects.

2.6.2 Experimental procedures

In order to determine the effects of parameters such as electrode-plate angle, electrode-feeding speed, travel speed, and weld pool length on the weld bead morphologies several bead-on-plate welds were deposited in dry and wet conditions. The values that gave the best welds were selected to make welds at three water depths. Again, the wet welds were deposited in the chamber shown in Figure 2.2.1 at simulated water depths of 25, 50, and 75 m with varying voltages as presented in Table 2.6.1

Table 2.6.1. Experimental matrix for the wet welds deposited in the hyperbaric chamber.

Selected voltage, V	Water depth, m		
	25	50	75
25	X	X	X
27	X	X	X
29	X	X	X
31	X	X	X
33	X	X	X
35	X	X	X
37	X	X	X

AWS E6013 grade electrodes of 355 x 3.9 mm in length and rod diameter respectively were used to deposit all the BOP welds. For the wet welds, the electrodes were waterproofed to protect the flux coating from water absorption using commercial varnish. The BOP welds were made on A36 steel plates 13 mm in thickness.

A gravity welder was modified by adding an electrical motor with adjustable speeds to move the electrode holder up and down (to feed the electrode). The modified setup is shown in Figure 2.6.1. With

the used of the motor the electrode is fed at a constant speed producing welds with better bead morphologies eliminating undercuts, humps, and other surface defects.

The constant voltage/GMAW process capabilities of a power source (Max. 40 V and 600 A) were used to deposit the BOP welds. For a selected voltage value, the welding current is adjusted automatically by the power source to melt the electrode at the feeding rate.

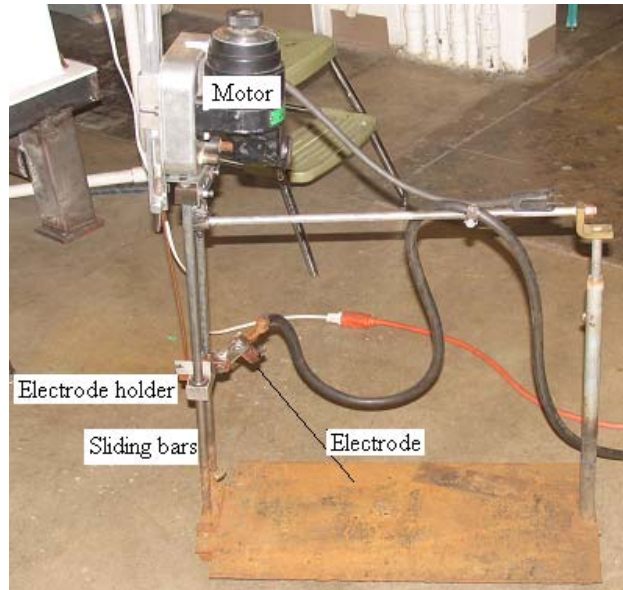


Figure 2.6.1. Welding system used for wet welding with flux-covered electrodes and constant voltage.

The welder was placed inside the chamber shown in Figure 2.2.1 to make the bead-on-plate wet welds at the three water depths.

2.6.3 Results

Only two BOP welds described in Table 2.6.1 were not made due to low voltage. Those were the ones with 25 volts at 50 and 75 m. Figure 2.6.2 shows four of the BOP wet welds deposited at 50 m water depth. A close-up of the central region of the BOP welds is shown in Figure 2.6.3 where besides surface irregularities due to internal porosity no other significant defects (undercutting and humping) were found.



Figure 2.6.2. Bead-on-plate wet welds made with E6013 electrodes, electrode positive polarity, and constant voltage at 50 m water depth. The numbers on the plate from left to right indicate water depth, voltage and weld number.



Figure 2.6.3. Close-up of the bead-on-plate wet welds shown previously.

Cross-sections were extracted from the BOP welds to measure width, penetration, and weld metal porosity. Figure 2.6.4 plots the weld width as a function of voltage illustrating that the weld beads became wider as voltage increased from 25 to 31 volts. Minor increases were observed in the range of 31 to 37 volts. All welds made in the three water depths exhibited similar behavior. Since higher arc voltages entail in longer and wider arcs, the welds became wider with increasing voltage.

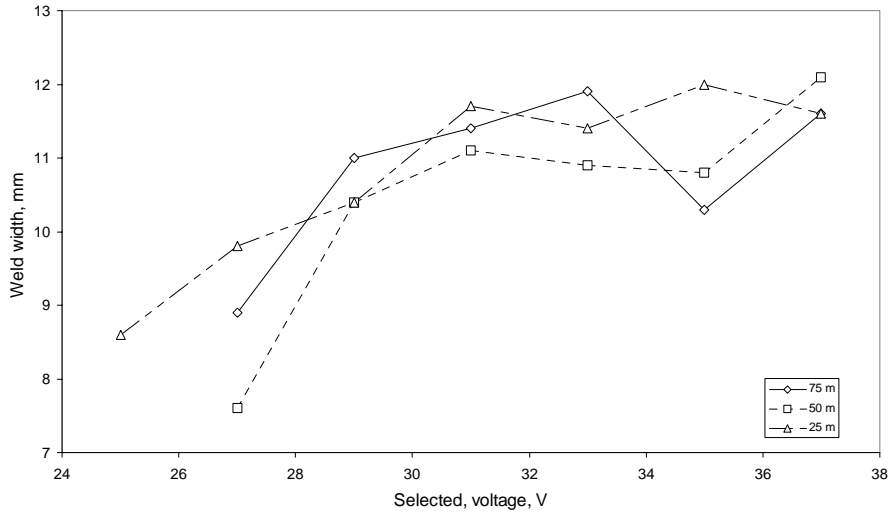


Figure 2.6.4. Width versus selected voltage of the BOP welds.

Figure 2.6.5 presents weld penetration as a function of voltage, with graphs showing increasing penetration with increasing voltage. Deeper penetration was observed in wet welds deposited at 25 m. Welds deposited at 50 and 75 m water depth showed essentially the same penetrations. The increase in penetration can be attributed to the increase in heat input, which can be expressed

as $Heat\ Input = \frac{I \cdot V}{S} \cdot \eta$. Where I and V represent current and voltage; S is travel speed and η is arc

efficiency. The decreased penetration with water depth is likely because of arc instability at the greater depths. With a wandering arc, the heat source becomes more diffused with heat dissipated more easily to the surroundings.

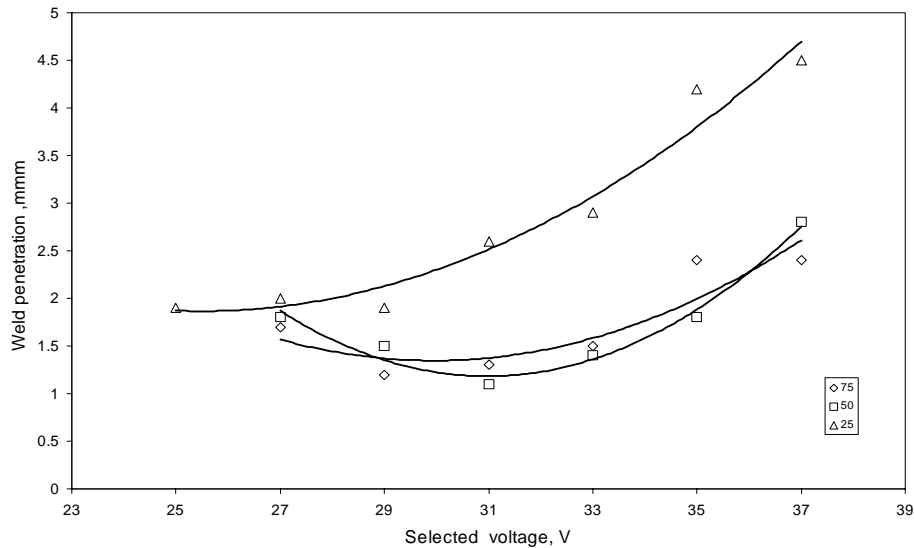


Figure 2.6.5. Penetration versus selected voltage of the BOP welds.

Similar to the findings in task 1, porosity varied along the weld bead, being greater at the beginning and smaller at the end side as shown in the radiographic images shown earlier (i.e. Figure 2.1.3b and 2.1.4b). Nevertheless, porosity is typically measured on cross-section macrographs where the total area of the pores is divided by the total area of the weld bead and the resulting value multiplied by 100 to obtain percentage. In this case, weld metal porosity was measured in a different way to obtain more precise values. Dry and submerged weights were obtained from small sections of the weld bead and by weight and density differences, porosity values were calculated. Since the actual volume of the weld is not determined with this method, the weld metal area was measured in cross-section and assumed constant along the weld. The porosity volume was divided by the weld metal volume then multiplied by 100 to obtain the porosity percentages presented in Figure 2.6.6. Although small differences were observed at 25 and 50 m, porosity percentages increased with increasing water depth. Larger porosity values were obtained in wet welds deposited at 75 m, particularly at the highest voltage values. Since this method can be conducted in much shorter time than the typical macrographic approach, it is anticipated that this method may ultimately replace the cumbersome metallographic technique in determining porosity. More tests should be conducted to give extensive correlation before deciding to replace the traditional technique.

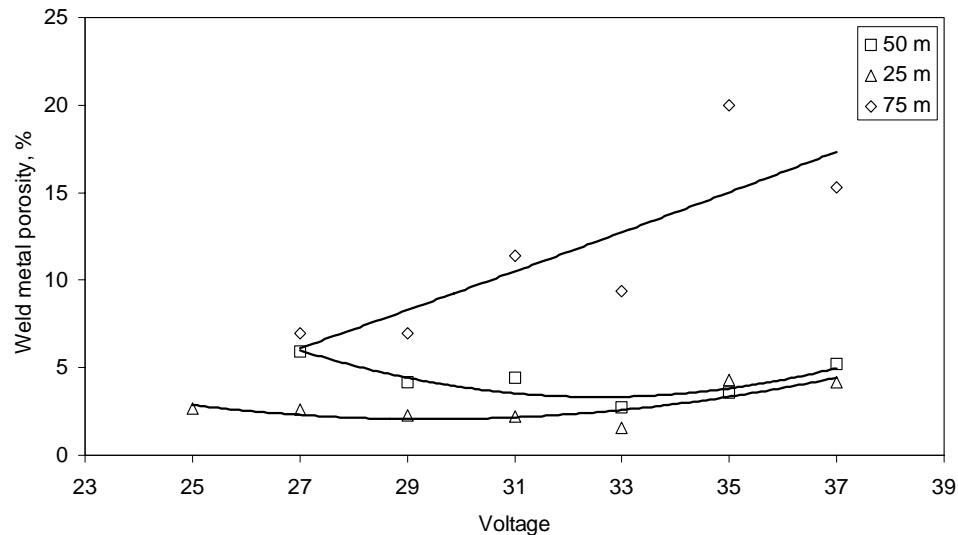


Figure 2.6.6. Porosity percent versus selected voltage of the BOP welds.

2.6.4 Conclusions

- Using the modified process, the arc is easily established when the flux-covered electrode contact the base metal, eliminating the need of inserting a low conductivity flux paste in between the electrode tip and base plate.
- Flux-covered electrodes can be used with constant voltage processes.
- Wet weld with less defects can be made with this new process.
- Power sources with pulsing capabilities could be used to reduce weld metal porosity.
- There is a better control of the arc length with the constant voltage processes.

3 GENERAL CONCLUSIONS AND RECOMMENDATIONS

3.1 Conclusions

Underwater wet welding at 150 m

- Porosity clearly limits wet welding at 150 m water depth to non-critical components and represents the main problem to be overcome in wet welding.
- Porosity in wet welds made at 150 m water depth ranged from 7.3 to 23.5 pct. and reduced considerably the tensile strength of the wet welds.
- Wet welds deposited with E6013 electrodes presented the lowest level of porosity and the highest tensile strength.
- The tensile strength of the weld metal was approximately 50% that of the base metal.
- Better arc stability was observed with the E6013 grade electrodes.
- Large electrode diameter increased the deposition rate producing large weld beads and large pores.

Performance of cellulosic electrodes

- The AWS E6010 type electrodes performed well underwater. At 50m water depth, a two-fold increase in weld penetration was obtained when compared with welds deposited with E6013 electrodes.
- The light slag produced was easily removed, without slag entrapment problem.
- Macro-cracks were observed along the fusion line of the BOP weld, however only a few micro-cracks were observed in the multipass welds made at 0.3 m and 50 m.
- In the V-groove welds, the average porosity was only 1.8 pct. due to the re-melting effect, which represents a 50% reduction from the BOP welds deposited at 50m.
- Carbon decreased with increasing water depth.
- Most alloying elements in the wet welds were in the form of oxide inclusions.
- Toughness and tensile strength decreased with increasing water depth.

Out-of-position welding

Vertical-down welding position

- E6013 grade electrodes produced the most stable arc and smallest droplets of the three electrodes tested at 0.5m water depth. E7018 electrodes produced the largest droplets with largest fluctuations in arc voltage.
- Wet welds deposited with E6010 electrodes produce discontinuous welds at 0.5 m water depth.
- Vertical-down wet welds were deposited with the specially designed gravity welder system at three water depths (0.5, 50, and 100m) using the E6013 electrode grade.
- The E6010 was not tested at 50 and 100 m due to the poor results obtained at 0.5 m.
- Porosity and arc instability were the main problems with the E7018 electrode at 50 m, thereafter no more tests were made at this depth or at 100 m.
- A loss of weld metal close to 50% was observed in welds deposited at 50 and 100 m with respect to the ones made at 0.5 m.
- Further work is needed to minimize the loss of weld metal in wet welds at 50 and 100 m water depth.

- Less porosity was measured on the wet welds deposited in the vertical-down welding position with respect to previous results reported for the flat welding position. However it is important to consider the difference in the reinforcement of the welds.

Vertical-up welding position

- Due to the lack of support of the molten weld pool, vertical-up wet welds were discontinuous and exhibited deep undercuts on both sides of the welds at 0.5 m water depth.
- Vertical-up wet welds were not deposited at 50m or 100 m water depths due to the poor results obtained at 0.5 m.

Rutile electrodes with nickel additions

- Different from what was found in the surface and shallow water wet welds, higher nickel content did not improve the impact toughness.
- The 50 m water depth welds had impact toughness ranging from 21 to 13 ft-lb (0.9 and 2.4 wt. pct. nickel), respectively.
- Ductile fracture was observed outside the pores. Thus, weld defects, instead of the microstructures, affected more significantly the mechanical behavior of these welds.

Mitigation of porosity

- Larger porosity percentages are associated with larger droplets detached from the electrode tip.
- Hollow droplets carry gas into the weld metal to result in weld porosity.
- As water pressure increases, the external pressure (arc pressure + hydrostatic pressure) acting on the weld metal also increases making it more difficult for the gas bubbles to escape.
- Mechanical gas entrapment in the droplet during droplet formation contributes significantly to weld porosity alongside with hydrogen diffusion.
- A wet weld deposited with pulsed current at 75 m water depth showed 3 pct. porosity compared to the 10.3 pct. porosity in a wet weld deposited at the same water depth with constant current.

Welding with covered electrodes using a constant voltage power source

- Using the modified process, the arc was easily established when the flux-covered electrode contacted the base metal, eliminating the need of inserting a low conductivity flux paste in between the electrode tip and base plate.
- Flux-covered electrodes can be used with constant voltage processes.
- Wet welds with fewer defects can be made with this new process.
- Power sources with pulsing capabilities can be used to reduce weld metal porosity.
- Better control of the arc length can be accomplished with the constant voltage processes.

3.2 Recommendations

Based on the results presented in this report, the following recommendations are suggested to further improve or ensure the quality of wet weld.

- Wet welds mechanically deposited at water depths beyond 100 m are not recommended, unless a procedure to reduce weld metal defects (particularly porosity) is implemented or if the strength of the wet welds is not important.
- Amongst the commercial electrodes tested, the AWS E6013 grade electrodes are recommended for underwater wet welding because of its low porosity percentages and good arc stability. The E6010 type electrodes also give good results if the carbon equivalent of the base metal is limited to below 0.40 wt. pct.
- Experimental electrodes with additions of alloying elements, i.e. proper formulation, are required to improve the mechanical properties of wet welds. Further experimental matrix for optimization is recommended to determine this formulation.
- Out-of-position vertical-down is the preferred position for wet welding at water depths of 50 and 100 m.
- More experimental work on rutile-grade electrodes with nickel additions is required to determine the optimum nickel content to obtain the highest impact toughness for a given water depth.
- Smaller diameter welding electrodes are recommended to reduce wet weld metal porosity.
- Extensive research work is required to reduce weld metal porosity with pulsed current.
- Constant voltage power sources can be used with flux-covered electrodes for wet welding. However high welding current values could be reached when the electrode short-circuits the base metal, which could be dangerous for the welder.

4 ACKNOWLEDGMENTS

The participants of this project acknowledge the support provided by the Minerals Management Service, in particular Dr. Charles Smith and Mr. Michael Else. The participants of this project also wish to acknowledge the support of the Instituto Mexicano del Petroleo.